LNA CONSIDERATIONS FOR SQUARE KILOMETRE ARRAY

A dissertation submitted to the University of Manchester
for the degree of Doctor of Philosophy
in the Faculty of Engineering and Physical Sciences

2012

By

Mina Panahi

School of Electrical and Electronic Engineering

Contents

Abstract **14**

Declaration **16**

Copyright **17**

Acknowledgements **19**

Glossary **20**

Publication List **22**

1 Introduction **24**

1.1 Introduction 24

1.2 Square Kilometre Array 25

1.3 LNAs for the SKA 26

1.4 Antenna Designs in SKA 32

1.5 SKA LNA Works Around the World 34

1.5.1 SKA LNA Developments 35

1.6 Ultra Wideband LNAs 38

1.7 Research Objectives 40

1.8 Thesis Organisation 41

2 Evolution of Low Noise Devices **44**

2.1 Introduction 44

2.2 Low Noise Amplifier History 44

2.3 High Electron Mobility Transistors(HEMT) 46

2.3.1 Technology of HEMTs 47

2.3.2 Topologies of HEMTs 48

2.3.3 HEMTs DC behaviour 50

2.4 Sources of Noise in HEMTs 51

2.5 Summary 53

3 Low Noise Amplifier Design Theory **54**

3.1 Introduction 54

3.2 S-parameters 55

3.2.1 2-Port S-Parameters 56

3.2.2 Multi-Port S-Parameters 60

3.2.3 Mixed Mode S-Parameters 61

3.2.4 4-Port Mixed mode S-Parameters [1] 62

3.2.5 3-Port Mixed Mode S-Parameters [1] 67

3.3 Noise Parameters 70

3.4 Fabrication Techniques 71

3.4.1 MICs 71

3.4.2 MMICs 72

3.5 Design Techniques 72

3.5.1 Multi-stage LNA 74

3.5.2 Noise Figure Matching 75

3.5.3 Impedance Matching 76

3.5.4 Passive Components 77

3.6 Parameters of LNAs 77
3.6.1 Gain 78
3.6.2 Noise Figure 79
3.6.3 Stability 79
3.6.4 Bandwidth 81
3.6.5 Power 82
3.6.6 Return Losses 82
3.7 Baluns [2, 3] 84
3.7.1 Lumped Component Baluns 85
3.7.2 Transformer Baluns 87
3.7.3 Other Variations of Baluns 87
3.8 Positional Impact of Balun in a Receiver [4] 88
3.8.1 SKA Front-end System Configuration Considerations [4] . 89
3.8.2 Balun followed by single-ended LNA [4] 90
3.8.3 2 LNAs followed by a balun [4] 91
3.9 Topologies 94
3.9.1 Single Ended LNA 94
3.9.2 Differential input and single ended LNA 95
3.9.3 Differential LNA 96
3.10 Summary 96

4 Designs **98**

4.1 Introduction 98
4.2 Avago ATF-58143 E-Mode pHEMT 99
4.3 Development of MIC LNAs 100
4.4 MIC AA-lo LNAs 102
4.4.1 SE-AAloV1, SE-AAloV2 and SE-AAloV3 103

4.4.2 Diff-AAloV1 and Diff-AAloV2 108
4.4.3 AA-lo LNA Packaging 112
4.5 MIC AA-mid LNAs 115
4.5.1 AAmidV1 and AAmidV2 116
4.5.2 AA-mid LNA Packaging 122
4.6 MMIC LNAs 123
4.6.1 TQP13N 130nm pHEMT Library 123
4.6.2 UMAN-SKAlowV1 126
4.6.3 UMAN8-Xband 129
4.6.4 MMIC LNA Packaging 132
4.7 DC Bias Networks 135
4.8 Summary 137

5 Measurement Bench **139**
5.1 Introduction 139
5.2 On-Wafer Transistor Measurement 139
5.3 MIC LNAs Measurements 142
5.3.1 S-Parameters 142
5.3.2 Noise Figure Measurement 145
5.4 Summary 146

6 Results and Analysis **147**
6.1 Transistor Measurements 148
6.1.1 TQP13 pHEMTs 148
6.2 LNAs 163
6.3 MIC AA-lo LNAs 166
6.3.1 SE-AAlo LNAs 166
6.3.2 Diff-AAlo LNAs 176

6.4 MIC AA-mid LNAs 189
6.5 MMIC UMAN-SKAlowV1 LNA 198
6.6 MMIC UMAN8-Xband LNA 201
6.7 Summary 204

7 Conclusion and Future Work **207**
7.1 Conclusion 207
7.2 Future Work 212

Bibliography **213**

List of Tables

1.1 LNAs in the SKA [5, 6] 27

1.2 Design specifications required for AA-lo LNAs [7, 6]. 28

1.3 Design specifications required for AA-mid LNAs [6]. 28

1.4 Summary of available commercial and non commercial LNAs for comparative study. 39

2.1 Properties of Si, InP and GaAs substrates [8, 9]. 48

4.1 Configurations of MIC LNAs for AA system. 101

4.2 Description of the components, functions and values in the AA-lo LNA. 104

4.3 Inductances of via holes for FR4 and RO4003C substrates. 107

4.4 Description of the components, their functions and values in the AA-mid LNA. 118

4.5 Description, functions and values of components in UMAN-SKAlowV1 LNA. 127

4.6 LNA design specifications of UMAN8-Xband 130

4.7 Description of the components, functions and the values in the UMAN8-Xband. 132

4.8 Summary of the designed LNAs. 138

6.1 DC sweeps used for TQP13N pHEMTs characterisation. 149
6.2 Summary of the DC characteristics of TQP13 pHEMTs. 152
6.3 Bias Points of TQP13 D mode pHEMTs for S-Parameter measurement. 153
6.4 Biases for stage-1 and 2 of the SE-AAloV1. 169
6.5 Biases for stage-1 and 2 of the SE-AAloV2. 170
6.6 Bias points for stage 1 and 2 of SE-AAloV3. 172
6.7 SKA and commercial LNAs operating over AA-lo frequency band. 175
6.8 Biasing points for stage-1 and 2 of the Diff-AAloV1. 179
6.9 Bias points of the Diff-AAloV2. 182
6.10 Summary of Diff-AAloV2 Measurements 187
6.11 Commercially available LNAs for Diff-AAlo LNAs. 189
6.12 Bias points for stage 1 and 2 of the AAmidV1 LNA. 193
6.13 Bias points for stage 1 and 2 of AAmidV2. 194
6.14 SKA and commercially available LNAs for AA-mid band. 197
6.15 Comparison of commercially available LNAs with UMAN-SKAlowV1.200
6.16 LNAs operating at X-band. 203
6.17 Summary of LNAs performances over the bandwidth. 204
6.18 LNAs designed for SKA AA system. 205

List of Figures

1.1 Signal path in the SKA AA system [10]. 29

1.2 Sky noise distribution over frequency [11]. 30

1.3 Antenna with differential output connected to an LNA with differential input and single ended output. 33

1.4 Antenna with differential output connected to a balun and a single ended LNA. 34

1.5 Antenna with differential output connected to a fully differential LNA. 34

2.1 Structure of a HEMT [8]. 49

3.1 S-parameter for a 2-port Network. 56

3.2 A 4-port network. 62

3.3 Presentation of a 3-port network. 67

3.4 General 2-port amplifier with matching networks. 75

3.5 An example of noise circles for a pHEMT. 76

3.6 Balanced and unbalanced signals. 84

3.7 Schematic view of a LC lumped component balun [12]. 86

3.8 Schematic view of a wire wound lumped component balun [12]. . . 88

3.9 Classical front-end configuration. 90

3.10 Front-end configuration with balun after LNAs. 91

4.1 Schematic view of the single ended mode of AA-lo LNA. 103
4.2 Layout of SE-AAloV1 LNA. 106
4.3 Layout of SE-AAloV2 LNA. 107
4.4 Layout of SE-AAloV3. 108
4.5 S-parameter performance of the transformer used in Diff-AAlo LNAs [13]. 110
4.6 Schematic view of the differential mode of AA-lo LNA. 110
4.7 Layout of Diff-AAloV1. 111
4.8 Layout of Diff-AAloV2. 111
4.9 Fabricated prototype Diff-AAloV1. 113
4.10 Fabricated prototype Diff-AAloV2. 114
4.11 Fabricated prototype SE-AAloV3 LNA. 115
4.12 Schematic view of the AA-mid LNA. 118
4.13 Layout of AAmidV1. 119
4.14 Fabricated prototype AAmidV1. 120
4.15 Layout of AAmidV2. 121
4.16 Fabricated prototype AAmidV2. 121
4.17 Packaged AA-mid LNA. 122
4.18 Simulated S_{21}, R_n and minimum noise figure performance of the TQP13N 4×50μm pHEMT with variation of V_g and frequency at V_d=2V. 125
4.19 Simulated S_{21}, R_n and minimum noise figure performance of the TQP13N 4×50μm pHEMT with variation of V_d and V_g at 8.5GHz. 125
4.20 Schematic view of the UMAN-SKAlowV1 MMIC LNA. 128
4.21 Layout of the UMAN-SKAlowV1 LNA. 129
4.22 The schematic view of the UMAN8-Xband LNA. 130
4.23 The layout of UMAN8-Xband LNA. 132

4.24 The layout of the board designed for measurement of the UMAN8-Xband LNA. 134
4.25 Prototype board designed for X-band LNA characterisation. . . . 135
4.26 The DC bias network used for 1 stage of a MIC AA-lo LNA at the gate. 136
4.27 The DC bias networks used at the gates of the UMAN8-Xband MMIC LNA with 3 stages. 137

5.1 An illustrative view of an on-wafer transistor. 140
5.2 Probe station for on-wafer transistor characterisation. 141
5.3 Block diagram representation of the DC and S-parameter measurement set-up for on-wafer transistors. 142
5.4 Agilent E5071B ENA. 143
5.5 Experimental set up for the single ended LNA measurements. . . 144
5.6 Experimental set up for differential to single ended LNA measurements. 145
5.7 Block diagram of the noise figure measurements for MIC LNAs. . 146

6.1 DC measurements of TQP13N pHEMT with gate width of $4 \times 25\mu$m. 149
6.2 DC measurements of TQP13N pHEMT with gate width of $4 \times 50\mu$m. 150
6.3 DC measurements of TQP13N pHEMT with gate width of $4 \times 75\mu$m. 150
6.4 DC measurements of TQP13N pHEMT with gate width of $4 \times 100\mu$m. 151
6.5 S-parameter responses of TQP13N pHEMT with gate width of $4 \times 25\mu m$. 154
6.6 S-parameter responses of TQP13N pHEMT with gate width of $4 \times 50\mu m$. 155
6.7 S-parameter responses of TQP13N pHEMT with gate width of $4 \times 75\mu m$. 156

6.8 S-parameter responses of TQP13N pHEMT with gate width of $4 \times 100\mu m$. 157
6.9 Minimum noise figure values of TQP13N pHEMTs with 4 different gate width dimensions. 161
6.10 Noise resistance values of TQP13N pHEMTs with 4 different gate width dimensions. 162
6.11 Γ_{opt} of TQP13N pHEMTs of 4×25μm, 4×50μm, 4×75μm and 4×100μm. 162
6.12 Diagram of the designed LNAs. 164
6.13 Simulated S-parameter responses of SE-AAlo. 167
6.14 Simulated noise figure responses of the SE-AAlo. 167
6.15 Measured S-parameter responses of the SE-AAloV1 LNA. 168
6.16 Measured noise figure of the SE-AAloV1. 169
6.17 Measured S-parameter responses of the SE-AAloV2. 171
6.18 Measured noise figure responses of the SE-AAloV2. 171
6.19 Measured S-Parameter responses of SE-AAloV3. 172
6.20 Measured noise figure of SE-AAloV3. 173
6.21 Simulated mixed mode S-parameter responses of the Diff-AAlo. . 177
6.22 Simulated noise figure responses of the Diff-AAlo. 178
6.23 Simulated common mode rejection ratio of the Diff-AAlo. 178
6.24 Measured mixed mode S-parameter responses of the Diff-AAloV1. 179
6.25 Measured noise figure of Diff-AAloV1. 180
6.26 Measured input and output return losses of the transformer used in Diff-AAloV1 and Diff-AAloV2 LNAs [13]. 181
6.27 Measured differential mode gain of Diff-AAloV2. 183
6.28 Measured common mode gain of the Diff-AAloV2. 183

6.29 Measured differential, common and single mode return losses of the Diff-AAloV2 at Bias1. 184
6.30 Measured differential, common and single mode return losses of Diff-AAloV2 at Bias2. 185
6.31 Measured differential, common and single mode return losses of Diff-AAloV2 at Bias3. 185
6.32 Measured noise figure responses of the Diff-AAloV2 LNA at 3 separate biases and the loss of the balun used in the LNA. 186
6.33 Measured common mode rejection ratio of the LNA2. 187
6.34 Simulated S-Parameter responses of the AA-mid LNA. 190
6.35 Simulated noise figure responses of the AA-mid LNA. 191
6.36 Simulated K-factors of the AA-mid LNA. 191
6.37 Measured S-Parameter responses of AAmidV1 192
6.38 Measured noise figure of the AAmidV1 193
6.39 Measured S-Parameter responses of the AAmidV2 LNA. 194
6.40 Measured noise figure responses of the AAmidV2. 195
6.41 Simulated S-parameter responses of UMAN-SKAlowV1. 199
6.42 Simulated Noise Figure of UMAN-SKAlowV1. 199
6.43 Simulated K-factor values for UMAN-SKAlowV1. 200
6.44 Simulated S-parameter responses of UMAN8-Xband. 202
6.45 Simulated noise figure of UMAN8-Xband. 202
6.46 Simulated K-factor of UMAN8-Xband. 203

Abstract

This thesis describes the design of low noise amplifier (LNA) for the international Square Kilometre Array (SKA) project. LNAs in radio astronomy receivers play an important role of amplifying very weak signals from the Universe and the significance of the LNAs become more crucial in the SKA which is the largest and most sensitive radio telescope in the World. The aperture array (AA) system proposed for SKA is projected to deploy tens of millions of LNAs in a receiver system to survey large areas of the sky simultaneously over the frequency bands of 70-450MHz and 400-1400MHz. Hence LNA power efficiency has a significant implication in the SKA AA system due to the large number of the LNAs required. This thesis describes the design of 9 LNAs for the SKA. Seven LNAs with very low power consumption were designed, fabricated and characterised for SKA AA system using MIC technology by employing COTS components. Single ended and differential to single ended configurations were used for the lower frequency band of SKA AA system. Low noise figures (noise temperatures) of 0.6dB (43K) were achieved with high gain of more than 30dB at a power consumptions of less than 25mW for lower frequency band of AA. The LNAs designed to perform at 400-1400MHz have a very low power consumption of 28mW with an average noise figure (noise temperature) of 0.45dB (32K). Two MMIC LNAs based on low noise TQP13N pHEMT process of TriQuint Semiconductors with gate length of 130nm were designed for the low (0.7-1.8GHz) and high (8-10GHz) frequency

ends of the SKA. The packaging and housing solutions of the SKA LNAs were implemented.

The work described in this thesis shows low noise figures (noise temperatures) with high gains are achieved at a very low power consumption of less than 30mW for the MIC LNAs in the SKA AA system by using commercially available components.

Declaration

No portion of the work referred to in this dissertation has been submitted in support of an application for another degree or qualification of this or any other university or other institute of learning.

Copyright

and commercialisation of this thesis, the Copyright and any Intellectual Property and/or Reproductions described in it may take place is available in the University IP Policy (see `http://www.campus.manchester.ac.uk/medialibrary/policies/intellectual-property.pdf`), in any relevant Thesis restriction declarations deposited in the University Library, The University Library's regulations (see `http://www.manchester.ac.uk/library/aboutus/regulations`) and in The University's policy on presentation of Theses

Acknowledgements

I would like to thank Dr. Danielle George for her efficient supervision, guidance and support throughout this undertaking. I would like to thank the Square Kilometre Array project for their help and support towards my work that has been reported in this thesis. I would like to take this opportunity to thank Mr. Neil Roddis for his technical insights, support and advice, Mr. Keith Williams (former employee of the University of Manchester) for his support and guidance in the laboratory, Mr. Peter Green, Dr. Graham Parkinson, Dr. Saswata Bhaumik and Dr. Mousumi Roy for their support.

Glossary

AA	Aperture Array
AA-lo	Aperture Array - lower frequency band
AA-mid	Aperture Array - higher frequency band
ADS	Advanced Design System
AlGaAs	Aluminium Gallium Arsenide
CAD	Computer Aided Design
CMOS	Complementary metal-oxide-semiconductor
COTS	Commercially available Off-The-Shelf
DC	Direct Current
DUT	Device Under Test
ECal	Electronic Calibration
ENA	Electronic Network Analyzer
ENR	Excess Noise Ratio
FET	Field Effect Transistor
GaAs	Gallium Arsenide
HBT	Heterojunction Bipolar Transistors
HEMT	High Electron Mobility Transistor
InAlAs	Indium Aluminium Arsenide
InGaAs	Indium Gallium Arsenide
InP	Indium Phosphide

LNA	Low Noise Amplifier
LRRM	Line-Reflect-Reflect-Match
mHEMT	metamorphic HEMT
MIC	Microwave Integrated Circuit
MMIC	Monolithic Microwave Integrated Circuit
NF	Noise Figure
NFM	Noise Figure Meter
NT	Noise Temperature
PCB	Printed Circuit Board
pHEMT	pseudomorphic HEMT
PSU	Power Supply Unit
RF	Radio Frequency
Si	Silicon
SiGe	Silicon Germanium
SKA	Square Kilometre Array
SOLT	Short-Open-Thru
SNR	Signal-to-Noise Ratio
VNA	Vector Network Analyser
VSWR	Voltage Standing Wave Ratio

Publication List

1. M. Panahi, S. Bhaumik, D. George, "Power-Efficient Ultra Wideband LNAs for the World's Largest Radio Telescope", submitted to *Review of Scientific Instruments*, 2012.

2. S. Bhaumik, M. Panahi, D. George, "Super Low Power Wideband LNA for Aperture Array Systems of Square Kilometre Array", submitted to *IEEE MTT-S International Microwave Symp.*, Dec. 2011.

3. M. Panahi, D. George, "Design of Low Noise amplifier for the Square Kilometer Array Design Study", *32nd ESA Antenna Workshop on Antennas for Space Applications Conference*, ESA/ESTEC, Noordwijk, The Netherlands, Oct. 2010.

4. M. Panahi, D. George, "Verification of Differential Low Noise Amplifier Measurement", *Widefield Science and Technology for the SKA, SKADS Conference*, Belgium, Nov. 2009.

5. S. Bhaumik, M. Panahi, D. Kettle, "Differential LNA considerations for the Square Kilometer Array", *13th International Symp. on Antenna Technology and Applied Electromagnetics and the Canadian Radio Science Meeting (ANTEM/URSI)*, pp.1-4, 15-18 Feb. 2009.

To my parents Mitra and Yousef

and

my brothers Kamran, Pouria and Pedram

Chapter 1

Introduction

1.1 Introduction

Low noise amplifiers (LNAs) are used in many applications that involve the detection and/or measurement of very weak signals. Examples of the LNA applications are in mobile phones, GPS receivers, wireless networks, satellite communication systems, Hall effect sensors, MRI scanners and radio astronomy receivers. Radio astronomy is a specific example which seeks to detect and measure extremely weak electromagnetic radiation from distant celestial sources. Radio astronomy enables the astronomers to observe and learn about the Cosmic Microwave Background radiations (CMB), Dark Ages before the birth of the first star and galaxies, black holes and many more. Some of these signals are remnants of the Big Bang and were emitted by the expanding universe shortly after its formation [14].

Radio astronomy observations concentrate on the objects emitting immense amount of energy from an astronomical distance to the Earth. Only a small amount of their signal is detectable on the surface of the Earth by a radio telescope due to the significant path loss of these objects and the Earth. Such signals can only be detected by a very large antenna connected to extremely low noise

amplifier. Therefore presence of a high sensitivity receiver is absolutely necessary in radio astronomy applications. Equation 1.1 gives an important relationship in the instrumentation of radio astronomy and it determines the minimum detectable signal of ΔT for a radio receiver [3, 15];

$$\frac{\Delta T}{T} \propto \frac{1}{\sqrt{B \times \tau}} \tag{1.1}$$

where ΔT is the minimum detectable signal which is treated as equivalent noise temperature, T is the noise temperature, B is the bandwidth and τ is the integration time. Equation 1.1 implies that the minimum detectable signal is proportional to the noise temperature of the system for a given bandwidth and integration time.

A detailed description of the international project to build the largest and most sensitive radio telescope called the "Square Kilometre Array" is given in Section 1.2.

1.2 Square Kilometre Array

The Square Kilometre Array (SKA) is an international radio astronomy project that has attracted the attention of the radio astronomers around the globe. The idea of the SKA was initially conceived in 1991 [16]. SKA project involves the development of the radio telescope that is the first in its type and is considered to be the new generation of the radio telescope [17, 18].

The SKA project will provide astronomers with the opportunity of further exploration of the birth, formation and evolution of the first stars and galaxies after Big Bang, search for extra terrestrial life, role of the cosmic magnetism and the nature of the gravity. Therefore SKA project enhances the possibility of new

discoveries [19].

The objectives of the SKA are achievable only if the telescope has high sensitivity and ability to process the data by innovative supercomputing [20]. The SKA has a collecting area of the order of one million square metre. The noise temperature of the front end receiver of SKA needs to be as low as possible which is defined according to the requirement of the systems. The sensitivity of the telescope will be at least 50 times more than the existing radio telescopes with a value of 10^4 m^2/K [18]. The design and development of the SKA has created a great opportunity for researchers to come up with innovations in the instrumentation and technical part of the radio astronomy. Thus this project has enabled researchers to get an insight in the design, development and implication of the new ideas in the different areas of the receiver system.

1.3 LNAs for the SKA

The SKA telescope is being designed and constructed to observe the sky over frequency range of 70MHz−10GHz [21]. Two main receptor types of Aperture Arrays (AA) and conventional parabolic dishes will be deployed to cover the required wide frequency band of the SKA [16, 22]. The frequency operation range of the SKA is divided primarily into 3 frequency bands consisting of AA-lo (70−450MHz), AA-mid (400MHz−1400MHz) and high frequency SKA (1.2GHz−10GHz) [19]. This thesis follows the nomenclature used by SKA Program Development Office (SPDO) for AA system.

AA designs are complementing the traditional radio telescope designs in order to realise the enormous collecting area of the SKA and provide a large field of view and capability of observing different parts of the sky instantaneously. Two types of AA systems are under development for the AA-lo and AA-mid frequency

bands. The AA-lo sparse aperture arrays cover frequency range of 70−450MHz while AA-mid dense aperture array operates over the frequency range of 400-1400MHz [19]. Details of the AA used in the SKA and the corresponding required LNAs are given in Table 1.1 [5, 6].

Table 1.1: LNAs in the SKA [5, 6]

	AA-lo LNA	AA-mid LNA
Collector Type	Aperture Array	Aperture Array
Frequency (MHz)	70-450	400-1400
Sensitivity (m^2/K)	4,000 at 100MHz	10,000 at 800MHz
Number	250 Arrays	250 Arrays
Size	Diameter 180m	Diameter 56m
Quantity of required LNAs	5,600,000	55,000,000

Generally, the overriding factor in the LNA designs for the radio astronomy applications is delivering the lowest noise figure possible with a flat gain across the band. Equation 1.2 gives the relationship between the noise temperature (NT) values in Kelvin (K) and noise figures (NF) values in dB.

$$NT = 290(10^{NF/10} - 1) \tag{1.2}$$

However, LNA design and development process in the SKA has equal emphasis on low noise, low power consumption and low production cost along with a flat and high gain over a wide frequency band. The necessity and importance of these requirements are driven by the large number of the LNAs required in the system as shown in Table 1.1. Hence, the LNAs must have low noise figure over wide frequency band along with a flat and high gain response at very low power consumption which are extremely challenging to achieve. Tables 1.2 and 1.3 give the required specifications of LNAs for AA-lo and AA-mid respectively. As shown in Tables 1.2 and 1.3, receiver noise temperature budget of less than 150K

was allocated to the AA-lo system while system noise temperature required for the AA-mid system was less than 38K. Noise temperature of AA-mid LNAs was projected to be less than 15K at room temperature. However, the performance of APERTIF at 1400MHz showed a receiver noise temperature of 58K [6].

Table 1.2: Design specifications required for AA-lo LNAs [7, 6].

Parameter	Specification
Bandwidth	70-450MHz
Receiver Noise	150 K
Gain	>20 dB
Power	<30mW

Table 1.3: Design specifications required for AA-mid LNAs [6].

Parameter	Specification
Bandwidth	400-1400MHz
T_{sys}	< 38K
Gain	>20 dB
Power	<30mW

The purpose of the thesis was to design LNAs to meet the required key performance parameters including noise temperature, power consumption and gain and possibly exceed the requirements. The SKA differs from the traditional radio telescope in its use of broad-band antennas with balanced outputs. Therefore, a balun must be utilised as an interface between the antennas with differential output and the LNAs. The optimum antenna performance is obtained by utilising either differential LNAs or baluns for converting the balanced signal to an unbalanced signal. Figure 1.1 illustrates the signal path of the SKA AA system.

It is absolutely essential for the AA system LNA designs to meet the following requirements;

- Lowest possible noise figure at ambient temperature

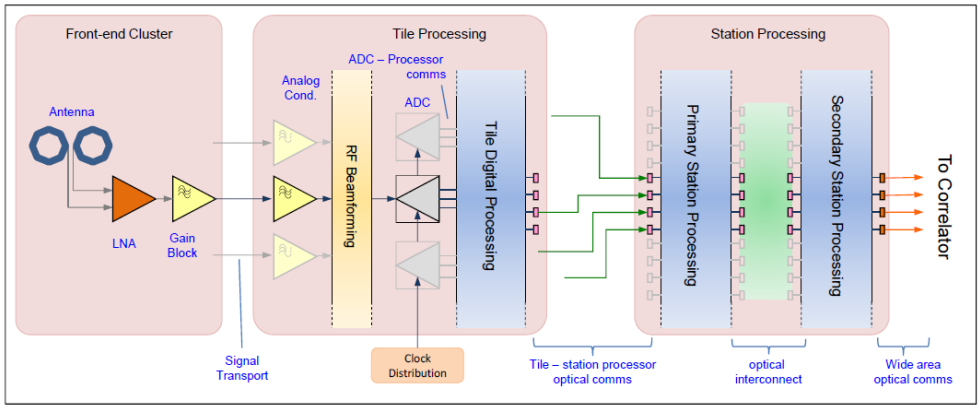

Figure 1.1: Signal path in the SKA AA system [10].

- Low power consumption
- Broad bandwidth
- Unconditional stability
- Low cost of manufacturing
- Differential input and single ended output

The importance and effect of the LNA requirements are described in further detail subsequently.

The overall system sensitivity is a vital specification of any radio receiver and in this instance is defined in Equation 1.3;

$$Sensitivity = \frac{A_{eff}}{T_{sys}} \tag{1.3}$$

where A_{eff} is the total effective collecting area and T_{sys} is the system noise temperature [19]. Two approaches which have been undertaken to increase the telescope sensitivity are to increase the collecting area of the telescope and also decrease the receiver temperature. Development of an ultra low noise LNA will help to achieve an ultra low noise receiver. Over the AA-lo frequency band, the

sky noise greatly increases as the frequency decreases. Sparse aperture arrays have been adopted for this frequency range as their effective area is proportional to wavelength (inversely proportional to frequency), thus reducing the variation in sensitivity with frequency caused by the sky noise. Figure 1.2 shows the distribution of the sky noise. It is perceived that below 200 MHz the sky noise is significantly high and dominates the noise temperature of the receiver. At frequencies above 200MHz, where the sky noise decreases dramatically, a low noise receiver will enhance the telescope sensitivity [19].

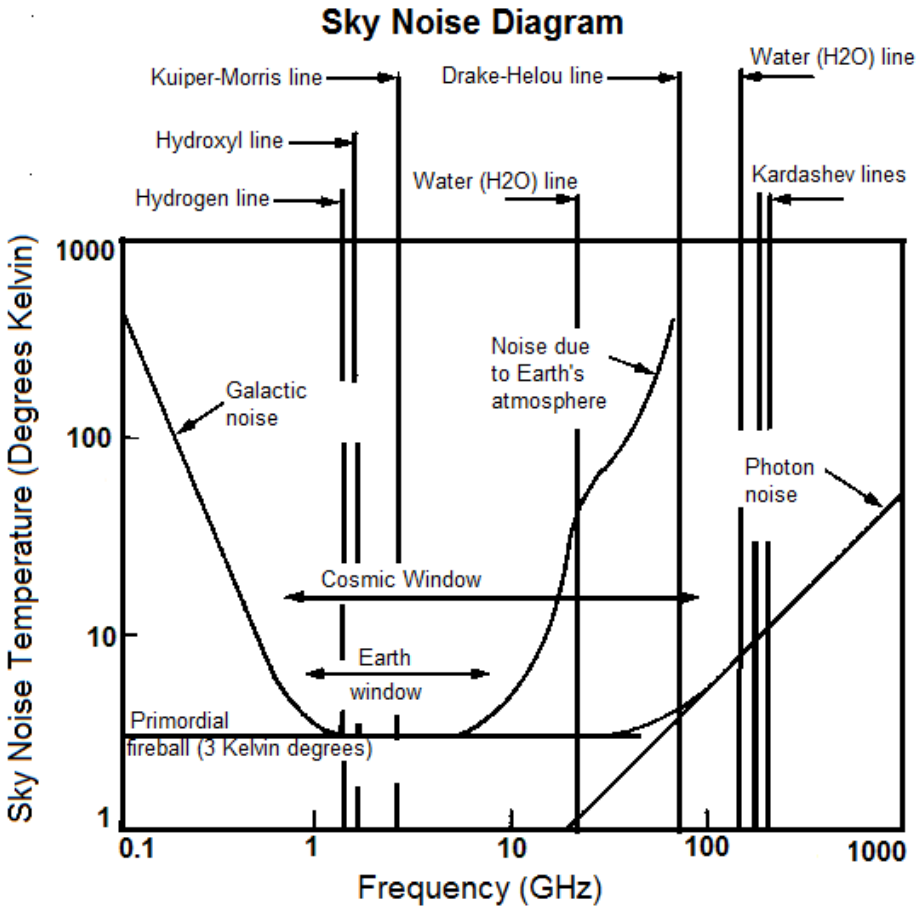

Figure 1.2: Sky noise distribution over frequency [11].

Various broad-band antenna designs are being investigated for this application

and majority of these antennas have differential outputs [23, 24, 25]. It is important to use a balun interface between the wideband antenna with differential output and the LNAs. The use of baluns prevents the single ended LNAs to affect the performance of the differential antenna by allowing unbalanced current to appear at the terminals of the antenna [26]. The baluns must be operational over a wide frequency band as a result of a broad band antenna. The baluns can be either passive or active. LNAs with differential input can be considered as active baluns that convert the balanced signal to the unbalanced signal at the output. Differential amplifiers must be low noise and have high Common Mode Rejection Ratio (CMRR) across the whole frequency band of operation. Passive baluns must prevent unbalanced currents reaching the antenna terminals over the whole frequency band and they must have low loss and sufficiently good impedance match. The prevention of the balanced signals from reaching the amplifier will prevent signal distortion whereas low loss nature of the antenna improves the system noise temperature. Good impedance matching is also necessary to reduce noise coupling and standing waves in the noise response.

Consequently an LNA with differential input is ideal to integrate with these antennas. A differential LNA avoids the necessity of a separate balun to convert the differential signal to an unbalanced signal. Various LNA designs with differential inputs have been investigated since the SKA project commenced [27].

The AAs proposed for the SKA will deploy tens of millions of LNAs in a receiver system that will be able to survey large areas of the sky very rapidly using multiple synthesized beams. This instrumentation will operate continuously for many years, and hence the power demand of the large number of LNAs will be significant. Thus the use of the most power efficient possible LNAs is essential to minimise the operating cost of the system.

Broad-band LNAs are vital for the receivers. As wide bandwidth relates to

high sensitivity in continuum radio observations, hence the LNA should function well over the entire AA frequency band and therefore the entire band can be observed simultaneously.

One other consequence of operating in an array is the impedance presented by the antenna element to each LNA will differ according to its location in the array, owing to mutual coupling between the antenna elements. This has implications for stability of the LNAs which is crucial, since an oscillating LNA could potentially disable the entire SKA system. Therefore, the developed LNAs must be unconditionally stable.

Microwave Integrated Circuits (MIC) and Monolithic Microwave Integrated Circuits (MMIC) are being exploited for the LNA designs in the SKA project [28, 9, 29]. Issues of low power, low cost, repeatability, availability and reproducibility will need to be resolved when mass production of the LNAs is undertaken. Utilising commercially available components and foundries assists the availability and reproducibility of the LNAs with cost effectiveness. Repeatability issue associated with the LNAs will be addressed by developing MMIC LNAs after the design technique and performance are successfully evaluated.

1.4 Antenna Designs in SKA

Antenna research work is being carried out for the different frequency ranges of SKA AA system around the World. Various research teams are concentrating on the antenna design and fabrication for AA-lo [30, 31, 32] and AA-mid frequency bands [33, 24, 34] with differential or single ended outputs. The output configuration and impedance of antenna dictates the input configuration and impedance of the LNA attached to it. Consequently a differential input LNA is required for

integration with a differential output antenna. Following approaches and configurations can be considered for the design of the LNAs after antennas with differential outputs:

- Differential input to differential output LNA
- Differential input to single ended output LNA
- Balun connected to a single ended LNA

Various configurations of LNAs with differential antenna are illustrated in Figures 1.3 to 1.5. An LNA with differential input and single ended output integrated with a differential output antenna is presented in Figure 1.3. The LNA is directly connected to the antenna and converts the balanced signal to an unbalanced signal at its output.

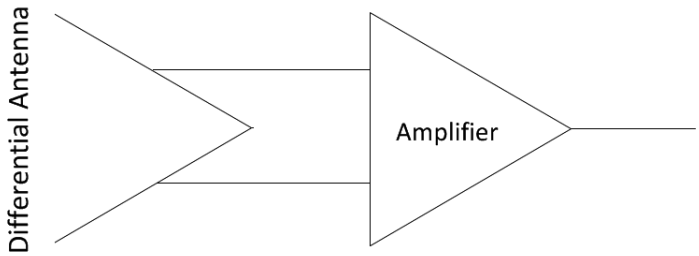

Figure 1.3: Antenna with differential output connected to an LNA with differential input and single ended output.

Figure 1.4 illustrates a configuration with a balun as an interface between the differential output antenna and the single ended LNA for the purpose of signal conversion. Figure 1.5 shows the configuration of a differential output antenna which is connected to a fully differential LNA.

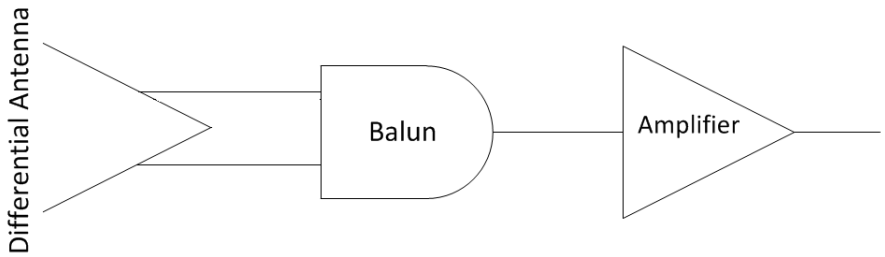

Figure 1.4: Antenna with differential output connected to a balun and a single ended LNA.

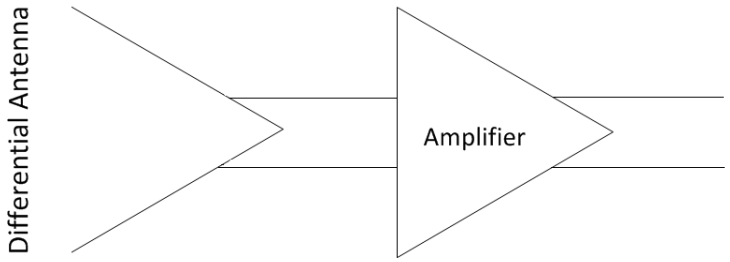

Figure 1.5: Antenna with differential output connected to a fully differential LNA.

1.5 SKA LNA Works Around the World

Various low noise foundries were characterised extensively for the purpose of LNA design and development for SKA project by research teams around the world. The low noise foundries based on Gallium Arsenide (GaAs), Indium Phosphide (InP), Silicon Germanium (SiGe) and Silicon (Si) were investigated with pHEMT, mHEMT, HBT and CMOS technologies. Over the past few decades, the HEMT technology has evolved as the low noise technology of choice. Minimum noise figure and noise resistance of the devices reduced dramatically with the arrival of the InP pHEMTs and GaAs mHEMTs; but they are expensive processes. The cost effective nature of CMOS has attracted industrial investments in large scales for the radio frequencies and hence they developed significantly [35]. The LNA developments carried out since the start of the SKA project are summarised in

Section 1.5.1.

1.5.1 SKA LNA Developments

The LNA design group in ASTRON, Netherlands Institute for Radio Astronomy [36], concentrated on the single ended LNA development. GaAs pHEMT devices of Avago Technologies and 70nm GaAs mHEMT process of OMMIC were used as part of APERTIF [37]. ASTRON has measured a 50Ω MIC LNA operating over the frequency band of 0.9-2GHz. The LNA has a flat gain of over 40dB and average return loss of better than -10dB. The noise temperature of the LNA was 35K. ASTRON and FG-IGN collaboration developed a MIC LNA using GaAs pHEMTs of Avago Technologies with a differential 150Ω input impedance which operates over the frequency range of 0.3-1GHz. The LNA has gain of over 26dB and average input return loss of -10dB and noise temperature of 40K [38, 39].

Australian SKA Programme (ASKAP) in CSIRO produced a differential input to single ended output MIC LNA with GaAs pHEMTs of Avago Technologies. The LNA has a differential input impedance of 300Ω and single ended output impedances of 50Ω. The LNA is operational over the frequency band of 0.7-1.8GHz. The LNA has performed a differential gain of 28dB and a noise temperature of 40K [35].

University of Calgary in Canada produced single ended and differential MMIC LNAs based on 90nm CMOS technology. The LNAs operate over the frequency band of 0.8-1.4GHz [40, 41, 35]. The LNA has differential impedance of 100Ω and shows 15dB differential gain and a noise temperature of 25K. The impedance of the single ended LNA is 85Ω with gain of 17dB. The return losses of the LNA are -11dB while the noise temperature is 14K.

The research team in the California Institute of Technology concentrated on

the SiGe HBT process and cryogenic temperatures. A single ended MMIC LNA operating over the frequency range of 0.1-5GHz was measured to have 17dB gain and 77K noise temperature at 300K ambient temperature. The average return loss was -10dB with a power dissipation of 76mW. The LNA at 15K ambient temperature has 30dB gain and input return loss of -14dB [42]. A balanced LNA with InP technology was reported to operate over the frequency band of 1-12GHz at 12K ambient temperature [43]. The LNA has 40dB gain and average noise temperature of 10K with a power consumption of 24mW [42, 43, 35]. Two identical LNAs were fabricated with one difference and the difference was the replacement of the input series inductor of one LNA with a wire for the other LNA. The LNAs consist of MIMIX CF003-03 GaAs HEMTs in the first stage and Avago VMMK1218 in the second and third stages. The noise temperature is less than 25K over the frequency range of 0.6-1.6GHz while at at 1.4GHz a noise of 22K was measured. The input and output return losses of the LNA is better than -10dB with an average gain of more than 40dB over the frequency range of 0.8GHz to 2.0GHz. The LNA without the inductor had higher noise temperature of 29K at 1.4GHz [44].

Research teams at the University of Manchester, UK have been involved with the design of LNAs for SKA. A single ended MMIC LNA with 70nm gate length mHEMT process of OMMIC was designed and characterised by Microwave and Communication Systems group (MACS) at University of Manchester. The LNA has a input impedance of 50Ω with dimension of 1.5mm×1mm. The bandwidth of the LNA was 0.7-4GHz with an average gain of 23dB. The noise temperature was measured to be 35K at room temperature with input return loss of -1.5dB [35]. A differential LNA was designed and characterised over the frequency range of 0.5-1GHz. The LNA has differential input and single ended output. The input and output impedances of the LNA were 150Ω and 50Ω respectively [45]. The

focus was given to the higher frequency band of SKA while the research work described in this thesis incorporates both lower and higher frequency bands of SKA AA.

The Microelectronics and Nano-structure research group in the University of Manchester has developed a 1μm InP pHEMT process. A single stage LNA operating over the frequency range of 0.2-2GHz was measured to have 10dB average gain, return loss of -2dB with power consumption of the 45mW. The LNA has average noise temperature of 123K over the frequency band of 1-2.5GHz at a power consumption of 75mW [46]. A MMIC LNA based on InGaAs/InAlAs/InP pHEMTs has been designed for the frequency range of 0.3-1.4GHz with simulated gain of more than 22dB. The LNA has noise figure of less than 0.5dB and power consumption of 190mW [47].

OPAR (Observatoire de Paris) developed a MMIC LNA with differential 100Ω input impedance using 250nm SiGe HBT. Noise temperature of 65K with gain of 27dB and input return loss of -17dB was reported over the frequency band of 0.3-1.9GHz. A 50Ω single ended LNA with gain of 24dB and noise temperature of 56K was reported [35].

INAF, national institute of astrophysics in Italy, has designed and investigated the commercially available LNAs. The commercial LNAs available from WanTcom and commercial MMIC from RFMD were considered. The designed LNA was based on the HEMT devices of Avago technologies. The LNAs have single ended or balanced configurations. Input and output impedances of the LNAs are 50Ω and 75Ω for the WanTcom LNA. The designed and characterised single ended MIC LNA is operational over the frequency range of 350-450MHz with gain of more than 20dB and noise temperature of less than 35K. The input return loss of the LNA are lower than -5dB while the output return loss is lower than -10dB from 370MHz. The power consumption of the LNA is 496mW. A

balanced MIC LNA operating over 350-450MHz was reported to have noise temperatures of less than 35K with an average gain of 25dB. The input and output return loss is better than -20dB due to the balanced configuration of the LNA. The minimum power consumption is 1.125W. A MIC single ended LNA was characterised for the frequency band of 130-500MHz which has average gain of 20dB with noise temperature of less than 100K. The average return losses of the LNA is lower than -10dB. The power consumption of the LNA is 510mW. The balanced version of the LNA was presented to have gain of 20dB and return losses of -20dB over the frequency band of 130-250MHz. The power consumption was 1.19W with noise temperature of 175K over the frequency range of 130-250MHz [48].

1.6 Ultra Wideband LNAs

Table 1.4 gives a list of the available ultra wide band LNAs within the frequency range of SKA AA system. Different technologies including GaAs pHEMTs, mHEMTs, SiGe HBTs, CMOS and AlGaN/GaN HEMT are used for the purpose of comparison. The LNAs were primarily selected for their frequency band of operation and hence various technologies are included due to the limited number of LNAs with GaAs pHEMT technology over the frequency band of interest. Both commercially available off the shelf LNAs and designed LNAs for different research projects are compared in Table 1.4. The bandwidth, gain, power consumption of the LNAs, noise figure, technology of the active devices and if the results are simulated or measured are outlined in Table 1.4.

Table 1.4: Summary of available commercial and non commercial LNAs for comparative study.

LNA	Bandwidth (MHz)	Gain(dB) Max-Min	Power (mW)	NF (dB) Min-Max	Technology	Simulated /Measured
[49]	$0-11500$	$12.5-13.2$	9.1	5.6	CMOS 0.13um	Measured
[50]	$5-2000$	$22.5-13.0$	18.81	$1-1.5$	SiGe HBT	Measured
[51]	$5-4000$	$35-16$	34.65	$1.5-2.8$	SiGe HBT	Measured
[52]	$20-1100$	$17.5-20$	18	$1.43-2.0$	CMOS 90nn	Measured
[53]	$50-860$	15.0	7.2	$2.2-3$	0.18um CMOS	Measured
[54]	$50-900$	$16.4-12.5$	14.4	$2.1-3.4$	CMOS 0.18um	Measured
[55]	$50-3000$	$21-12$	440	$0.9-1.6$	–	Measured
[56]	$50-6000$	15.4	400	1.5	E-pHEMT	Measured
[57]	$100-1000$	$12-15$	9.6	$3.1-4$	CMOS 0.13um	Measured
[58]	$200-9000$	$7.5-11$	20	$4.2-7$	CMOS 90nm	Measured
[59]	$300-1000$	$26-36$	2880	$0.6-0.75$	ATF-34143 pHEMT	Measured
[60]	$300-4000$	17.7	100	$1.2-2$	Dual Gate AlGaN/GaN HEMT	Measured
[60]	$300-4000$	18	100	$1.5-3.5$	Dual Gate AlGaN/GaN HEMT	Measured
[61]	$400-10000$	$11-12.4$	12	$4.4-6.9$	CMOS 0.18um	Measured
[62]	$470-870$	$21.0-18.0$	11.2	$3.4-3.8$	CMOS 0.18um	Simulated
[63]	$500-11000$	$7.5-10.2$	14.4	$3.9-4.5$	CMOS 0.18um	Measured
[64]	$600-2000$	$16.7-13.0$	–	$0.37-0.79$	70nm mHEMT	Simulated
[65]	$700-1800$	$14.9-18.3$	40.78	$0.56-0.67$	0.25um SOS	Measured
[66]	$1000-3000$	13.4	33.0	3.2	CMOS 0.35um	Measured
[67]	$1500-2500$	$12.0-5.0$	2.0	$2.0-4.5$	–	Measured

1.7 Research Objectives

The primary objective of the research was concentrated on the design and characterisation of LNAs for the international SKA project which will be the largest and most sensitive radio telescope in the world. AAs and conventional dishes with various feeds are employed in SKA project to acquire information from scanning the whole sky instantaneously up to frequency of 10GHz. Therefore, design of LNAs using MIC and MMIC technologies were motivated to operate over the low and high end of the SKA.

The primary objectives of the thesis for SKA AA LNAs are as follows:

- broad-band instantaneous bandwidth for unconditionally stable LNAs
- LNA with power consumption of less than 30mW
- High gain of more than 25dB
- Lowest possible noise figure over the complete instantaneous bandwidth
- Differential input and single ended output configuration for the LNA
- Cost effective LNAs developed based on commercially available robust and inexpensive components.

The objective of broad-band instantaneous bandwidth in the SKA LNAs was to achieve higher sensitivity. Low power consumption of less than 30mW for the SKA LNAs was estimated to make the system cost effective because millions of LNAs are required for both AA-lo and AA-mid. Lower noise figures of LNA over the wideband instantaneous bandwidth decreases the noise temperature of the receiver and the system. The noise figure and sensitivity of the AA-lo LNAs are dominated by high sky noise which is illustrated in Figure 1.2. However, the sky noise influence decreases at frequencies above 450MHz and hence LNA noise

figure becomes a very crucial parameter at higher frequencies. Therefore lowest noise figures were aimed for while the primary aim of the LNA was focused to obtain the optimum LNA performance at very low power consumption for the frequency bands of interest.

High gain of more than 25dB is required over the instantaneous bandwidth to reduce the noise contribution over the complete instantaneous bandwidth from subsequent stages significantly.

One of the objectives of thesis was to design an AA-lo LNA with differential input and single ended output for direct connection to a differential antenna and the subsequent unbalanced stages of the front-end system.

LNA designs using MMIC fabrication method for both low and high frequency bands of SKA are also studied to meet the required low manufacturing cost and high reliability factors. A multi-purpose MMIC LNA design was required to investigate the design approaches for the high end frequency bands of the SKA.

The main purpose of the thesis was to meet and possibly exceed the minimum key performance parameter defined for each LNA which are extremely challenging to achieve.

1.8 Thesis Organisation

The thesis consists of 7 chapters. Introduction chapter gives a detailed description of the LNA necessity in radio astronomy receivers and especially in SKA which is the next generation of radio telescopes. The special requirements and differences of the SKA and the conventional radio astronomy receivers are outlined in the Introduction. A comprehensive summary of SKA LNA research work around the world since the start of the project along with their achievements is given in this chapter.

Chapter 2 describes the history of the HEMTs and LNAs in detail. The literature is reviewed for the technology and topologies of the HEMT devices along with the explanation of noise sources in the HEMTs.

Chapter 3 gives a complete description of LNA design theory. Small signal model of 2-port, 3-port and 4-port networks are explained. The description and importance of the mixed mode S-parameters are given in chapter 3. The LNA design techniques, fabrication technologies and important parameters in LNA designs are further discussed. The theory of baluns and the various balun types are studied in great detail. The effect of baluns position in the low noise receiver is explained.

Chapter 4 gives a full description of 9 LNAs designed using MIC and MMIC fabrication techniques. There are 7 MIC LNAs for both AA-lo and AA-mid frequency bands in the SKA AA system. The AA-lo LNAs consist of single ended input and output configuration along with differential input to single ended output configuration. The detailed description of AA-mid LNAs with single ended input and output configuration is given in chapter 4. Details of 2 MMIC LNAs named as UMAN-SKAlowV1 and UMAN8-Xband using TQP13N pHEMT process of TriQuint Semiconductor are explained. The schematics and layout designs of the LNAs are illustrated in this chapter. Details of the fabrication process, housing and packaging of the LNAs are discussed.

Chapter 5 describes the measurement bench of the transistors and the LNAs. The test bench of the DC, RF and noise measurements of the pHEMTs and LNAs are given in detail.

Chapter 6 gives an insight to the results and data analysis of the LNA designs discussed in chapter 4.

Finally, chapter 7 provides a summary and conclusion of the work in the thesis and suggests the potential future works that can be undertaken for the

future investigation and characterisations of the MIC and MMIC LNAs.

Chapter 2

Evolution of Low Noise Devices

2.1 Introduction

This chapter gives the history of LNAs and HEMTs in more detail. Section 2.2 describes the history of the LNAs with a detailed explanation of their noise and performances. Sections 2.3 describes the advent of the HEMTs and their various technologies and topologies. Variation of the HEMTs and the DC behaviour of the HEMTs are explained briefly. HEMTs generally use III-V semiconductor compounds such as Gallium Arsenide (GaAs) and Indium Phosphide (InP). The widespread implication of the HEMT based transistors in the LNA designs are explained. Section 2.4 discusses the noise sources and their origins in HEMTs.

2.2 Low Noise Amplifier History

Vacuum tube amplifiers were used for the noise characterisation purposes in the early twenty century. North and Ferris measured and modelled the electron stream fluctuations of the input circuity in 1941 [68]. The investigation and theoretical analysis of the random variation in space current inducing the current

fluctuations in the control-grid circuit and the grid-voltage fluctuation proportional to the input impedance were carried out by Ballantine in 1928 [69].The early noise was measured by R.C.A. Communications engineers at Riverhead while studying the noise sources in the receiving circuits operating over 10MHz to 20MHz. The main focus of the North effort was on the formula of Nyquist which was on the mean-square short-circuit current fluctuations in a passive network. This formula is expressed in Equation 2.1;

$$\bar{i^2} = 4kT\Delta f \tag{2.1}$$

where T is the temperature of the network, k is Boltzmann constant and Δf is the frequency bandwidth. A noise measuring method in the receiving system which includes the antenna was described by North in 1942 [70]. The details of state of the art LNAs in the radar systems was given by Lewis in 1946 [71]. After this, the LNA design works attracted various independent research works by [72], North and Herold and Malters [73, 74, 75, 76]. Majority of these researches used the equivalent networks of the noisy devices where the resistances and conductances were considered as noiseless and different voltages or currents were supplied to the noise sources. These works made the assumption that there is no correlation between the various noise sources. This research formed the basis of the Rothe and Dalhke work [77] which plays a significant role in the low noise transistor modelling. Friss formulated the overall noise factor of a receiver system in 1944 where he considered the noise contribution and available gain of each stage of the system [78]. Friis' work has served as a fundamental basis of the LNA designs and noise budgeting in a receiver system. Wallman, Macnee and Gadsden reported an LNA circuit with high gain and noise figures of 0.25dB at 6MHz and 1.35dB at 30MHz [79]. The double-tuned circuits at the inputs of

high frequency amplifiers were presented by Lebenbaum to obtain very low noise devices [80]. Currie and Forster developed a state of the art amplifier of the time with noise figure performance of less than 4dB [81]. A detailed description of the low noise klystron amplifiers was presented by Rockwell [82] and 6.7dB was the lowest noise figure reported by him for a C-band pre-amplifiers. It proved that the noise figures were considerably higher than the low noise transistors counterparts. Parametric LNA with silicon mesa diode was developed by Weglein and Keywell to operate over the X-band. The LNA performance illustrated noise figures of less than 2dB and gain of 17dB at 8.5GHz [83]. A detailed review of the LNAs with different technologies was made which consists of the performances of the vacuum tube amplifiers, transistors, masers, tunnel diodes and parametric amplifiers based on semiconductor diodes [84]. As a result of this study masers were identified as the low noise technology of the time. Lauritzen and Leistiko from Fairchild Semiconductor established the idea of utilising FETs as low noise technology in 1962 [85]. The LNA design progressed rapidly after the FETs were introduced as the low noise technology. The progression of FETs to MESFETs which lead to the appearance of the HEMTs played a significant role in the low noise amplifiers designs.

2.3 High Electron Mobility Transistors(HEMT)

The idea of High Electron Mobility Transistors (HEMTs) was conceived by T. Mimura [86]. The first HEMTs were produced by the research team developing GaAs MESFETs for Fujitsu Laboratories in Japan in 1979. The HEMTs were the new fabricated field effective transistors with extremely high speed microwave capabilities [87]. The low noise and high gain characteristics of HEMTs led them towards the low noise applications. By 1985 HEMTs were announced as the

lowest noise transistors in the world and HEMTs were being implemented in most satellite communication applications worldwide. The low noise technology evolution until 1989 is summarised and available in [88, 89]. A summary of the subsequent low noise technology development is available in [90].

2.3.1 Technology of HEMTs

The important properties of GaAs and InP substrates based HEMTs which enhance their suitability for low noise applications are discussed in this section. GaAs substrates have been used extensively for HEMT developments in the past 3 decades [91]. The basic properties of the GaAs, InP and Silicon (Si) substrates at an ambient temperature of 300 K are given in Table 2.1 [9]. Electron mobility and electron drift velocity are important parameters as the speed and low noise performance of the substrates are determined with these parameters. In the devices with small gate lengths, higher electron drift velocities reduce the electron transit times and consequently increase the cut-off frequency of the devices. Higher mobilities and drift velocities can result lower parasitic resistances and larger values of transconductance. GaAs FETs performance for low noise applications at microwave and millimetre-wave frequencies improve significantly due to the enhanced conduction of the GaAs compound compared to Silicon [91]. Performances with excellent low noise and high cut-off frequencies (greater than 115GHz) were observed for InP based HEMTs [9]. High cost, fragile structure and unavailability in large scales can be counted as the disadvantages of the InP based HEMTs compared to the GaAs counterparts [92].

Table 2.1: Properties of Si, InP and GaAs substrates [8, 9].

Parameters	Units	GaAs	InP	Si
Dielectric Constant		10.9	9.6	11.7
Peak Electron Velocity	$\times 10^7$ cms^{-1}	1.6-2.3	2.5-3.5	0.3-0.7
Electron Mobility	cm$^2V^{-1}s^{-1}$	5500-7000	10000-12000	900-1100
Saturated Drift Velocity	$\times 10^6$ cm^{-2}	5	6	8.5
Energy Gap	eV	1.4	1.3	1.1
Intrinsic Resistivity	Ωcm	3.3×10^8	8.6×10^7	3.2×10^5

2.3.2 Topologies of HEMTs

This section explains the operating principle of the HEMTs in details. HEMTs were designed in such a way so that the mobility of the electrons in the transistors are enhanced considerably [91]. Hetero-junction principle is utilised to create the two dimensional electron gas. This is created between a wideband gap material such as AlGaAs and a narrower band gap semiconductor such as GaAs. Carrier flow is confined within the intrinsic layer due to the difference between the band gaps. High carrier concentration and high mobility are achieved by separation between the doping layer and the channel. The result of the confined carrier concentration and high electron mobility determines the current and transconductance of transistors. Thus, confined carrier concentration and high mobility enhance the performance and noise of the transistors. The performance of the transistor enhances by adding an un-doped spacer layer [93, 94]. A typical structure of a HEMT is presented in Figure 2.1 [8]. The 2 varieties of the HEMTs are pseudomorphic HEMTs (pHEMT) and metamorphic HEMTs (mHEMT) that are described in the following subsections.

pseudomorphic HEMTs (pHEMTs)

Although the HEMTs exhibited a superior performance in terms of noise and gain at microwave frequencies, the HEMTs with GaAs/AlGaAs structure have serious

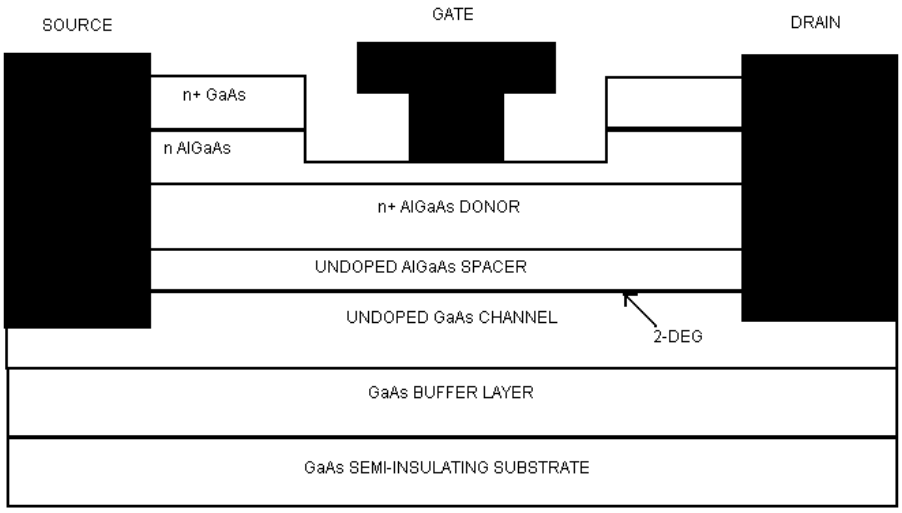

Figure 2.1: Structure of a HEMT [8].

limitations which are inherent to the AlGaAs material [94, 92]. The solutions to the shortcomings of the HEMTs are given by pseudomorphic HEMTs (pHEMTs). pHEMTs are structures that are grown with a slight difference in their lattice constants. The InGaAs compound with an indium concentration in the range of 20-30% forms the pseudomorphic layer [15]. Therefore a strained channel is formed as the lattice constant of the channel is larger than the GaAs substrate, AlGaAs donor and spacer layer. Although the structure is still fabricated on the GaAs substrate, it benefits from the indium addition (InGaAs) and its enhanced mobility performance. Therefore the RF performance of the device improves compared to the conventional HEMTs [91, 94, 15].

metamorphic HEMTs (mHEMTs)

A buffer layer is positioned between the lattice mismatched channel layer InGaAs and the substrate GaAs in the metamorphic HEMTs (mHEMTs). The buffer layer is constructed from InAlAs. The indium concentration is graded to

match the lattice constants of GaAs and InAlAs on each side. mHEMT is a comparatively new technology and has not reached a matured state [8, 95].

2.3.3 HEMTs DC behaviour

The HEMTs devices are classified as either depletion mode (D-mode) or the enhancement (E-mode) mode in terms of their DC behaviour. The current can flow between the drain and the source at zero gate bias for the depletion mode transistors. However, for the enhancement mode transistors, the current cannot flow unless a positive gate bias is applied [94].

The transconductance (g_m) of a transistor is one of the most important parameters for investigation of the DC behaviour of a transistor. Transconductance of a device is defined as the ratio of change in the drain source current (I_{ds}) to the change in the gate source voltage (V_{gs}) with a constant drain source voltage (V_{ds}). The mathematical definition of the transconductance at a constant V_{ds} is given in Equation 2.2;

$$g_m = \frac{dI_{ds}}{dV_{gs}} \tag{2.2}$$

The unit of g_m is Siemens. Transconductance of a device depends on the device dimension and is proportional to the device gate width [94]. Therefore, normally g_m is expressed as the transconductance per unit gate width, i.e, mS/mm.

According to [96], the minimum noise figure of a transistor, among all combinations of gate and drain bias voltages, can be achieved at a bias where the parameter $\sqrt{I_d}/g_m$ of a transistor has a minimum value.

2.4 Sources of Noise in HEMTs

The knowledge of the noise sources in HEMTs must be incorporated with the small signal equivalent circuit of the HEMTs for the low noise amplifier design purposes. The 4 main noise sources of the HEMTs are described in further details in this section.

Thermal (Johnson) Noise

The random changes in the motion of the conduction band carriers are caused by temperature variations. Hence, the carriers experience collisions with the vibrating atoms or each other. This is the reason of a noise source called thermal noise.

The spectral density of the short-circuit current fluctuations ($S_{I,x}$) in A^2/Hz is given in Equation 2.3 [97, 15];

$$S_{I,x} = (\frac{1}{2}hf + \frac{hf}{exp(hf/kT) - 1})/R \tag{2.3}$$

where h and k are the Planck and Boltzmann constants respectively, f is the frequency, T is the temperature and R is the resistance. Equation 2.3 for $hf/KT << 1$ is represented in Equation 2.4.

$$S_{I,T} = \frac{4kT}{R} \tag{2.4}$$

Shot Noise

Theory of shot noise was described by Schottky in 1918 [98]. The shot noise definition is expressed as Equation 2.5;

$$\bar{i_n^2} = 2qI_{DC}\Delta f \tag{2.5}$$

where q is the electronic charge and is 1.6×10^{-19}C, I_{DC} is the flowing DC current in the device and Δf is the bandwidth. The shot noise is caused by fluctuations of the emission rates of the carriers and the resulting fluctuations in the current [99, 15, 8].

Flicker ($1/f$) Noise

The flicker noise is also known as "$\frac{1}{f}$" noise as it is inversely proportional to the frequency. Flicker noise is dominant at low frequencies [99]. Although flicker noise is ubiquitous and is present in most of the electronic devices but their definite cause has not been proved yet [15]. An empirical expression for Flicker noise is given in Equation 2.6 [100, 15];

$$S_I(f) = \frac{\alpha}{f^n N} \tag{2.6}$$

Generation-Recombination Noise

Sometimes generation-recombination noise is known as g-r noise [97, 15]. When a free electron combines with a free hole to move to another valance band which is more stable, some energy is released. These random trapping and de-trapping are due to the traps and recombination centres in the semiconductors and cause fluctuations in the number of free charge carries (N) per unit time. Therefore the conductance of the device fluctuates. Equation 2.7 gives the power spectral density of the generation-recombination noise [97, 15];

$$S_N(f) =< \Delta N^2 > \frac{4\tau}{1 + (2\pi f\tau)^2} \tag{2.7}$$

where the variance of the N is shown as $< \Delta N^2 >$, f is the frequency and τ is the carrier lifetime.

2.5 Summary

This chapter talks about the evolution of low noise devices including LNAs and HEMTs. The history of the LNA designs using different technologies was discussed in detail. Various technologies and topologies of the HEMTs were described. The HEMT based transistors are ideal choices for the LNA designs due to their high gain and low noise performances. A brief discussion was given for the different variations of the HEMTs and their operating principals. The cut off frequencies of the pHEMTs and mHEMTs are higher which implies lower noise figures. The reduction in the Couloumbic effects, delta doping and spacer layer in the above mentioned devices which are fabricated on low loss substrates like GaAs, InP, with high Indium content in the channel, enhance the electron mobility of the transistors. This enhancement in electron mobility is also reflected on high cut-off frequency and ultra low minimum noise figure of the device. This chapter explained why the HEMT based devices are widely used in microwave LNA designs. The noise sources in the HEMTs were outlined and explained in this chapter.

Chapter 3

Low Noise Amplifier Design Theory

3.1 Introduction

Low Noise Amplifiers (LNA) amplify very weak signals detected from antennas without adding substantial noise to them. However, LNAs are the major producer of noise in a low noise receiver system. The primary objective of LNAs is to achieve a minimum noise figure possible with high gain. This chapter will describe the matching techniques used for attaining the desired LNA performance and several important aspects in the design of LNAs. Noise and impedance matching are explained in detail. The extensive use of Computer Aided Design (CAD) tools has simplified the design of LNAs significantly as majority of the original graphical and analytical matching methods in the LNA designs are removed. However, a good understanding and knowledge of amplifier design principles and fundamentals are still essential. The generic theory of baluns is explained in this chapter. The effect of balun position in a low noise receiver is discussed in this chapter.

3.2 S-parameters

In the representation of a device in terms of Z, Y and h-parameters, the open and short circuit currents and voltages are measured. The Z-parameters are determined by open circuiting the ports in succession as various terms become zero. The Y or admittance parameters are determined by short circuit conditions. Combinations of open and short circuit conditions determine the hybrid parameters. The Z, Y and H parameters are expressed by currents and voltages at the ports. At low frequencies, the popularity of these representation for characterising the system depends on the ability of determination of the parameters experimentally. Measuring short circuit current and open circuit voltage of devices for small signal characterisation at high frequencies are highly inaccurate. It is convenient to terminate the ports in short and open circuits at low frequencies for 2-port description as various terms become zero and simplify the maths. Therefore a different set of parameters is required to evade the experimental problems at higher frequencies for system characterisation. These parameters are called Scattering parameters or S-parameters. The S-parameters define the input and output variables in terms of incident and reflected voltage waves as it is difficult to define the port voltages and currents at high frequencies [101, 102]. S-parameters are related to the incident and reflected power and their magnitude do not vary along the transmission lines. Unstable oscillation of the active devices are avoided as the impedance matching conditions are present for the S-parameter measurements [103].

3.2.1 2-Port S-Parameters

The insight of using S-parameters in microwave circuits and the analysis of S-parameter characterisation of multi-port microwave devices were given by Mathews [104]. The generalised S-parameters were defined by Kurokawa [102]. These describe the inter-relationship between a set of variables a_i and b_i that are normalised complex voltage waves incident on and reflected from the i^{th} port of the network. Definition of these variables are in terms of the terminal voltage (V_i), terminal current (I_i) and an arbitrary reference impedance (Z_i) and are given in Equations 3.1 and 3.2.

$$a_i = \frac{V_i + Z_i I_i}{2\sqrt{|R_e Z_i|}} \tag{3.1}$$

$$b_i = \frac{V_i - Z_i I_i}{2\sqrt{|R_e Z_i|}} \tag{3.2}$$

Figure 3.1 illustrates the wave function used to define the S-parameters for a 2-port network.

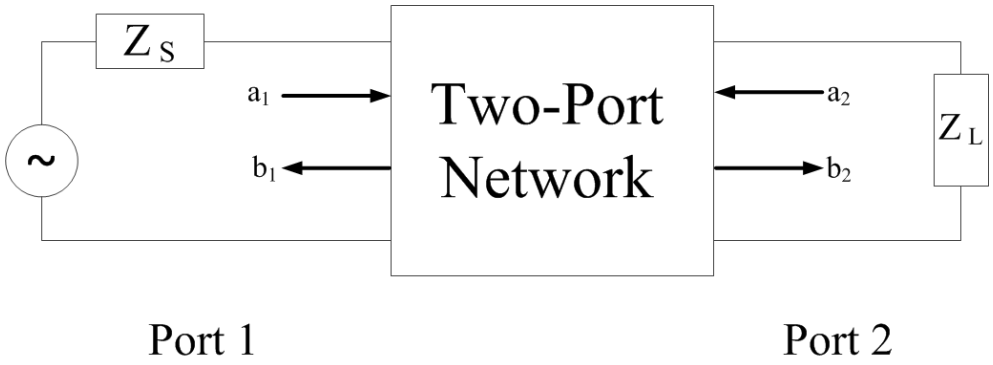

Figure 3.1: S-parameter for a 2-port Network.

Equations 3.3 and 3.4 give the independent variables of a_1 and a_2 respectively, which are normalised incident voltages:

$$a_1 = \frac{V_1 + Z_0 I_1}{2\sqrt{Z_0}} = \frac{\text{Voltage wave incident on port 1}}{\sqrt{\text{Z}_0}} = \frac{V_{i1}}{\sqrt{Z_0}} \tag{3.3}$$

$$a_2 = \frac{V_2 + Z_0 I_2}{2\sqrt{Z_0}} = \frac{\text{Voltage wave incident on port 2}}{\sqrt{\text{Z}_0}} = \frac{V_{i2}}{\sqrt{Z_0}} \tag{3.4}$$

This is only true for a system with uniform Z_0, otherwise the voltage wave is a root power wave.

The normalised reflected voltages denoted as b_1 and b_2 are dependent variables. Equations 3.5 and 3.6 give b_1 and b_2 respectively.

$$b_1 = \frac{V_1 - Z_0 I_1}{2\sqrt{Z_0}} = \frac{\text{Voltage wave reflected from port 1}}{\sqrt{\text{Z}_0}} = \frac{V_{r1}}{\sqrt{Z_0}} \tag{3.5}$$

$$b_2 = \frac{V_2 - Z_0 I_2}{2\sqrt{Z_0}} = \frac{\text{Voltage wave reflected from port 2}}{\sqrt{\text{Z}_0}} = \frac{V_{r2}}{\sqrt{Z_0}} \tag{3.6}$$

The linear equations which describe the relationships of a 2-port network are given in Equations 3.7 and 3.8.

$$b_1 = S_{11} a_1 + S_{12} a_2 \tag{3.7}$$

$$b_2 = S_{21} a_1 + S_{22} a_2 \tag{3.8}$$

The S-parameter relationships of the 2-port network can also be written in a matrix format as shown in Equation 3.9

$$\begin{bmatrix} b_1 \\ b_2 \end{bmatrix} = \begin{bmatrix} S_{11} & S_{12} \\ S_{21} & S_{22} \end{bmatrix} \begin{bmatrix} a_1 \\ a_2 \end{bmatrix} \tag{3.9}$$

The S-parameters of a 2-port network are defined in Equations 3.10 to 3.13.

Equation 3.10 shows the input reflection coefficient of the 2-port network when the output port is terminated by a matched load.

$$S_{11} = \frac{b_1}{a_1} \mid_{a_2=0} \tag{3.10}$$

Equation 3.11 gives the output reflection coefficient of the 2-port network when the input port is terminated by a matched load.

$$S_{22} = \frac{b_2}{a_2} \mid_{a_1=0} \tag{3.11}$$

Equation 3.12 shows the forward transmission (insertion) gain of the 2-port network when output port is terminated by a matched load.

$$S_{21} = \frac{b_2}{a_1} \mid_{a_2=0} \tag{3.12}$$

Equation 3.13 gives the reverse transmission (insertion) gain of the 2-port network when the input port is terminated by a matched load.

$$S_{12} = \frac{b_1}{a_2} \mid_{a_1=0} \tag{3.13}$$

Therefore, the S-parameters of a 2-port network can be defined in Equations 3.14 to 3.17.

$$|S_{11}|^2 = \frac{\text{Power reflected from the network input}}{\text{Power incident on the network input}} \tag{3.14}$$

$$|S_{22}|^2 = \frac{\text{Power reflected from the network output}}{\text{Power incident on the network output}} \tag{3.15}$$

$$\begin{aligned} |S_{21}|^2 &= \frac{\text{Power delivered to a } Z_0 \text{ load}}{\text{Power available from a } Z_0 \text{ source}} \\ &= \text{Transducer power gain with } Z_0 \text{ load and source} \end{aligned} \tag{3.16}$$

$$|S_{12}|^2 = \text{Reverse transducer power gain with } Z_0 \text{ load and source} \tag{3.17}$$

As shown earlier, the S-parameter responses of a 2-port network describe the input and output behaviour of the network and are expressed by power ratios of the inputs and outputs of the network. The S-parameters can be measured directly by using a Vector Network Analyser (VNA).

The reflection coefficient and the impedance relationship constructs the basis of the Smith Chart transmission line calculator. Thus the impedance parameters can be derived if the input and output reflection coefficients (S_{11} and S_{22}) are plotted on the Smith Chart to optimise a circuit design.

3.2.2 Multi-Port S-Parameters

A multi-port network can be described using S-parameter matrix for multiple ports. VNAs with multi-ports can be used for the multi-port S-parameter measurements directly. Devices under test with multi-ports are becoming more common. Multi-port network S-parameters are utilised to describe and characterise the behaviour of the devices.

Three-port S-parameters are required to characterise a 3-port network. The standard S-Parameter representation of a network with 3 ports is specified in Equation 3.18.

$$\begin{bmatrix} b_1 \\ b_2 \\ b_3 \end{bmatrix} = \begin{bmatrix} S_{11} & S_{12} & S_{13} \\ S_{21} & S_{22} & S_{23} \\ S_{31} & S_{32} & S_{33} \end{bmatrix} \begin{bmatrix} a_1 \\ a_2 \\ a_3 \end{bmatrix} \tag{3.18}$$

Four-port S-parameters are required to characterise a 4-port network. Four-port S-parameter has the reflected and incident power waves information of 4 ports of the network. Full differential amplifiers, a pair of coupled transmission lines or transformers are described by a 4-port S-parameter. Equation 3.19 gives the S-parameter representation of a 4-port network.

$$\begin{bmatrix} b_1 \\ b_2 \\ b_3 \\ b_4 \end{bmatrix} = \begin{bmatrix} S_{11} & S_{12} & S_{13} & S_{14} \\ S_{21} & S_{22} & S_{23} & S_{24} \\ S_{31} & S_{32} & S_{33} & S_{34} \\ S_{41} & S_{42} & S_{43} & S_{44} \end{bmatrix} \begin{bmatrix} a_1 \\ a_2 \\ a_3 \\ a_4 \end{bmatrix} \tag{3.19}$$

A complete description of an N-port network is given by its S-parameter matrix. A network with N-ports contains N^2 elements in the S-parameter matrix. Each element in the S-parameter matrix of the N-port network is denoted as S_{xy} where x and y are the ports and vary from 1 to n. Equation 3.20 shows the S-parameter representation of a network with N ports. Each element describes the relationship between 2 ports of the network. The S-parameters can be plotted on the Smith Chart and converted to the impedance parameters to optimise a design.

$$[S] = \begin{bmatrix} S_{11} & \dots & S_{1n} \\ \vdots & \ddots & \vdots \\ S_{n1} & \dots & S_{nn} \end{bmatrix} \tag{3.20}$$

3.2.3 Mixed Mode S-Parameters

The extensive use of active and passive differential components has resulted in the appearance and evolution of the mixed mode S-Parameters. Traditional S-parameter theory was extended for the analysing the responses of differential circuits by Bockelman et. al [105]. The complete characterisations of differential circuits consist of differential mode, common mode and any mode conversion responses of the circuit as the differential circuits respond to both differential mode and common mode stimulus. The mixed-mode S-parameter responses examine the behaviour of the differential networks accurately [106]. The calibration and measurement procedures have been developed during the last decade [107, 108].

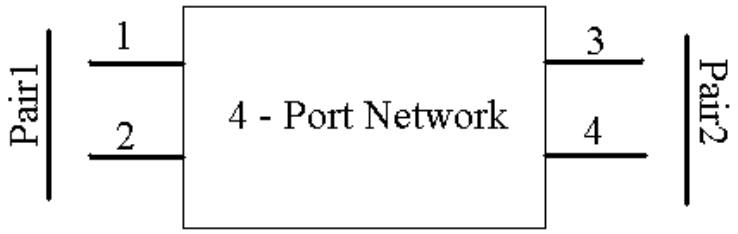

Figure 3.2: A 4-port network.

3.2.4 4-Port Mixed mode S-Parameters [1]

The response of a 4-port network to differential and common mode stimulus signals are described with mixed mode S-parameters. Figure 3.2 illustrates a 4-port network which has 2 pairs of signals at the input and output. Ports 1 and 2 are assumed as Pair1 and ports 3 and 4 as Pair2. Pair1 and Pair2 are driven with common mode and differential mode signals [1]. Mixed mode S-parameters of a 4-port network is expressed in Equation 3.21. Details and description of Equation 3.21 are given in the following;

$$\begin{bmatrix} b_{d1} \\ b_{d2} \\ b_{c1} \\ b_{c2} \end{bmatrix} = \begin{bmatrix} S_{d1d1} & S_{d1d2} & S_{d1c1} & S_{d1c2} \\ S_{d2d1} & S_{d2d2} & S_{d2c1} & S_{d2c2} \\ S_{c1d1} & S_{c1d2} & S_{c1c1} & S_{c1c2} \\ S_{c2d1} & S_{c2d2} & S_{c2c1} & S_{c2c2} \end{bmatrix} \begin{bmatrix} a_{d1} \\ a_{d2} \\ a_{c1} \\ a_{c2} \end{bmatrix} = \begin{bmatrix} S_{dd} & S_{dc} \\ S_{cd} & S_{dd} \end{bmatrix} \begin{bmatrix} a_{d1} \\ a_{d2} \\ a_{c1} \\ a_{c2} \end{bmatrix} \tag{3.21}$$

where a_{d1} and a_{d2} are the differential input signal for Pair1 and 2 respectively. The common mode input signal for Pair1 and 2 are a_{c1} and a_{c2} respectively. Equation 3.22 gives the definition of the differential and common mode input signals for Pair1 and 2. The definition of the differential and common mode

signals for Pair1 and 2 are given in terms of individual incident power waves on each port.

$$\begin{aligned} a_{d1} &= \tfrac{1}{\sqrt{2}}(a_1 - a_2) \\ a_{d2} &= \tfrac{1}{\sqrt{2}}(a_3 - a_4) \\ a_{c1} &= \tfrac{1}{\sqrt{2}}(a_1 + a_2) \\ a_{c2} &= \tfrac{1}{\sqrt{2}}(a_3 + a_4) \end{aligned} \tag{3.22}$$

Similarly, b_{d1} is the differential output signal of Pair1, b_{d2} is the differential output signal of Pair2, b_{c1} is the common mode output signal of Pair1 and b_{c2} is the common mode output signal of Pair2. Equation 3.23 shows the mixed mode output signals of the 4-port network. As shown in the Equation 3.23, the differential and common mode signals of the output are related to the reflected power waves of each port in the Pair1 and 2.

$$\begin{aligned} b_{d1} &= \tfrac{1}{\sqrt{2}}(b_1 - b_2) \\ b_{d2} &= \tfrac{1}{\sqrt{2}}(b_3 - b_4) \\ b_{c1} &= \tfrac{1}{\sqrt{2}}(b_1 + b_2) \\ b_{c2} &= \tfrac{1}{\sqrt{2}}(b_3 + b_4) \end{aligned} \tag{3.23}$$

The mixed-mode S-parameters matrix shown in Equation 3.21 gives a full description of differential and common mode inputs (stimuli) and outputs (responses) of a 4-port network. Equation 3.19 gives the full description of the individual ports of a 4-port network. The stimulus signals on Pair1 and 2 are differential and common modes. The response signal contains differential and common modes for Pair1 and 2. The mixed mode S-parameters of Pair1 and 2 of the 4-port network which is illustrated in Figure 3.2, are derived in terms of the

individual S-parameters of ports 1, 2, 3 and 4.

The first quadrant on the upper left of the mixed mode S-parameters in Equation 3.21 describes the differential stimulus and differential response characteristics of the 4-port network. This quadrant includes the S_{d1d1}, S_{d1d2}, S_{d2d1} and S_{d2d2} parameters which are defined in Equations 3.24 to 3.27. S_{d1d1} is the differential input return loss, S_{d1d2} is the output differential insertion loss, S_{d2d1} is the input differential insertion loss and S_{d2d2} is the differential output return loss.

$$S_{d1d1} = \frac{1}{2}\left(S_{11} - S_{21} - S_{12} + S_{22}\right) \tag{3.24}$$

$$S_{d1d2} = \frac{1}{2}\left(S_{13} - S_{23} - S_{14} + S_{24}\right) \tag{3.25}$$

$$S_{d2d1} = \frac{1}{2}\left(S_{31} - S_{41} - S_{32} + S_{42}\right) \tag{3.26}$$

$$S_{d2d2} = \frac{1}{2}\left(S_{33} - S_{43} - S_{34} + S_{44}\right) \tag{3.27}$$

The second quadrant is located on the upper right of the mixed-mode S-parameter matrix in Equation 3.21. These parameters describe the common mode stimulus and differential response characteristics of the 4-port network. The parameters of this quadrant are S_{d1c1}, S_{d1c2}, S_{d2c1} and S_{d2c2}. These parameters are defined in Equations 3.28 to 3.31.

$$S_{d1c1} = \frac{1}{2}\left(S_{11} - S_{21} + S_{12} - S_{22}\right) \tag{3.28}$$

$$S_{d1c2} = \frac{1}{2}\left(S_{13} - S_{23} + S_{14} - S_{24}\right) \tag{3.29}$$

$$S_{d2c1} = \frac{1}{2}\left(S_{31} - S_{41} + S_{32} - S_{42}\right) \tag{3.30}$$

$$S_{d2c2} = \frac{1}{2}\left(S_{33} - S_{43} + S_{34} - S_{44}\right) \tag{3.31}$$

The third quadrant is on the lower left of the mixed mode S-parameter matrix in Equation 3.21. These parameters describe and characterise the differential mode stimulus and common mode response of the 4-port network. The quadrant includes S_{c1d1}, S_{c1d2}, S_{c2d1} and S_{c2d2} parameters. The relationships of these parameters are given in Equations 3.32 to 3.35.

$$S_{c1d1} = \frac{1}{2}\left(S_{11} + S_{21} - S_{12} - S_{22}\right) \tag{3.32}$$

$$S_{c1d2} = \frac{1}{2}\left(S_{13} + S_{23} - S_{14} - S_{24}\right) \tag{3.33}$$

$$S_{c2d1} = \frac{1}{2}\left(S_{31} + S_{41} - S_{32} - S_{42}\right) \tag{3.34}$$

$$S_{c2d2} = \frac{1}{2}\left(S_{33} + S_{43} - S_{34} - S_{44}\right) \tag{3.35}$$

The fourth quadrant is the lower right of the mixed-mode S-parameter matrix in Equation 3.21. These parameters describe the common mode stimulus and common mode response characteristics of the 4-port network. Parameters S_{c1c1}, S_{c1c2}, S_{c2c1} and S_{c2c2} are defined in Equations 3.36 to 3.39 respectively. The input and output common mode return loss of the network are S_{c1c1} and S_{c2c2} respectively.

$$S_{c1c1} = \frac{1}{2}\left(S_{11} + S_{21} + S_{12} + S_{22}\right) \tag{3.36}$$

$$S_{c1c2} = \frac{1}{2}\left(S_{13} + S_{23} - S_{14} + S_{24}\right) \tag{3.37}$$

$$S_{c2c1} = \frac{1}{2}\left(S_{31} + S_{41} + S_{32} + S_{42}\right) \tag{3.38}$$

$$S_{c2c2} = \frac{1}{2}\left(S_{33} + S_{43} + S_{34} + S_{44}\right) \tag{3.39}$$

Differential LNAs must be designed for a high differential mode gain and minimum common mode gain transmission to the output. Common Mode Rejection Ratio (CMRR) is useful measure in the differential LNAs to measure the differential signal amplification to the common mode signal amplification of the amplifier. The CMRR of a full differential amplifier is defined as the ratio of differential gain to the common mode gain [109].

$$CMRR = \frac{S_{d2d1}}{S_{c2c1}} \tag{3.40}$$

Equation 3.40 gives the CMRR of an amplifier with 4-ports. Higher values of CMRR is more desirable for differential amplifiers as it means more differential signal is propagating to the output of the amplifier compared to the common mode signal.

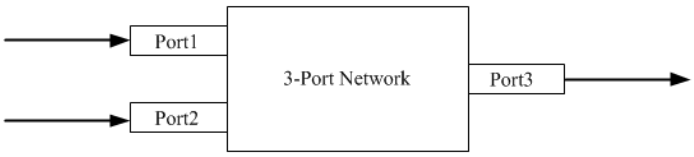

Figure 3.3: Presentation of a 3-port network.

3.2.5 3-Port Mixed Mode S-Parameters [1]

This section concentrates on describing the mixed-mode S-parameters of a 3-port network. Mixed-mode S-parameters of a 3-port network gives a complete description of responses of the network to differential and common mode signals. Figure 3.3 illustrates a 3-port network that consists of a differential input and a single ended output. The designed differential LNAs for SKA project are considered as 3-port networks as they are constructed of differential input and a single ended output. The differential input to the single ended output configuration of the SKA LNAs are due to the connection of the LNA input to an antenna with a differential output while the output of the LNA is connected to the rest of the subsequent amplification stages in the receiver which is single ended.

The mixed-mode S-parameter responses of a 3-port network are given in Equation 3.41 [1]. As illustrated in Figure 3.3, ports1 and 2 correspond to the differential inputs of the 3-port network and port3 is the single ended output.

$$\begin{bmatrix} b_s \\ b_d \\ b_c \end{bmatrix} = \begin{bmatrix} S_{ss} & S_{sd} & S_{sc} \\ S_{ds} & S_{dd} & S_{dc} \\ S_{cs} & S_{cd} & S_{cc} \end{bmatrix} \begin{bmatrix} a_s \\ a_d \\ a_c \end{bmatrix} \tag{3.41}$$

In Equation 3.41, a_s is the single ended input on port3, a_d is the differential input signal on ports1 and 2 while a_c is the common mode signal of input ports1 and 2. The allocations of these ports are illustrated in Figure 3.3. The definitions

of a_d and a_c are shown in terms of the individual incident power waves on each port at the differential input of the network.

$$\begin{aligned} a_d &= \tfrac{1}{\sqrt{2}}(a_1 - a_2) \\ a_c &= \tfrac{1}{\sqrt{2}}(a_1 + a_2) \end{aligned} \tag{3.42}$$

Similarly, b_d is the differential output signal of ports1 and 2 while b_c is the common mode output signal of the ports. Definitions of b_d and b_c are given in Equation 3.43. b_s is the single ended output of the port3.

$$\begin{aligned} b_d &= \tfrac{1}{\sqrt{2}}(b_1 - b_2) \\ b_c &= \tfrac{1}{\sqrt{2}}(b_1 + b_2) \end{aligned} \tag{3.43}$$

Mixed mode S-parameter matrix in Equation 3.41 consists of all the parameters required to describe the performance of a differential input to single ended network to differential and common mode signals. The mixed mode S-parameter responses of a 3-port network are derived from the standard 3-port S-parameter representation shown in Equation 3.18.

In Equation 3.41, S_{ss} is the reflection coefficient of the single ended port. Differential gain of the 3-port network is S_{sd} while the common mode gain is S_{sc} which are defined in Equations 3.44 and 3.45

$$S_{sd} = \frac{1}{\sqrt{2}}(S_{31} - S_{32}) \tag{3.44}$$

$$S_{sc} = \frac{1}{\sqrt{2}}(S_{31} + S_{32}) \tag{3.45}$$

Equation 3.46 defines S_{ds} which is the reverse differential transmission coefficient. S_{cs} is the reverse common mode transmission coefficient of input and single ended output and is given in Equation 3.47.

$$S_{ds} = \frac{1}{\sqrt{2}}(S_{13} - S_{23}) \tag{3.46}$$

$$S_{cs} = \frac{1}{\sqrt{2}}(S_{13} + S_{23}) \tag{3.47}$$

S_{dd} is the differential return loss while S_{cc} is the common mode return loss. Definitions of S_{dd} and S_{cc} are given in Equations 3.48 and 3.49 respectively.

$$S_{dd} = \frac{1}{2}(S_{11} - S_{12} - S_{21} + S_{22}) \tag{3.48}$$

$$S_{cc} = \frac{1}{2}(S_{11} + S_{12} + S_{21} + S_{22}) \tag{3.49}$$

S_{dc} is the coefficient of common mode input and differential mode output and S_{cd} is the coefficient of differential mode input and common mode output. Equations 3.50 and 3.51 define the values of S_{dc} and S_{cd} respectively.

$$S_{dc} = \frac{1}{2}(S_{11} + S_{12} - S_{21} - S_{22}) \tag{3.50}$$

$$S_{cd} = \frac{1}{2}(S_{11} - S_{12} + S_{21} - S_{22}) \tag{3.51}$$

CMRR is a measure of differential LNA performance in terms of its differential signal amplification compared to the common mode signal amplification and CMRR of an LNA with differential input and single ended output is defined in Equation 3.52 [110, 109].

$$CMRR = \frac{S_{sd}}{S_{sc}} \tag{3.52}$$

3.3 Noise Parameters

Definition of noise factor (F) is the input signal-to-noise ratio divided by the output signal-to-noise ratio which is given in Equation 3.53 [78]. Noise factor is used as a measure of the noise performance of a 2-port network. Noise figure (NF) is noise factor expressed in decibels and is defined in Equation 3.54. Noise figure is affected by source or input impedance and the noise sources within the 2-port network. The noise figure of a 2-port network with any source impedance can be derived from Equation 3.55 or Equation 3.56:

$$F \equiv \frac{SNR_{input}}{SNR_{output}} \tag{3.53}$$

$$NF = 10\, logF \tag{3.54}$$

$$NF = NF_{min} + \frac{R_n}{G_s}\left[(G_s - G_{opt})^2 + (B_s - B_{opt})^2\right] \tag{3.55}$$

where G_s is the source conductance, G_{opt} is the optimum conductance, B_s is the source susceptance, B_{opt} is the optimum susceptance and R_n is the equivalent noise resistance.

$$NF = NF_{min} + \frac{4R_n \left|\Gamma_s - \Gamma_{opt}\right|^2}{\left(1 - \left|\Gamma_s\right|^2\right)\ \left|1 + \Gamma_{opt}\right|^2} \tag{3.56}$$

where Γ_s is defined in Equation 3.57 and Γ_{opt} is the optimum source reflection coefficient. In Equation 3.57, source impedance is defined in terms of source resistance (R_s) and source reactance (X_s). Z_0 is the system impedance which is normally 50Ω.

$$\Gamma_s = \frac{R_s + jX_s - Z_0}{R_s + jX_s + Z_0} \tag{3.57}$$

The 4 noise parameters of a 2-port network are minimum noise figure (NF_{min}), the optimum source admittance (Y_{opt}=G_{opt}+jB_{opt}) at which the NF_{min} occurs and the equivalent noise resistance (R_n). The noise parameters show how noisy a 2-port network would be.

Minimum noise figure of a device is achieved at Γ_{opt}. Therefore, a low noise device must be matched to the impedance of the Γ_{opt} in order to achieve the lowest possible noise figure of the device. R_n indicates how much the noise figure changes as the source impedance deviates from the optimum conditions and is matched to other impedances. A large value of R_n shows high sensitivity of the noise figure as the source impedance deviates from the optimum conditions and therefore achieving and maintaining the optimum conditions are more difficult.

3.4 Fabrication Techniques

Two approaches of MIC and MMIC technologies are used as fabrication techniques of LNAs. The primary difference between MICs and MMICs is the method of fabrication and manufacturing process. The sizes and values of the components which can be used in MMIC designs are constrained while larger values of components can be employed easily in the MIC designs.

3.4.1 MICs

MIC or Hybrid Integrated circuits are constructed from individual active and passive components. The active components are transistors and diodes while passive components are resistors, inductors, capacitors and transformers. The

active and passive components of a MIC LNA are connected and bonded onto a substrate or printed circuit board (PCB). The material of the substrate depends on the application and frequency band of operation. The advantage of MIC designs is the complete freedom of using components with large values and sizes like big capacitors and inductors as part of the design. The other advantage of the MICs is the possibility of replacing the individual components if necessary. MIC designs can consist of single or multi layers.

3.4.2 MMICs

MMIC is a type of design that can be employed for the LNA design and fabrication. In MMIC technology all the active and passive components are constructed on the same substrate. The materials used for the fabrication of the low noise HEMT substrates are generally a III-V compound semiconductor, i.e GaAs, GaN, InP. The substrates consist of different layers which are used to construct the active and passive components and their connections. The sizes and values of available components are limited in MMIC design due to the small dimension of the MMIC chips. A complete characterisation of few MMIC chips from one wafer are essential as the performance of the MMIC chips fabricated on the same wafer are similar. The small dimension and mass production are the advantages of the MMIC chips. Mass production of MMICs make them cost effective [9].

3.5 Design Techniques

Noise figure matching and gain matching are implemented at various stages in the LNA design. The networks of noise figure and gain matching consist of passive components. Values of passive components are derived using Smith Chart. Initially the ideal lumped components available from the design software libraries

are used in each network in order to develop the LNA design. It is essential to check the device thoroughly after the synthesis of noise figure matching network is completed in the first stage. Testing the noise figure matching network can be carried out using the design software. Test must be performed as the subsequent stages of the LNA would have negligible effect in the noise figure of the LNA. As design progresses, it is very important to test the circuit after each stage using the design software. The reason is that the individual stages of the LNA cannot be tested after LNA fabrication as it is impossible to terminate each stage to 50Ω.

The lumped element components in the matching networks of each stages are determined by utilising Smith Chart either conventionally on paper or by using the available Smith Chart tool in ADS software [111]. Using the ADS Smith Chart [111], the load impedance is considered as 50Ω and the source impedance depends on the required impedances in each stage. Source impedance is the optimum noise impedance for noise matching stage, while the source impedance is maximum power transfer impedance for other stages. A mis-matching technique can be applied in the design for obtaining a desired trade-off between noise figure and power gain by using ADS software. The gain, return losses and reverse transmission are monitored during the matching process with the lumped element components. Some filtering circuitry might be required in the design of the LNA to maintain the gain only in the frequency band of interest. Biasing networks are necessary for transistors in each stage to obtain the required performance of the transistors and for the protection of the transistors. The biasing networks of the transistors would provide the required bias current for the transistor. Ideal lumped components must be substituted with the real components after achieving a desirable performance. Real elements are lossier compared to the ideal lumped components and hence the LNA design must be tuned until a satisfactory response is obtained. Microstrip transmission lines are employed to connect the elements.

The designed LNAs should have flat and acceptable gain with good return losses along with minimum noise figure over the frequency range of interest.

3.5.1 Multi-stage LNA

A combination of lowest noise figure possible with high and constant gain over the frequency range of interest must be achieved in a broadband LNA design. Noise matching of the LNA is achieved by matching the load to Γ_{opt} impedance while the conjugate of the load is matched to the source impedance. The noise figure matching and impedance matching of the low noise transistors are accomplished over different stages because the noise and gain circles are located in different sections of Smith Chart.

The noise factor of a multi-stage amplifier can be calculated by Friis' formula given in Equation 3.58,

$$F = F_1 + \frac{F_2 - 1}{G_1} + \frac{F_3 - 1}{G_1 G_2} + \frac{F_4 - 1}{G_1 G_2 G_3} + ... \tag{3.58}$$

where F_n is the noise factor in nth stage and G_n is the power gain of component n in the chain. Equation 3.58 shows that it is very important to have a low value noise factor in the first stage as the overall noise factor of the chain is dominated by the noise factor from the first stage. The contribution of the noise factor from subsequent stages are reduced by the gain of the preceding stages. Consequently, the primary objective of LNA designs in the first stage is to obtain the lowest noise figure possible. The subsequent stages of the LNA are designed for higher gain as the noise figure becomes less important in those stages. Determination of number of stages, required noise figure and gain from each stage are crucial aspects of multi-stage LNA designs.

Figure 3.4 shows a general 2-port amplifier with the matching network. The

input matching network mainly deals with the matching of the first transistor for low noise, while the other stages are focused to match the devices for maximum gain which is flat across the bandwidth of the LNA.

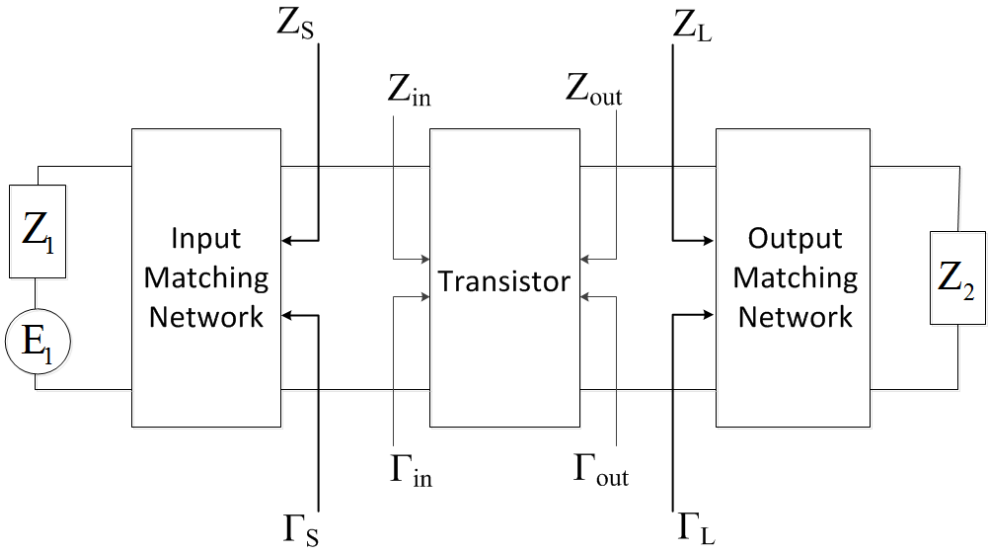

Figure 3.4: General 2-port amplifier with matching networks.

3.5.2 Noise Figure Matching

The primary objective of the LNA design is to achieve and match to minimum noise figure or noise factor ($F_{min} = 10^{\frac{NF_{min}}{10}}$). Therefore gate of the transistor must be presented by optimum impedance (Z_{opt}) or the reflection coefficient value (Γ_{opt}). Noise circles with constant noise figure values are formed in Smith Chart while moving away from the optimum noise matching conditions.

Figure 3.5 illustrates an example of noise figure circles of a transistor. The noise figure values of formed noise circles are higher than noise figure at the Z_{opt}. The complex relation of source impedance and noise figure are displayed by noise circles. Noise figure of a transistor is given in Equation 3.55. The relation between noise figure and the equivalent noise resistance (R_n) of a device is evident in Equation 3.55. The equivalent noise resistance (R_n) of a transistor indicates

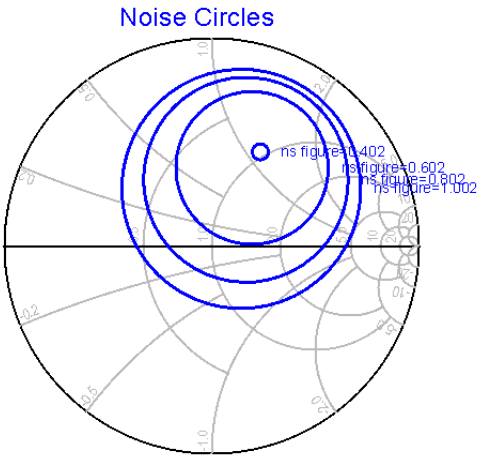

Figure 3.5: An example of noise circles for a pHEMT.

how fast the noise figure degrades when Γ_s moves away from Γ_{opt}. A lower value of R_n is more desirable as it shows that the noise figure is less sensitive to the noise impedance mismatch which makes the broadband LNA design comparatively convenient. Hence, it is essential to choose a transistor with small R_n and perform noise figure matching once the noise and gain circles of the device has been studied thoroughly.

3.5.3 Impedance Matching

Impedance matching is implemented from the second stage onwards in the LNA designs. Available gain (G_a) of a device driven by a specific source impedance is given in Equation 3.59. G_a can be determined from the S-parameters of the device and source reflection coefficient (Γ_s) as shown in Equation 3.59.

$$G_a = \frac{(1-|\Gamma_s|^2)|S_{21}|^2}{|1-S_{11}\Gamma_s|^2\,(1-|S_{22}+\frac{S_{12}S_{21}\Gamma_s}{1-S_{11}\Gamma_s}|^2)} \tag{3.59}$$

Source gain circles are obtained when Γ_s is plotted on Smith Chart for constant values of the gain. Gain circles illustrate the relation between gain and source impedance in a convenient way.

3.5.4 Passive Components

In the design of LNAs, passive components are very important as they form the majority of the components used for the LNA design. It is vital to choose the right passive components for the LNA designs due to self resonant frequency of the components which may lead the LNA to oscillations. Another important aspect of choosing passive component is their behaviour consistency at higher frequencies for the associated parasitics. Presently, high quality, state of art components are available for all the frequency ranges with very low loss and hence they can be implemented in the first stage of the LNA. The passive component for MIC designs are available in various and compact packagings. The S-parameters and/or models of passive components are available from manufacturing companies to assist designers to obtain a realistic response for the LNA. For passive components, there are some aspects to be taken into account while choosing commercially available off the shelf Components (COTs) in the MIC designs. A capacitor must have low inductance, low loss and very high self resonant frequency. The loss and self resonant frequency of the inductors must be considered.

In the MMIC LNA design, passive components are developed using the different layers of the process. MMIC foundries provide the models of the on chip passive components as the components are part of the process library.

3.6 Parameters of LNAs

Prior to commencing LNA design various fundamental aspects and specification of the LNA must be considered. In the following subsections the fundamental aspects of LNA design and characterisation are explained briefly.

3.6.1 Gain

Transducer power gain (G_T) of an LNA is defined as the ratio of the power delivered to the load to the power available from source which depends on source impedance (Z_s) and load impedance (Z_L). Equation 3.60 gives the transducer gain of an LNA which is commonly referred to as the gain of the LNA.

$$G_T = \frac{Power\ delivered\ to\ the\ load}{Power\ available\ from\ the\ source} = \frac{P_L}{P_{AvS}} \tag{3.60}$$

The definition of Available Gain (G_a) is given in Equation 3.61. G_a is the measurement of the ratio of power available from a 2-port network to the power available from the source.

$$G_a = \frac{Power\ available\ from\ the\ 2-port\ network}{Power\ available\ from\ the\ source} = \frac{P_{AvN}}{P_{AvS}} \tag{3.61}$$

Power gain (G_p) is the ratio of dissipated power in the load (Z_L) to the power delivered to the input of the 2-port network. Equation 3.62 shows the definition of the power gain.

$$G_p = \frac{Power\ delivered\ to\ the\ load}{Power\ input\ to\ the\ 2-port\ network} = \frac{P_L}{P_{in}} \tag{3.62}$$

Available gain (G_a) and power gain (G_p) of the transistors are examined completely for middle stages of the LNA to maximise the transducer gain (G_T).

Gain is one of the main parameters to be considered in the design of an LNA. The potential transistors for each stage of the LNA must be investigated completely before allocating the required gains to each stage. Number of stages is determined based on the available and maximum available gains of the transistors in each stage. The LNA must be designed in such a way to exhibit the required

gain over the frequency band of interest. Therefore, the gain must roll off outside the frequency band of LNA operation to prevent any possibility of oscillation [28, 112].

3.6.2 Noise Figure

Noise is an undesirable and inevitable product in the LNAs and plays a vital role in the LNA designs and characterisations. Source or input impedance and the noise sources within a 2-port network can effect the noise figure. The noise figure of the LNA can be calculated by using Equation 3.56. The primary objective of the LNA design is to achieve minimum noise figure in the first stage of the amplifier. The noise introduced to the LNA from the subsequent stages is insignificant as the noise is minimised by the gain of the preceding stages as seen in Equation 3.58.

3.6.3 Stability

One of the crucial considerations in LNA design is the stability of the LNA. Stability of an LNA shows its resistance towards the oscillations. Stability can be calculated from the S-parameters and matching networks and terminations of the LNA. Oscillations in a 2-port network are possible if either the input or output impedances has a negative real part. Thus it implies that $|\Gamma_{in}| > 1$ and $|\Gamma_{out}| > 1$. The stability condition of an LNA is frequency dependant as it is calculated from the S-parameters that are functions of frequency. It is possible for an LNA to be stable within the operation frequency band of the LNA but unstable at frequencies outside the operation frequency band. Thus, it is absolutely essential to check the stability of the LNA at various frequencies in Smith Chart. An amplifier is unconditionally stable if $|\Gamma_{in}| < 1$ and $|\Gamma_{out}| < 1$ for all the source and

load impedances which means $|\Gamma_S|$ <1 and $|\Gamma_L|$ <1. The unconditionally stable conditions are given in Equations 3.63 to 3.66.

$$|\Gamma_S| < 1 \tag{3.63}$$

$$|\Gamma_L| < 1 \tag{3.64}$$

$$\Gamma_{in} = \left| S_{11} + \frac{S_{12}S_{21}\Gamma_L}{1 - S_{22}\Gamma_L} \right| < 1 \tag{3.65}$$

$$\Gamma_{out} = \left| S_{22} + \frac{S_{12}S_{21}\Gamma_S}{1 - S_{11}\Gamma_S} \right| < 1 \tag{3.66}$$

The conditions of unconditional stability given in Equations 3.65 and 3.66 are simplified to S_{11} <1 and S_{22} <1, for a unilateral device where S_{12}=0. Stability circles of the load and source are plotted using Smith Chart. The stability circles define the boundaries of the stability of the 2-port network. The amplifier is unconditionally stable if the stability circles are completely outside the Smith Chart or encircle the Smith Chart. The load and source stability circles are drawn on the Γ_S and Γ_L planes respectively. The centre (C_L) and radius (R_L) of the output stability circle is defined by Equations 3.68 and 3.69 respectively. Δ is the determinant of the scattering matrix and is defined in Equation 3.67.

$$\Delta = S_{11}S_{22} - S_{12}S_{21} \tag{3.67}$$

$$C_L = \frac{(S_{22} - \Delta S_{11}^*)^*}{|S_{22}|^2 - |\Delta|^2} \tag{3.68}$$

$$R_L = \left| \frac{S_{12}S_{21}}{|S_{22}|^2 - |\Delta|^2} \right| \tag{3.69}$$

The input stability circle is defined with a centre (C_S) and radius (R_S) given in Equations 3.70 and 3.71 respectively.

$$C_S = \frac{(S_{11} - \Delta S_{22}^*)^*}{|S_{11}|^2 - |\Delta|^2} \tag{3.70}$$

$$R_S = \left| \frac{S_{12}S_{21}}{|S_{11}|^2 - |\Delta|^2} \right| \tag{3.71}$$

If all the conditions stated in Equations 3.63 to 3.66 are met for all biases and frequencies, then the LNA is unconditionally stable. Rollet stability factor (K) [113, 114] is another important measure of the LNA stability that gives an indication in regards of LNA stability. Rollet's factor is defined in Equation 3.72. LNA is unconditionally stable if K>1 over the frequency range of operation.

$$K = \frac{1 - |S_{11}|^2 - |S_{22}|^2 + |\Delta|^2}{2|S_{12}S_{21}|} \tag{3.72}$$

3.6.4 Bandwidth

Bandwidth of an LNA requires a constant power gain over the frequency band of interest. The variation of the gain with frequency is compensated by surrounding the device with external elements. The gain flatness is achieved by feedback techniques and selective impedance mismatching of the input and output networks. It is vital that the LNA has flat gain over the operational frequency band and a sharp roll-off outside the operational band.

3.6.5 Power

Power consumption of the LNA plays a crucial role in the design of LNAs especially for the systems that consist of large number of LNAs. It is very important to provide the power supply in the best and most effective way possible which is dependant of the requirements and conditions of the systems that the LNA is designed for. For example for SKA AA LNAs must be extremely power efficient as millions of LNAs are required for installation on the site. The cost of the LNA power supply is decreased dramatically if the designed LNAs are power efficient. Primarily, the power consumptions of the LNAs are derived by the power consumption of the transistors used in the LNA design. The power consumption of the transistors are a property of the process used in the transistors as some processes are more power hungry. Therefore power consumption of the active devices must be considered during the transistor selection process. However the power consumption of the amplifiers can be reduced to some extent with power efficient designs and a compromise in the gain. DC power supply of the gate voltage (V_{gs}) of the transistors can be either negative or positive which depends on the technology mode of the transistor. A negative V_{gs} must be provided if the transistor is in depletion mode, whilst a positive V_{gs} is supplied if the transistor is in enhancement mode. Consequently the need of negative voltages are eliminated if the enhancement mode transistors are used in the LNA designs making the DC power supply more convenient.

3.6.6 Return Losses

Return Loss is ratio of reflected power to the incident power when the load is mismatched because not all the available power from the generator is delivered to the load. Return loss is defined in Equation 3.73 and is expressed in decibels

[115].

$$Return\ Loss\ (dB) = -20\ log|\Gamma| \tag{3.73}$$

Reflection Coefficient (Γ) is defined in Equation 3.74 when load impedance (Z_L) and source impedances (Z_S) are known:

$$\Gamma = \frac{Z_L - Z_S}{Z_L + Z_S} \tag{3.74}$$

Input and output return loss parameters should be considered during LNA design. Low values of return losses are essential for an LNA to perform properly. Achieving low return losses in the LNA design is a challenge due to the required matching technique which is in contradiction with low noise matching. Isolators are non-reciprocal passive devices as the power is conducted in one direction only. Using isolators improve the return loss but this is not a practical solution for LNA design perspective due to the lossy nature of the isolators. Input and output return loss of a 2-port network is given in Equations 3.75 and 3.76 respectively. The power level available to the first stage of the transistor is degraded if the input return loss of the LNA is poor. The noise figure of the LNA deteriorates as a result of poor input return loss.

$$\Gamma_{in} = S_{11} + \frac{S_{21}S_{12}\Gamma_L}{1 - S_{22}\Gamma_L} \tag{3.75}$$

$$\Gamma_{out} = S_{22} + \frac{S_{21}S_{12}\Gamma_S}{1 - S_{11}\Gamma_S} \tag{3.76}$$

3.7 Baluns [2, 3]

Balun constitutes a very important and significant module in receiver systems where the antenna is differential. The balun usually is placed immediately after the differential antenna and serves as the interface between the antenna and subsequent amplification stages which maybe single ended. The importance of the balun in low noise receiver is further enhanced as the challenge is to keep the insertion loss very low. The challenge is overcome in cryogenically cooled systems due to the absence of thermal losses. But at room temperature systems, it is a primary objective to attain a balun with very low noise temperature.

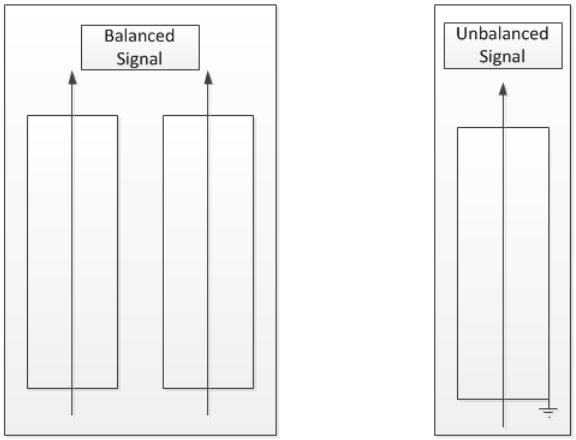

Figure 3.6: Balanced and unbalanced signals.

Fundamentally, a balun is a device which converts a balanced signal to an unbalanced signal and vice versa. The signal conversion is done by employing several techniques and the important ones are discussed later in this section. The representations of balanced and unbalanced signals are illustrated in Figure 3.6. In the balanced port the signal travels between the 2 arms of the balanced conductors. The signal in true sense is floating in nature due to the absence of any

physical ground. An example of the balanced line which has been widely implemented is the twin-line conductor where the balanced signal travels between 2 parallel conductors. This twin-line conductor is widely used in terrestrial communication systems and also in television. The unbalance port of the balun is more commonly used for the present communication RF networks. Coaxial lines and microstrip lines are the examples of an unbalanced line. In the unbalanced coaxial transmission line the outer references conductor is electrically connected to the ground or serves as the ground to the signal travelling in the inner conductor. The unbalance is achieved by either cancelling or removing the current on the outer side of the outer conductor in case of a coaxial line. This cancellation of current or RF signal can be attained by many techniques depending on the suitability to the system and technical requirements [2].

Baluns differ with respect to several parameters like technology and impedance conversion. In terms of technology, a balun can be designed based on lumped components, microstrip lines, coaxial lines, striplines, Co-Planar Waveguide (CPW) and many more. Each of the mentioned technologies can be implemented at different frequencies and applications. Baluns designed with lumped elements may be low loss naturally but their instantaneous bandwidth is usually smaller than microstrip or stripline baluns and microstrip baluns are lossier in nature. They can be inadequate for low frequency applications because of their dimensions at low frequencies. Stripline baluns have demonstrated both broadband and low loss characteristics.

3.7.1 Lumped Component Baluns

The lumped element balun consists of LC circuits and an example is shown in Figure 3.7 [12]. The objective of the design is to eliminate the phase difference

between signals in the same arm of the balun. The basic design of this balun consists of two 90° phase lines that provide the required 180° split between the 2 arms at the output of the balun. One of the arms of the balun is grounded making the signal at the output unbalanced. This configuration is essentially a bridge and is known as a lattice-type balun. It consists of 2 capacitors and 2 inductors, which produce the ±90° phase shifts.

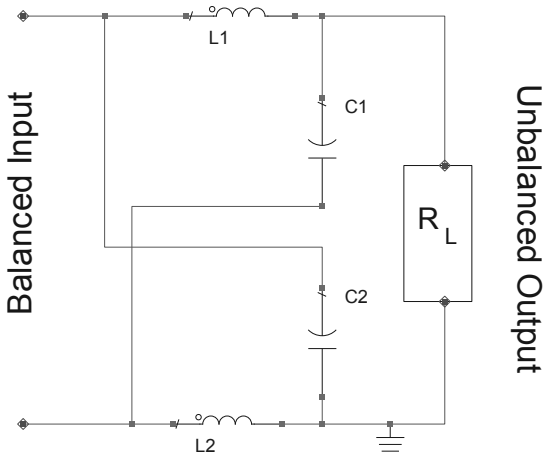

Figure 3.7: Schematic view of a LC lumped component balun [12].

The essential parameters based on which the balun is designed are the frequency of operation and impedance of the balun. The values of the lumped components in the design are calculated to optimise the performance at required frequency and impedance. When the operating frequency of the balun is f, the inductor and capacitor values of the configuration are determined by Equations 3.77 and 3.78 where Z_c is expressed in Equation 3.79.

$$L = \frac{Z_c}{\omega} \tag{3.77}$$

$$C = \frac{1}{\omega Z_c} \tag{3.78}$$

$$Z_c = \sqrt{R_I R_L} \tag{3.79}$$

These baluns have very small bandwidth with low loss characteristics. With the advent of MMIC based high frequency lumped components these baluns can be implemented at very high frequencies. The electrical parasitics and self resonant frequency of the various components must be taken into account while designing the baluns.

3.7.2 Transformer Baluns

Wire wound baluns can be classed as wire wound transformers which also performs the task of baluns. Wire wound transformer baluns are constructed from the wire wounded around a ferrite or iron core very similar to classical transformers. The operation of these baluns are limited to low frequency generally below 2.5GHz. The isolation between the primary and secondary sections of the baluns are high and respective ports have very good return loss. Wire wound transformers are commercially available with considerably small dimension. Although the commercially available transformers cover a wide frequency band their optimum performance is limited to narrower frequency range. Figure 3.8 shows the electrical equivalent circuit of a transformer balun. [116]

3.7.3 Other Variations of Baluns

There are different variations of baluns in terms of the design technology. These baluns can be designed and implemented at various frequencies depending on their application. Transmission line transformers can be realised from lines with a length of $\lambda/4$. In addition to the balanced to unbalanced signal conversion , they can be utilised for impedance transformation purposes. Marchand baluns

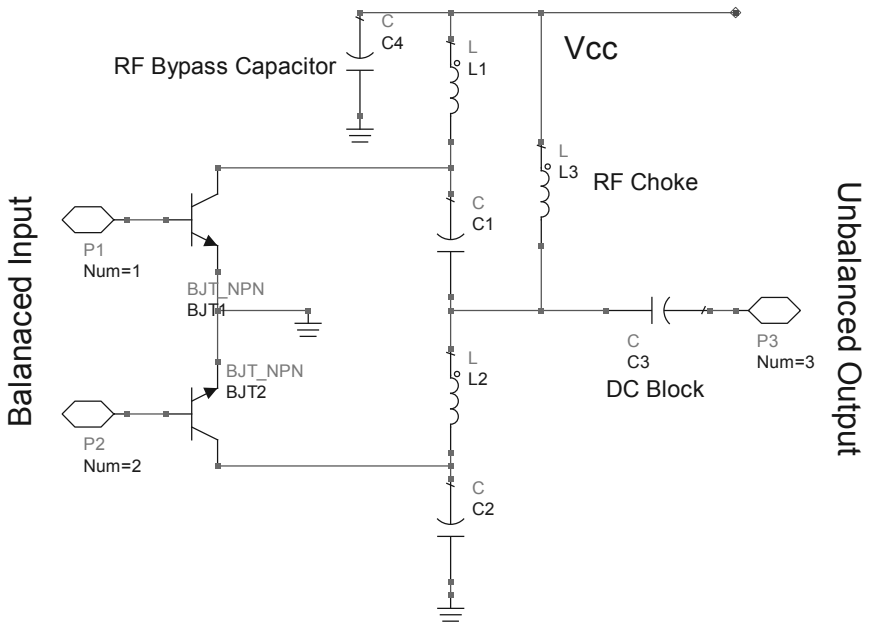

Figure 3.8: Schematic view of a wire wound lumped component balun [12].

overcame the problem of isolation in the transmission line baluns and they were coaxial lines originally [117]. Microstrip baluns are the other types of the baluns that can be fabricated on a suitable substrates. The dimension of these baluns are large at lower frequencies. Coupled line baluns are a simple version of the microstrip line baluns. The Marchand version of the coupled line is commonly used. [117, 118]

3.8 Positional Impact of Balun in a Receiver [4]

In this section, the advantages and disadvantages of 2 separate approaches are considered for designing the SKA front-end with differential antennas followed by LNAs. Approach 1 is a differential MIC LNA which includes a balun before the LNA. Approach 2 consists of 2 single ended LNAs with a balun after the LNAs.

3.8.1 SKA Front-end System Configuration Considerations [4]

Noise temperature of all radio astronomy telescopes is the primary parameter which defines system performance and the SKA is not exception. The feed and connection losses include the transmission losses associated with balun. An aperture array antenna system in SKA essentially comprises of differential antenna with a single ended back-end. The balanced signal at the antenna must be converted to unbalanced form before being fed to the digital back-end. Classically in radio receiver systems baluns are used to attain this transformation from balanced to unbalanced signal. But due to the low operational frequency of AA-lo in SKA, the dimension of baluns will be considerably large. Moreover the challenge also lies in the realisation of a low loss wideband balun suitable for SKA. The large dimension of baluns imply the associated losses are also considerably higher than 7K. Though microstrip and strip line baluns are low loss in nature, their dimension is considerably large. In order to meet the 7K added noise requirement the passive balun would need to have less than 0.1 dB loss. This would be very challenging, and would be likely to need a large balun structure. A differential LNA is ideal for integration into aperture array AA-lo system. But few HEMT based differential LNAs have been developed and have faced issues such as stability and poor common mode rejection ratio. The feasible options with single ended LNAs suitable for SKA front-end are shown in Figure 3.9 and Figure 3.10. Figure 3.9 shows the classical radio receiver configuration where a low loss balun can be used to transform balanced signal from balanced antenna to unbalanced signal to be fed to the LNA. This configuration demands a very low loss balun which has a maximum loss of 7K for SKA. Figure 3.10 shows the alternative configuration of incorporation of single ended LNA in SKA front-end.

In the Australian SKA program this configuration is being researched [35]. In the following sections the issues related to each configuration are discussed.

3.8.2 Balun followed by single-ended LNA [4]

The configuration, shown in Figure 3.9 is matured in system design and integration. The advantages are its maturity and success in existing systems. But the primary challenges of this topology are achieving very low loss and wideband balun response below 450MHz. Above 1GHz promising responses have been achieved by microstrip feed and balun in APERTIF program [38]. At AA-lo frequency band the dimension of the balun will also be significantly large which will not only be expensive but also cumbersome to facilitate integration. The alternative solution to this issue is to develop a low loss and wideband balun based on discrete components or coils. This is an extremely challenging task with discrete components because very low loss components will have high Q-factor which will serve as a opposing factor to achieve wideband response.

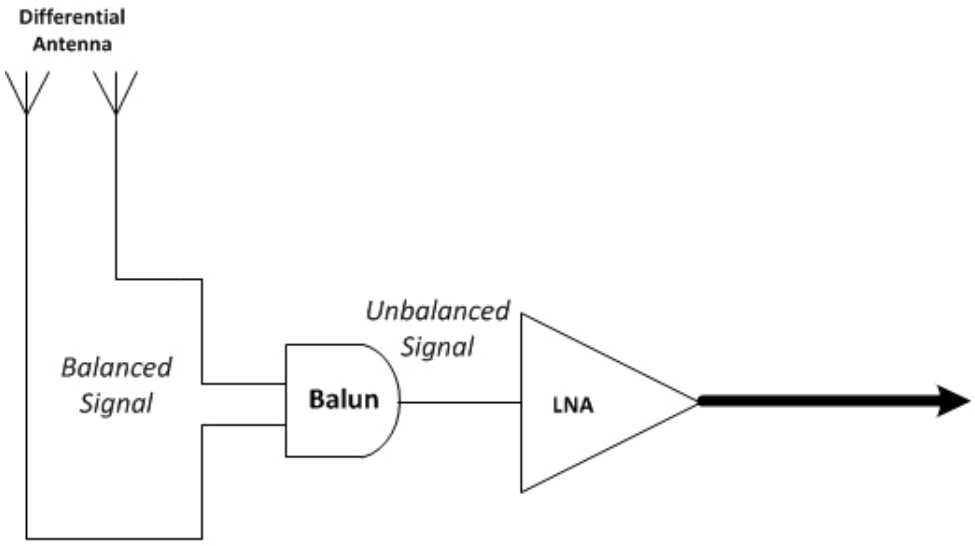

Figure 3.9: Classical front-end configuration.

3.8.3 2 LNAs followed by a balun [4]

Figure 3.10 shows approach 2 to the front end arrangement discussed in this section for the SKA project. The issues that are associated with this configuration are stability, poor common mode rejection ratio, imbalance of drain current in each arm. In a LNA design a common practice for achieving wideband and stable response is to use resistors in the drain bias circuit usually denoted by R_d. In a MIC topology, COTS components are used to build the LNA. These components typically have 2% of tolerence. This 2% shift in tolerence limit of each component in LNA1 and LNA2 of Figure 3.10 to opposite polarities can contribute significantly to the distortion of the balanced signal from the antenna. The discussed problems will be more challenging to solve in a MIC LNA.

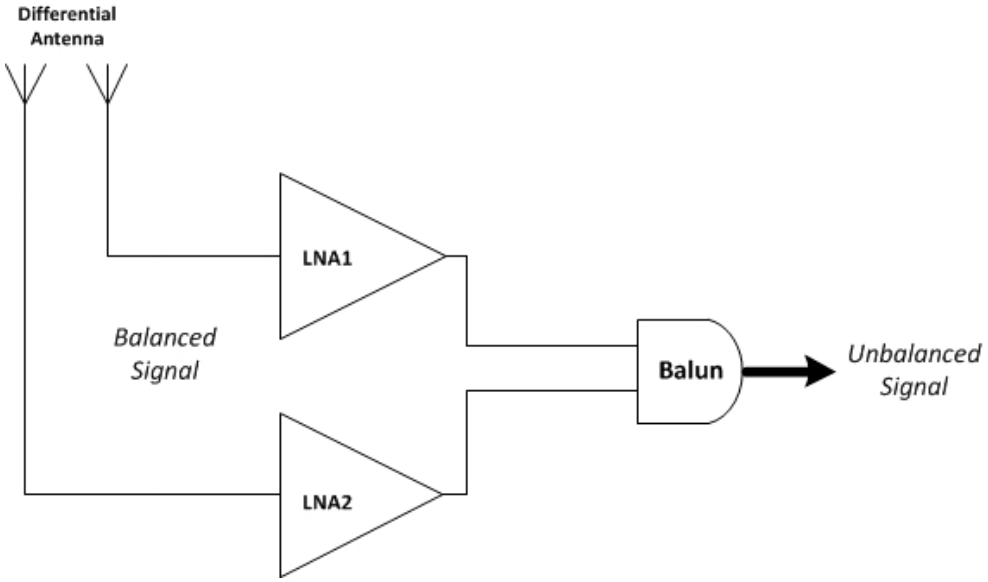

Figure 3.10: Front-end configuration with balun after LNAs.

Equation 3.80 [119] and Equation 3.81 are the expressions of drain current of a HEMT in terms of its electrical parameters including bias conditions. A different value of R_d in the 2 LNAs will place the quiescent points on different locations on the load line of the LNAs at same V_{DD} and V_{GS}. Effectively the

drain currents I_{d1} and I_{d2} of the 2 LNAs will differ causing imbalance of drain currents in the 2 LNAs. This imbalance of drain current may lead to distortion of the balanced signal. If the drain current is kept same with different V_{GS} the drop across the resistors of the 2 LNAs will be different for different tolerance values. This difference in potential drops across the R_Ds of the 2 LNAs will bias the drains of the LNAs at different voltage values. Equation 3.82 is an expression of transconductance of a HEMT. It is not only a function of V_{GS}, alternatively I_d, but also V_{DS}. Though this case will not cause drain current imbalance in the 2 LNAs but will bias them at different quiescent points. Effectively the transconductance and optimum noise impedances of the 2 LNAs will be different causing distortion in the balanced signal.

$$I_d = \frac{qN\mu_0 W Z_G}{L_a}\left[V_{DS} - \frac{2}{3}(V_p + V_{Bo}) \left\{\left(\frac{V_{Bo}+V_{GS}+V_{DS}}{V_p+V_{Bo}}\right)^{\frac{3}{2}} - \left(\frac{V_{Bo}+V_{GS}}{V_p+V_{Bo}}\right)^{\frac{3}{2}}\right\}\right] \quad (3.80)$$

$$= K_1\left\{V_{DS} + \frac{2}{3}(V_p+V_{Bo})^{-\frac{1}{2}} \left[(V_{Bo}+V_{GS}+V_{DS})^{\frac{3}{2}} - (V_{Bo}+V_{GS})^{\frac{3}{2}}\right]\right\} \quad (3.81)$$

$$g_m = \frac{dI_d}{dx} = K_1(V_p+V_{Bo})^{-\frac{1}{2}} \left[(V_{Bo}+V_{GS}+V_{DS})^{\frac{1}{2}} - (V_{Bo}+V_{GS})^{\frac{1}{2}}\right] \quad (3.82)$$

Let I_{d1} and I_{d2} be the drain currents with PSU voltages for drains as V_{DS1}

and V_{DS2} of LNA1 and LNA2 respectively. Let the variation of R_D for LNA1 and LNA2 be $+\Delta R_D$ and -ΔR_D respectively. Equations 3.83 and 3.84 show the voltages at the drains of LNA1 and LNA2.

$$\begin{aligned} V_{d1} &= V_{DD} - I_{d1}R_D \\ V_{d2} &= V_{DD} - I_{d2}R_D \end{aligned} \tag{3.83}$$

$$\begin{aligned} V_{d1} &= V_{DD} - I_{d1}\left(R_D + \tfrac{\Delta R_D}{2}\right) \\ V_{d2} &= V_{DD} - I_{d2}\left(R_D - \tfrac{\Delta R_D}{2}\right) \end{aligned} \tag{3.84}$$

Equation 3.85 shows the drain currents of the LNAs after rearrangements of Equation 3.84. By changing V_{GS1} and V_{GS2} the condition I_{d1}=I_{d2}=I_d can be achieved.

$$\begin{aligned} I_{d1} &= \tfrac{V_{DD}-V_{d1}}{R_D+\frac{\Delta R_D}{2}} \\ I_{d2} &= \tfrac{V_{DD}-V_{d2}}{R_D-\frac{\Delta R_D}{2}} \end{aligned} \tag{3.85}$$

Subtracting the equations in Equation 3.84, Equation 3.86 is derived.

$$V_{d2} - V_{d1} = I_d\left(-R_D + \frac{\Delta R_D}{2} + R_D + \frac{\Delta R_D}{2}\right) \tag{3.86}$$

Assuming a nominal 2% variation of R_D gives Equation 3.87. Further taking a nominal value of R_D as 50Ω leads to Equation 3.88.

$$\begin{aligned} \Delta R_D &\approx 2\% R_D \\ V_{d2} - V_{d1} &= I_d \Delta R_D = I_d \tfrac{R_D}{50} \end{aligned} \tag{3.87}$$

$$V_{d2} - V_{d1} = I_d \text{Volts} \tag{3.88}$$

From Equation 3.88 it is apparent that the difference between the drain bias voltages caused because of 2% variation of R_Ds between LNA1 and LNA2 may make at least 10% difference between the drain bias voltages of the same if it is assumed that a typical LNA works at 10mA drain current. A minimum 10% swing between drain bias voltages of the 2 LNAs will bias the transistors at very different g_m and $\sqrt{I_d}/g_m$ which are indices of gain and minimum noise figure respectively. This analysis effectively implies that the 2 arms of the differential antenna will experience a difference in amplification and also addition of noise. The imbalances will result in signal distortion, reduction in CMRR and oscillations.

3.9 Topologies

Classically LNAs have single ended input and single ended output topology. LNAs with single ended configurations have been designed, characterised and fabricated successfully over the time. Other topology that is being used in the design of the LNAs is differential configuration. SKA AA project requires LNAs with differential input to single ended output configuration.

3.9.1 Single Ended LNA

Single ended amplifiers receive an unbalanced single input signal with respect to the ground and amplify the received signal and pass it through to the single ended output with respect to the ground. LNAs with single ended input and output topology is matured. The design and characterisations of these amplifiers are well established and well known. The single ended input and output amplifiers can

consist of one or multiple stages. From noise perspective in single ended LNAs the source impedance of first stage is matched to the optimum noise impedance of the transistor. The noise from external sources like power supplies, cables, etc. are prevalent in the performance and contribute to the LNA noise temperature. But this configuration is vastly used in present systems because of its simplicity subsequent system architecture. Single ended LNAs are not compatible for a differential system which interprets balanced signals.

3.9.2 Differential input and single ended LNA

Differential amplifiers amplify the voltage difference between 2 input signals or balanced signal and transfers the signal to the single ended output. SKA project requires LNAs with differential input and single ended output as the antennas have differential output. Therefore, an LNA with this configuration must be designed. The LNAs can consist of a single stage or multiple stages. Design of an LNA with differential inputs and single ended output is very complicated as the signal must be converted from balanced to unbalanced within the LNA. The noise matching must be done for both of the transistors simultaneously while the transistors are loaded with effect of each other. The grounding is another issue involved with the differential to single ended LNA designs. These problems were solved by implication of balun at the input of the LNA. Therefore, the balanced signal from the antenna are fed through the balanced input of the balun. Then the balanced signal is converted to an unbalanced signal by the balun and is passed to the LNA that has been designed using the single ended LNA. The performance of the balun was considered in the LNA design to optimise the performance. This was carried out in the LNA design phase and the 3-port simulations were utilised for the design of the LNA.

3.9.3 Differential LNA

Fully differential amplifiers amplify balanced signals and keep it intact at its output. The ground reference of the LNA is floating in nature. Differential amplifiers are used extensively and are implemented in various applications like medical science instrumentation and astronomy. The differential amplifiers can consist of a single stage or multiple stages. The number of active and passive elements in the differential LNA is double of that in a single ended LNA. Accordingly the differential LNA consumes double quantity of the power. From noise perspective it has the advantage of cancelling the noise which is common to both the arms of the LNA. This helps in minimising the noise from external sources like power supplies and other common interfering sources. The primary disadvantage of differential LNAs over the single ended LNAs is that the 2 arms of the LNA must be identical to preserve the efficiency, linearity and improved noise performance. This aspect calls for implementing differential LNAs in MMIC technology to facilitate identical components on each arm. Noise matching technique in differential LNA is more complex because, in common source configuration, each transistor is loaded with its differential pair which may alter the optimum noise impedance of transistors.

3.10 Summary

This chapter covers a complete description of the LNA design techniques. The reasons of employing the techniques in the LNA design is discussed thoroughly. The important parameters and crucial aspects that must be considered during the LNA design have been explained separately. Normal and mixed mode S-parameters for 2, 3 and 4-port networks are described in this chapter. A comprehensive description of the LNA design theory is portrayed in this chapter.

The detailed explanation of the LNA topologies and the fabrication methods are given in this chapter. The baluns were studied and used in the LNA designs for converting the unbalanced signal to a balanced signal. The LC lumped element and wire wounds baluns were described. The impact of the balun position in a low noise receiver was also explained. Single ended and differential LNA configurations were described along with the differential to single ended configuration required by the SKA AA system.

Chapter 4

Designs

4.1 Introduction

In this chapter MIC and MMIC LNA designs are described in detail. Commercial off-the-shelf (COTS) components are utilised in the design of MIC LNAs. Two MIC LNAs were designed, fabricated and characterised for the SKA AA system on the basis of the requirements in the LNA operational frequency bands. The MIC LNAs are defined as low frequency Aperture Array (AA-lo) and high frequency Aperture Array (AA-mid) LNAs which cover frequency ranges of 70-450MHz and 400-1400MHz respectively. The detailed description of the AA-lo and AA-mid LNAs are given in Sections 4.4 and 4.5 respectively. Single ended and differential LNA topologies were designed for AA-lo system. Three versions of the single ended and 2 versions of differential LNA were developed for AA-lo band. A number of LNA versions were characterised as the LNA designs evolved to meet the required key performances of the LNAs. The AA-mid LNAs consist of 2 separate versions with single ended inputs and outputs. Different versions differ primarily in their circuit component values and layouts. The transistors used for the MIC LNAs are ATF-58143 of Avago Technology. ATF-58143 are GaAs

E-mode pHEMTs which were selected primarily due their low power consumption for low noise performance. The MMIC LNAs were designed based on using the low noise TQP13N GaAs pHEMT process of TriQuint Semiconductors. Detailed description of the TQP13N process is given in Section 4.6.1. Sections 4.6.2 and 4.6.3 are dedicated to the explanation of the MMIC LNA designs over the frequency ranges of 0.7-1.8GHz and 8-12GHz respectively.

The key performance parameters of all the MIC and MMIC LNA designs described in this chapter are outlined as follows

- Required bandwidth coverage
- Lowest noise figure possible
- High gain
- Low power consumption
- Unconditional stability.

The packaging and housing of the LNAs are explained in Sections 4.4.3 and 4.5.2 for MIC LNAs and Section 4.6.4 for MMIC LNAs.

4.2 Avago ATF-58143 E-Mode pHEMT

ATF-58143 pHEMT of Avago Technologies operates in enhancement mode. Positive gate voltages are required in E-mode pHEMTs and hence the negative gate voltages requirement associated with depletion mode transistors are eliminated. Therefore E-mode pHEMTs are more convenient for operational and voltage supply purposes. The low noise ATF-58143 pHEMTs are housed in a 4-lead (SC-70) low cost and small surface mount plastic package of SOT-343. Combination of

low noise, high gain and high linearity performance of ATF-58143 pHEMTs make them a suitable choice for low noise amplifier designs. Maximum drain source voltage (V_{ds}) and gate source voltage (V_{gs}) of the ATF-58143 pHEMTs are 5V and 1V respectively and application of higher voltages cause permanent damage to the device. Maximum total power dissipation (P_{diss}) and drain current (I_{ds}) of the pHEMT are 500mW and 100mA respectively. Typical value of V_{gs} is 0.51V for V_{ds} of 3V and I_{ds} of 30 mA. The pHEMT has gain of more than 20dB and 15dB up to frequencies of 1.5GHz and 2.5GHz respectively [120]. Noise figure of the pHEMT is less than 0.5dB for conditions of 3V and 30mA at 25°C. Typical values of 1dB compressed output power (P1dB) are 18dBm and 19dBm for frequencies of 0.9GHz and 2GHz respectively when V_{ds}=3V and I_{ds}=30mA [120].

4.3 Development of MIC LNAs

The LNAs were designed for 2 frequency bands of AA system known as AA-lo and AA-mid to cover the frequency bands of 70-450MHz and 400-1400MHz respectively. The LNAs were specifically designed to meet the exceptional criteria required by the system. LNAs for the AA system must have low noise and high gain like all the other radio astronomy LNAs, along with very low power consumption due to the large number of the LNAs required in the project. Tens of millions of the LNAs are required for each frequency band in the AA system as mentioned in Section 1.3. Therefore, it is vital to design LNAs with low noise and high gain with very low power consumption to reduce the total power supply of the system and hence whole system becomes cost effective. LNAs with differential input to single ended configurations are required as part of the AA system. The LNA configuration is dictated as a result of the connection of input of the LNA to an antenna with differential output and a single ended system at the output of the

LNA as outlined in Chapter 1. Consequently, it is essential to design differential to single ended LNAs with high differential gain and low common mode gain. Repeatability and reproducibility factors of the LNAs are met by utilising COTS components in the MIC LNAs. Due to the large scale of SKA project , it is essential that a more automated approach is taken for the receiver subsystems such as mass production of the LNAs to reduce the fabrication costs. A summary of configurations used to design, fabricate and characterise the MIC LNAs in the AA system is given in Table 4.1.

Table 4.1: Configurations of MIC LNAs for AA system.

LNA	Configuration
AA-lo	Single ended input and output
	Differential input to single ended output
AA-mid	Single ended input and output

Focus was given to a reduced set of performance parameters outlined in Section 4.1 as the design of MIC LNAs for AA system evolved to obtain an optimum performance. Therefore a number of versions were designed for the MIC LNAs in the AA system. A detailed description of the AA-lo LNAs is given in Section 4.4 which consist of single ended LNAs and differential input to single ended output LNAs. Design and development of 3 versions of the single ended AA-lo LNA and 2 versions of differential AA-lo LNAs are explained in detail in Section 4.4. Section 4.5 describes the design of the single ended LNAs for AA-mid. Two separate versions of single ended LNA were designed and developed for AA-mid frequency band.

4.4 MIC AA-lo LNAs

The design procedure, layouts and packaging of 5 AA-lo LNAs are discussed in this section. The single ended AA-lo LNA consists of 3 versions and are named as "SE-AAloV1", "SE-AAloV2" and "SE-AAloV3". The AA-lo LNAs with differential input and single ended output have 2 versions and are named as "Diff-AAloV1" and "Diff-AAloV2".

The design of LNAs were carried out by using ADS software. The MIC AA-lo LNAs consist of 2 stages and operate over the frequency range of 70-450MHz. The input and output impedances of the single ended LNAs are 50Ω.

The primary objective of the SE-AAloV1 and Diff-AAloV1 LNAs was to achieve the required wide frequency band of 70-450MHz with a flat gain of more than 20dB. Subsequent versions of the AA-lo LNAs were designed to maintain the main performance parameters of the LNAs outlined in Section 4.1 and improve the subset parameters. Therefore, SE-AAloV2 and Diff-AAloV2 LNAs were designed and fabricated to further improve the aims of SE-AAloV1 and Diff-AAloV1 LNAs while concentrating on the reduced set of key parameters. Flat gain over the bandwidth of interest, lower power consumption, size reduction and lower noise figures were targeted to meet and possibly exceed the required AA-lo LNA specifications for SE-AAloV2 and Diff-AAloV2. A flat and broad-band gain of greater than 25dB was required at power consumption of less than 30mW which was the target set for the AA system [6]. The primary objectives of the AA-lo LNAs were met and exceeded by SE-AAloV2 and Diff-AAloV2 in terms of power consumption, high and flat gain over the frequency band of operation. SE-AAloV3 LNA was designed and fabricated to further reduce the noise figure and dimension of the single ended AA-lo LNAs.

4.4.1 SE-AAloV1, SE-AAloV2 and SE-AAloV3

The schematic design, layouts and fabrication process of 3 versions of the single ended AA-lo LNAs are described in this section.

Design

The schematic design of the LNA is illustrated in Figure 4.1. It consists of 2 stages with the input and output impedances of 50Ω.

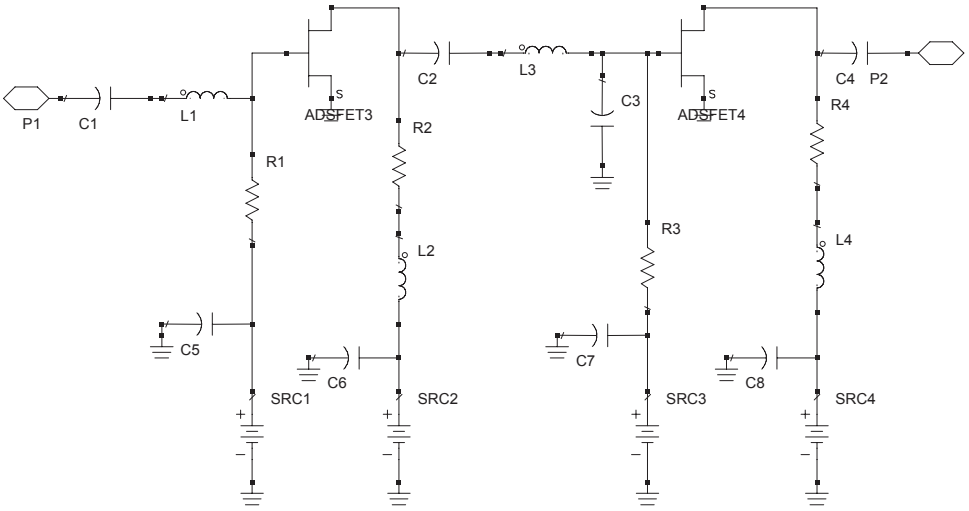

Figure 4.1: Schematic view of the single ended mode of AA-lo LNA.

The primary aim of the LNA design was noise matching in the first stage along with achieving sufficient gain of more than 10dB in order to minimise noise contribution from the second stage. In the first stage of the LNA, the optimum impedance for minimum noise figure of the transistor was matched to a 50Ω. An inductor was used to achieve the noise matching in the first stage. The main priority in the second stage was the impedance matching in order to

increase the gain and performance of the LNA. Input, output DC blocks and the interstage decoupling capacitors were chosen for the purpose of gain optimisation and flatness in the LNA. By-pass capacitors were employed in the circuit to eliminate the feedback through the DC bias lines and maximise the stability. The capacitors are used to decouple the DC supply lines from the RF of the amplifier. Rollet's factor (K-factor) was used as an indicator of unconditional stability of the LNAs. High values of resistors were used at the gates of the pHEMTs in each stage of the LNA to maintain the gate bias voltage (V_{gs}) and reduce noise addition from leakage current. High value resistors at the gates were used also to protect the gates of the transistor. Low value resistors and inductors were used at drains of each stage. The inductors were used to decouple the RF from the DC power supply units. The low resistances were used to make the LNA stable and reduce gain of the transistors. The resistances also help to achieve a broad-band response across the frequency band. Table 4.2 states the functionality of individual components used in the design of the AA-lo LNAs.

Table 4.2: Description of the components, functions and values in the AA-lo LNA.

Function	Components	Values
Input DC Block	C_1	50pF
Output DC Block	C_4	50pF
Interstage Decoupling	C_2	5pF
Noise Matching	L_1	35nH
Impedance Matching	L_3, C_3	17.5nH, 3pF
By-pass Capacitors	C_5, C_6, C_7, C_8	100pF, 100pF, 100pF, 100pF
Gate Resistor	R_1, R_3	7KΩ, 7KΩ
Drain Resistor	R_2,R_4	50Ω, 50Ω
RF and DC decoupling	L_2,L_4	1.5nH, 2nH

The gate and drain voltages of the pHEMT for stage 1 and 2 are biased through separate channels. The biases were kept separate and therefore individual stages were controlled to optimise the performance of the LNA with respect to

the noise and bandwidth. BNC cables are employed to connect the power supply unit and the gate and drain of each stage of the LNA. BNC cables were chosen to provide a good RFI shield and maintain a common ground for DC and RF signals. SMA connectors are used for the connection on the RF input and output.

Layout

The layout designed for SE-AAloV1 is shown in Figure 4.2. Availability, low cost and repeatability of the LNAs are vital requirements in the SKA project. Therefore the SE-AAloV1 LNA was fabricated on a FR4 substrate for the low cost of substrate. The FR4 substrate has a thickness of 1.6mm, dielectric constant (ϵ_r) of 4.7 and dissipation factor (tanδ) of 0.02. Dimension of the fabricated SEAAloV1 LNA was 72.2mm×41.8mm. The footprints of the SMAs are drawn on the layout of the LNA with 3 pads on the left and right hand side of Figure 4.2. The middle pad on the SMA footprint conducts the RF signals while the pads on either side are for the ground connections to the back of the board. The coaxial pin of the SMA is connected onto the middle pad of the SMA footprint. RF input and output of the LNA are located on the left and right hand-side of the board. DC paths of the drains and gates of both stages are on the top and bottom of the layout respectively.

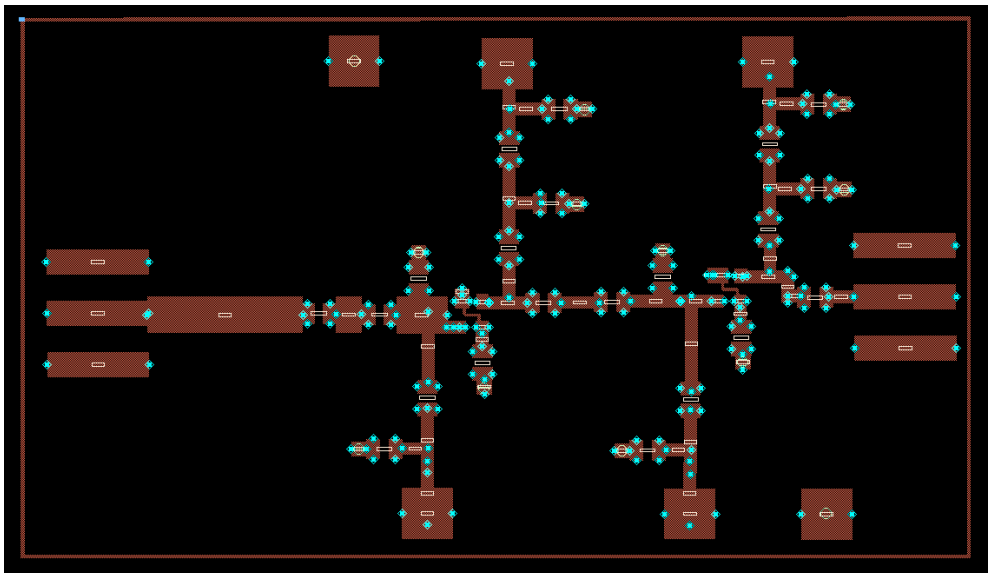

Figure 4.2: Layout of SE-AAloV1 LNA.

Figure 4.3 illustrates the layout of SE-AAloV2 which was fabricated on a Rogers RO 4003C substrate. RO 4003C substrate has a thickness of 0.51mm, dielectric constant (ϵ_r) of 3.38 and dissipation factor (tanδ) of 0.0022.

The difference between SE-AAloV1 and SE-AAloV2 are the noise matching inductor values in the first stage and the sizes of the LNAs. The LNA has dimension of the 57.9mm×33.4mm. Six footprints for the SMA connectors are drawn in the layout of the LNA in Figure 4.3. The SMA connector footprint consists of 3 pads with the middle pad for the RF signal and DC bias voltages respectively and the 2 pads on either side are connected to the ground on the other side of the board via the SMA. The drain and gate voltages are supplied through the DC paths on the upper and lower parts of the layout.

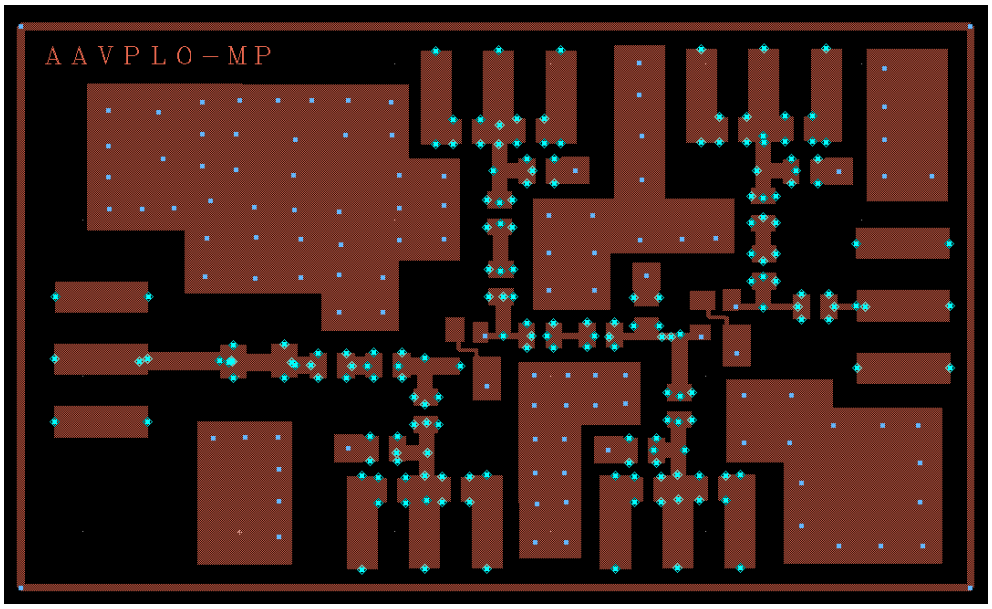

Figure 4.3: Layout of SE-AAloV2 LNA.

Source inductive feedback is attained by transmission line tracks and substrate via holes at the sources of the transistors. For FR4 substrates the source via holes are 1.6mm long while the source via holes of Rogers RO 4003C are 0.51mm long. The trade-off is between high gain and low input return loss for the LNAs. The via holes on the source of the ATF-58143 pHEMTs introduces different inductive feedback depending on the substrate. Table 4.3 gives the inductive feedback produce by 1 via hole on the source pin of the transistor for both FR4 and Rogers RO4003C substrates.

Table 4.3: Inductances of via holes for FR4 and RO4003C substrates.

Frequency(GHz)	FR4	RO4003C
0.05	0.32 nH	0.030 nH
0.25	0.26 nH	0.030 nH
0.50	0.26 nH	0.032 nH
0.75	0.25 nH	0.032 nH
1.00	0.25 nH	0.024 nH
1.25	0.25 nH	0.026 nH
1.50	0.25 nH	0.027 nH

Figure 4.4 shows the layout of SE-AAloV3 fabricated on the Rogers RO4003C substrate which is an updated version of SE-AAloV2 with a reduction in the size of the LNA. The dimension of the LNA is 41.5mm×31.2mm.

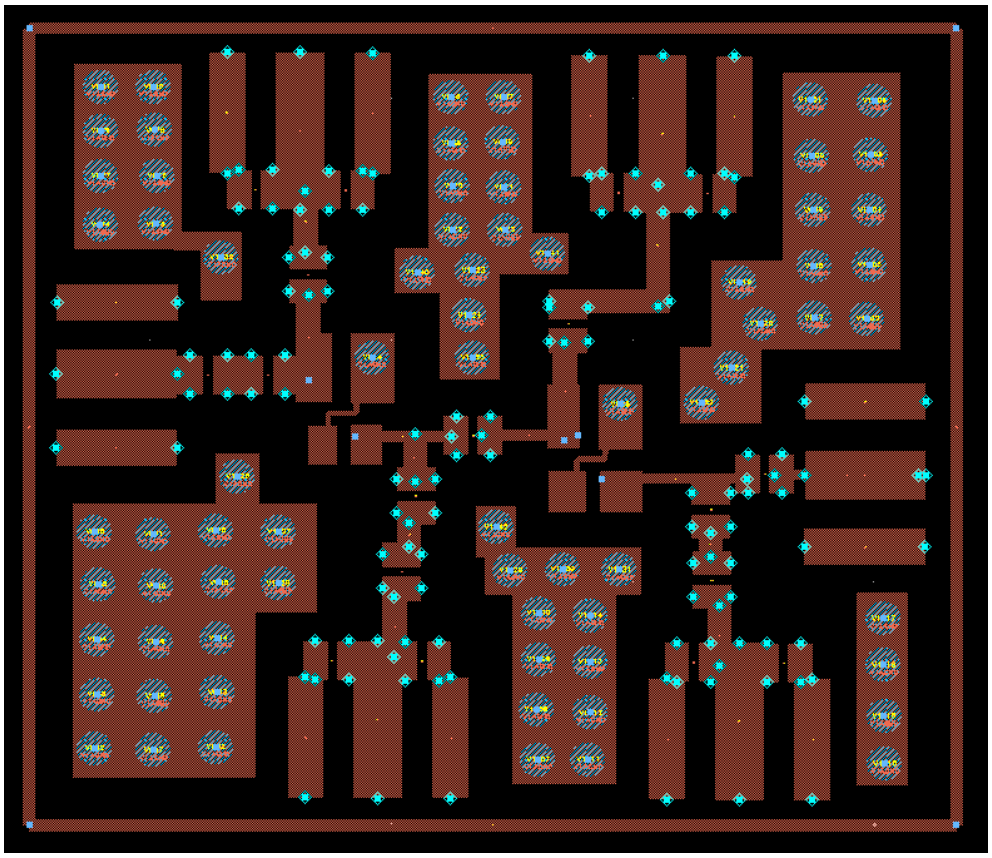

Figure 4.4: Layout of SE-AAloV3.

As illustrated in Figures 4.3 and 4.4, several via holes were included in the layouts of the SE-AAloV2 and SE-AAloV3 to provide a stable RF ground for the LNAs in order to reduce the oscillation possibilities.

4.4.2 Diff-AAloV1 and Diff-AAloV2

The design, layout and fabrication process of 2 versions of differential to single ended AA-lo LNAs are described in this section. The LNAs are named as "Diff-AAoV1" and "Diff-AAoV1" and consist of 2 stages with ATF-58143 E-mode

pHEMTs.

Designs

The design of an LNA with differential input was explored because the AA antenna system is differential. A commercially available RF transformer with a 1:1 transfer ratio was employed in the design of the differential AA-lo LNA. The transformer operates over a wide frequency band of 4.5-3000MHz [121]. Figure 4.5a shows the measured insertion loss of the balun. The insertion loss of the balun is less than 0.6dB up to frequency of 1GHz. The insertion loss of the balun is between 0.2dB and 0.3dB over the frequency band of 70-450MHz. Measured input and output return losses of the balun are illustrated in Figure 4.5b. The return losses of the transformer are lower than -20dB up to 1GHz [13]. The transformer was implemented in the design to convert the differential input signal to a single ended signal. The differential LNA design consists of a transformer followed by a single ended LNA. The single ended LNA has been explained in Section 4.4.1. The response of the transformer was considered as part of the LNA response in the design phase. The schematic view of the differential LNA is given in Figure 4.6. The inputs and output terminations have an impedance of 50Ω.

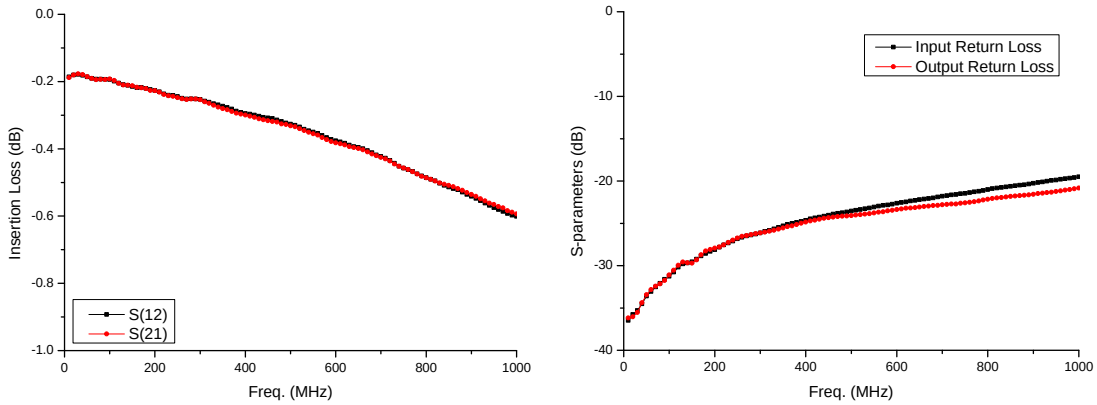

(a) Insertion loss (b) Return losses

Figure 4.5: S-parameter performance of the transformer used in Diff-AAlo LNAs [13].

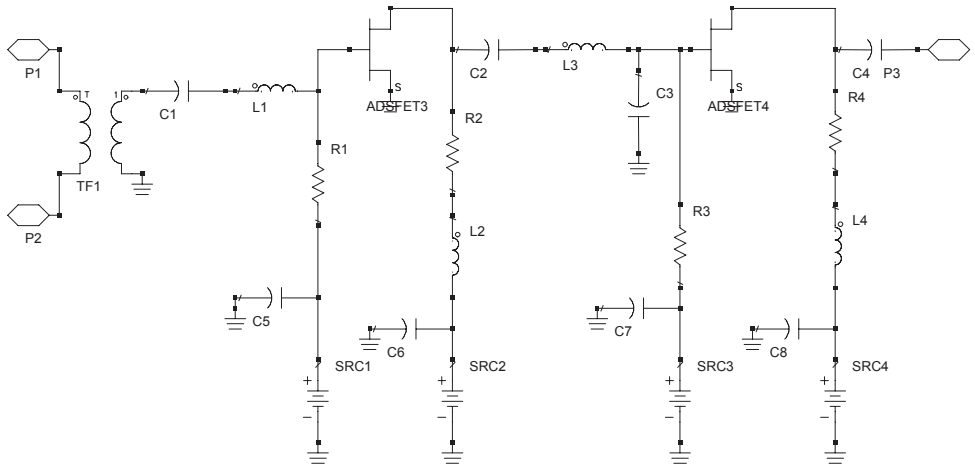

Figure 4.6: Schematic view of the differential mode of AA-lo LNA.

Layout

The layouts designed for Diff-AAloV1 and Diff-AAloV2 are shown in Figures 4.7 and 4.8 respectively. The Diff-AAloV1 and Diff-AAloV2 LNAs are fabricated on

FR4 and Rogers RO4003C substrates respectively.

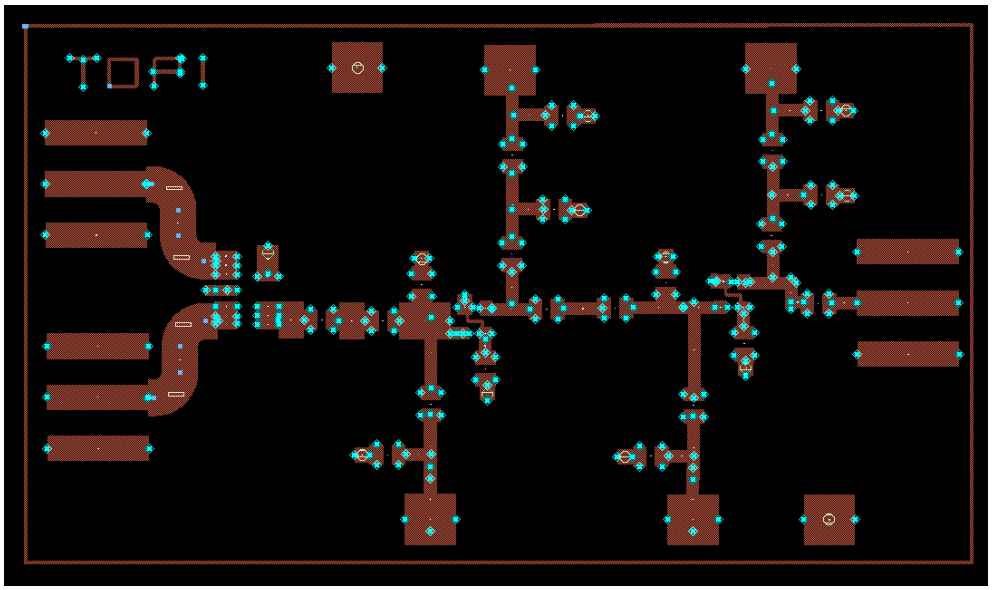

Figure 4.7: Layout of Diff-AAloV1.

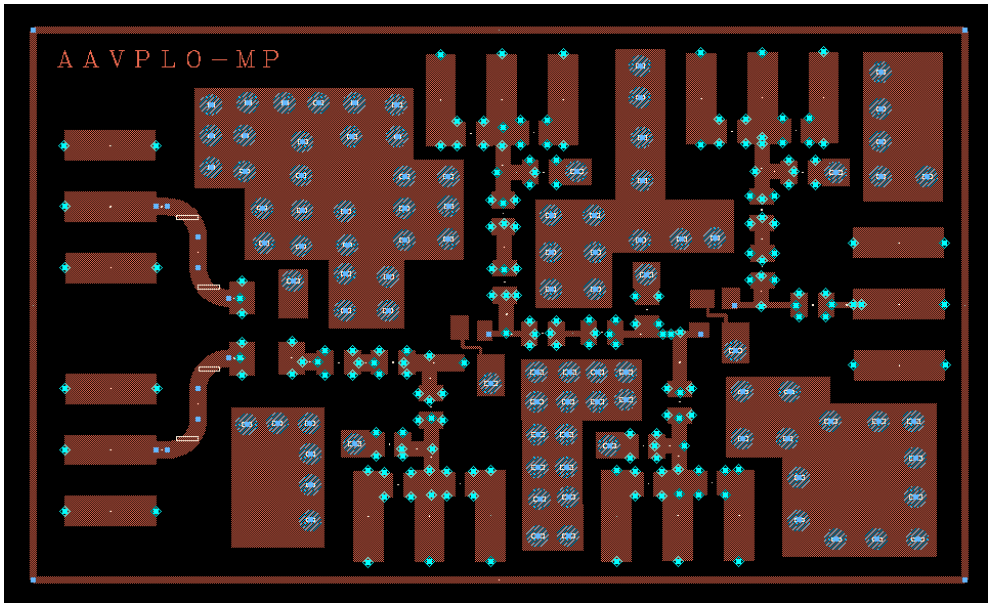

Figure 4.8: Layout of Diff-AAloV2.

4.4.3 AA-lo LNA Packaging

Five AA-lo prototypes were fabricated which include the single ended AA-lo LNAs (SE-AAloV1, SE-AAloV2 and SE-AAloV3) and differential AA-lo LNAs (Diff-AAloV1, Diff-AAloV2).

SE-AAloV1 and Diff-AAloV1

Figure 4.9 shows the packaging style used for SE-AAloV1 and Diff-AAloV1. The LNAs were packaged in a copper body. The length, width and height of the copper body are 82.5mm, 45mm and 25mm respectively. End launch jack SMAs were used at the input and output of the LNA. The SMAs are coaxial type with an impedance of 50Ω. The external length and width of the SMAs are 6.35mm. The SMAs are mounted at the edges of the LNA. The coaxial pin of the SMA is connected to the input and output of the LNA for the RF signal. The ground connection of the LNA is through the via holes on the board to the ground at the back. Two external pins of the SMA on either side of the coaxial pin are connecting the top and bottom sides of the LNA together to construct a well connected ground. The DC power for gates and drains of each stage of the LNA is supplied through individual wires onto the board. The individual wires are connected to the power supply through a crimp socket inside a 8-way crimp housing on the board. Each of these wires are connected to the power supply unit by using a shielded cable to reduce the possibility of the picking up the unwanted signals through the individual and thin wires.

Figure 4.9: Fabricated prototype Diff-AAloV1.

SE-AAloV2, Diff-AAloV2 and SE-AAloV3

Figure 4.10 illustrates the copper housing style used for packaging both SE-AAloV2 and Diff-AAloV2. The length, width and height of the illustrated housing body is 65mm, 40mm and 20.3mm respectively. Four cylindrical shapes were connected to the corners of the amplifier housing for the lid enclosing purpose. The screws are held in these cylindrical shapes in order to keep the lid and body of the enclosure connected without touching the LNA board. The coaxial pin of the end launch jack SMAs were used for the RF signal and DC power supply to the LNA. The impedance of the SMA connectors are 50Ω. The SMAs at the input and output of the LNAs are for RF signal. The DC power of the drains and gates for each stage of the LNA were supplied through the coaxial pin of the

SMAs on the DC paths. BNC cables were used to supply the DC from the power supply units to the LNA. BNC cables were selected to provide a good RFI shield and maintain a common ground for DC and RF signals. The SMA external pins are connected to the top of the LNA and ground at the back and therefore the grounds on both sides of the LNA are well connected. The fabricated SE-AAloV3 LNA is shown in Figure 4.11.

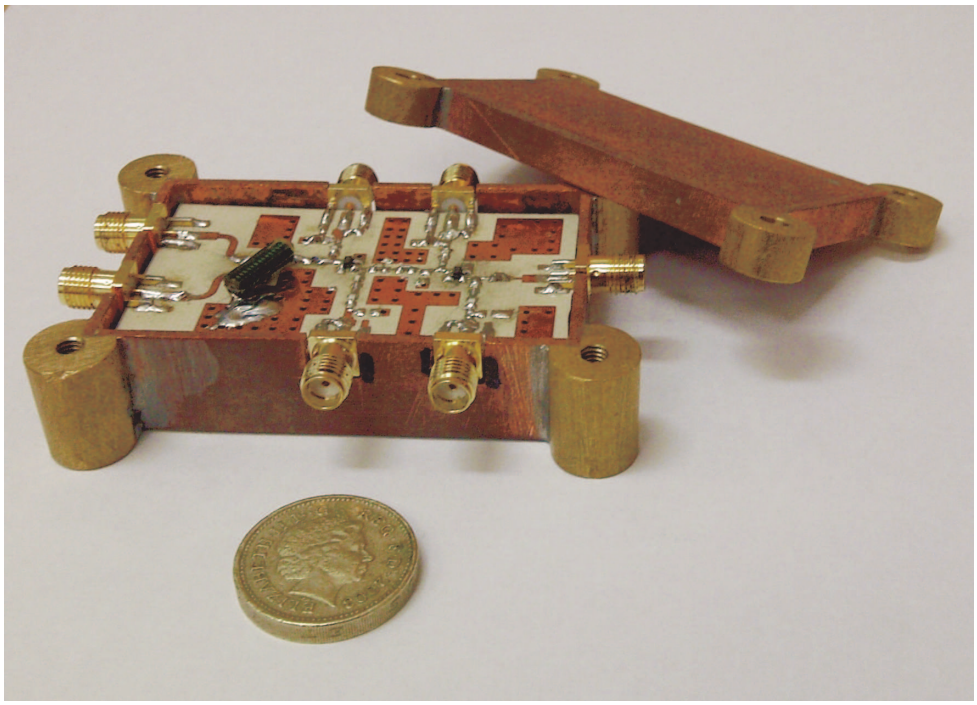

Figure 4.10: Fabricated prototype Diff-AAloV2.

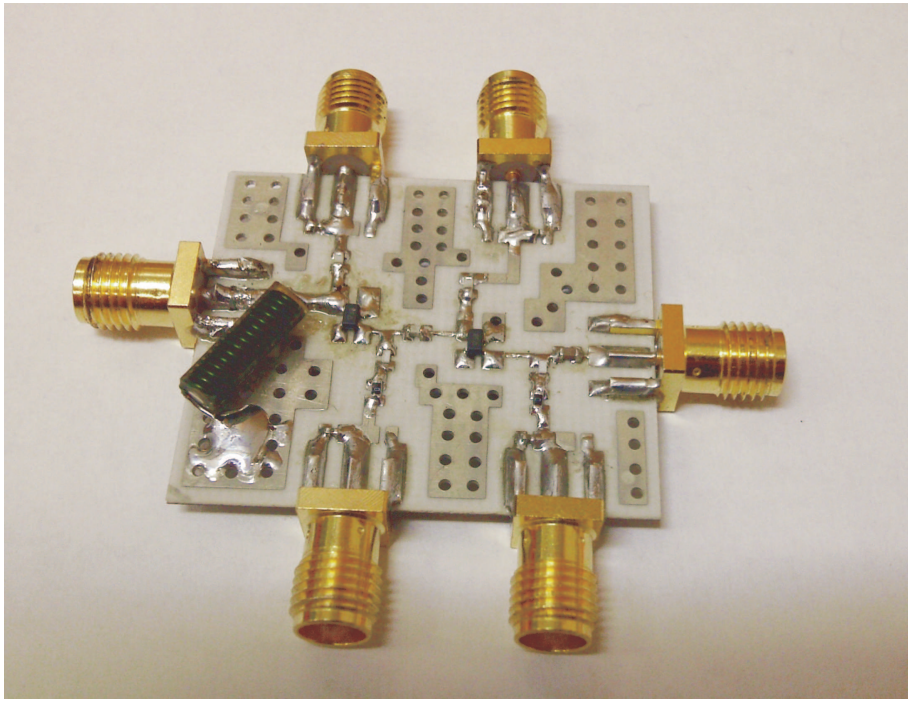

Figure 4.11: Fabricated prototype SE-AAloV3 LNA.

4.5 MIC AA-mid LNAs

This section describes the design procedure, layouts and fabrication of 2 AA-mid LNAs. The LNAs have single ended input and output configuration. Designed and characterised AA-mid LNAs are termed as "AAmidV1" and "AAmidV2". AA-mid LNAs operates over the frequency band of 400-1400MHz to cover the higher frequency band of the AA system. The LNA designs were carried out using ADS software. The primary objective of the LNA development was to achieve the minimum possible noise figure at room temperature along with a considerable gain to meet the criteria set for AA-mid system. The key performance parameter of AAmidV1 was to achieve a flat gain of more than 20dB over the frequency band of interest along with the lowest noise figure possible.

AAmidV2 was designed to further improve the AAmidV1 performance to meet

and if possible exceed the requirement of AA-mid LNAs. Therefore, a flat gain of more than 25dB over the bandwidth of interest, lowest possible noise figures across the band at power consumption of less than 30mW were the primary objectives of the AAmidV2 design along with a considerable reduction in the LNA dimension [6].

4.5.1 AAmidV1 and AAmidV2

The schematic design, layouts and fabrication process of 2 versions of AA-mid LNAs are described in this section.

Design

The focus was with equal emphasis on low noise, low power consumption and low production cost. In this section the LNAs with low power consumption and low noise are discussed. Two versions of the AA-mid LNAs differ in several design and layout aspects but the designs are fundamentally similar in topology. The detailed discussion on the designs of the LNAs are covered in subsequent sections.

Figure 4.12 shows the schematic of the AA-mid LNA design with 2 stages. ATF-58143 pHEMTs are used in both stages of the design. The choice of the devices in stages 1 and 2 of the LNA are a reflection of the trade-off between the noise figure and power efficiency of the transistor. In the first stage, the optimum impedance for minimum noise figure of the transistor has been matched to 50Ω system. The linear noise models of the transistor were used for the purpose of noise matching. Source inductive feedback has been used in stage 1 to achieve close proximity of the optimum noise and gain circles. The source degeneration has been implemented with transmission line and substrate via. Noise matching has been achieved with high impedance transmission line at the input of the

transistor. A high resistive shunt feedback from drain to gate is used to improve the gain bandwidth and noise flatness over the band. The gain of the LNA has been sacrificed to some extent in stage 1 to ensure that LNA is biased at optimum bias condition for minimum noise figure. According to Friis formula given in Equation 3.58, the overall noise figure of the LNA is dominated by the noise figure from the first stage of the LNA. Hence minimum noise figure must be achieved in the first stage as the noise figure contribution of the subsequent stages in the LNA is very low. The value of the drain resistor in stage 1 was kept small to reduce the gain and noise from the stage with improvement in the stability of the LNA. Stage 2 had a higher drain resistance to increase the gain of the LNA and achieve an overall flat gain response over the whole frequency band of operation. An impedance matching resistor had been incorporated after the final stage of the LNA to achieve a good output return loss. High value capacitors are used at the DC biases to decouple the DC bias power supplies from the RF path on the LNA. Description of the components used in the AA-mid LNAs design and their functions are summaries in Table 4.4. The gate and drain voltages of the pHEMTs in the LNA are biased through separate channels. The biases were separate to control the performance of each stage individually in order to optimise the noise and bandwidth of the LNA. DC connections of the LNA and the power supply units are by BNC cables for providing RFI shield and maintaining a common ground.

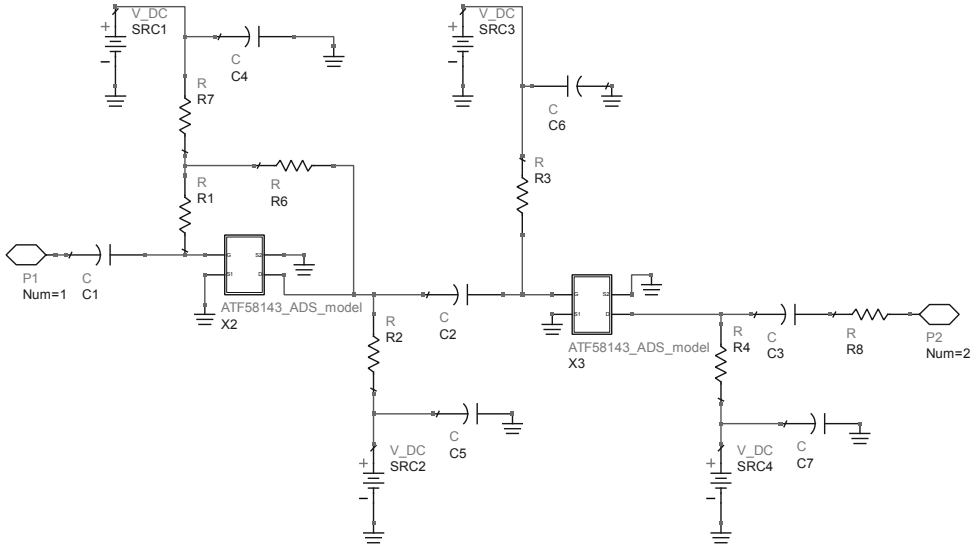

Figure 4.12: Schematic view of the AA-mid LNA.

Table 4.4: Description of the components, their functions and values in the AA-mid LNA.

Function	Components	Values
Input DC Block	C_1	100nF
Output DC Block	C_3	100nF
Interstage Decoupling	C_2	100nF
Noise Matching	C_1	100nF
Impedance Matching	C_2	100nF
By-pass Capacitors	C_4, C_5, C_6, C_7	100nF, 100nF, 100nF, 100nF
Gate Resistor	R_1, R_3	7KΩ,7KΩ
Drain Resistor	R_2,R_4	5Ω, 68Ω
Shunt feedback	R_1,R_6	4KΩ, 7KΩ

Layout

The layout of the AAmidV1 produced in ADS is shown in Figure 4.13. The dimension of the LNA board is 51mm×31mm. The LNA was designed and fabricated on a FR4 substrate. High volume LNA production is required for the AA

system in the SKA project and hence the fabrication cost plays as a main driving factor. FR4 substrate was used in the fabrication of AAmidV1 due to the low cost and robustness nature of the substrate. Thickness of 1.6mm, dielectric factor (ϵ_r) of 4.7 and dissipation factor (tanδ) of 0.02 are the specifications of the FR4 substrate used for the LNA fabrication. There are 6 footprints of the coaxial SMA connectors in Figure 4.13. The RF input and output of the LNA are the SMA connectors on the left and right hand-side of the board respectively. The DC power is supplied to the LNA through the SMA connectors. The gate and drain channels of both stages are on the top and bottom side of the layout respectively. As illustrated in Figure 4.13, there are several substrate via holes presented in a distributed fashion in the LNA layout to provide a stable RF ground to the LNA for reducing the possibilities of oscillations. The fabricated AAmidV1 LNA is illustrated in Figure 4.14.

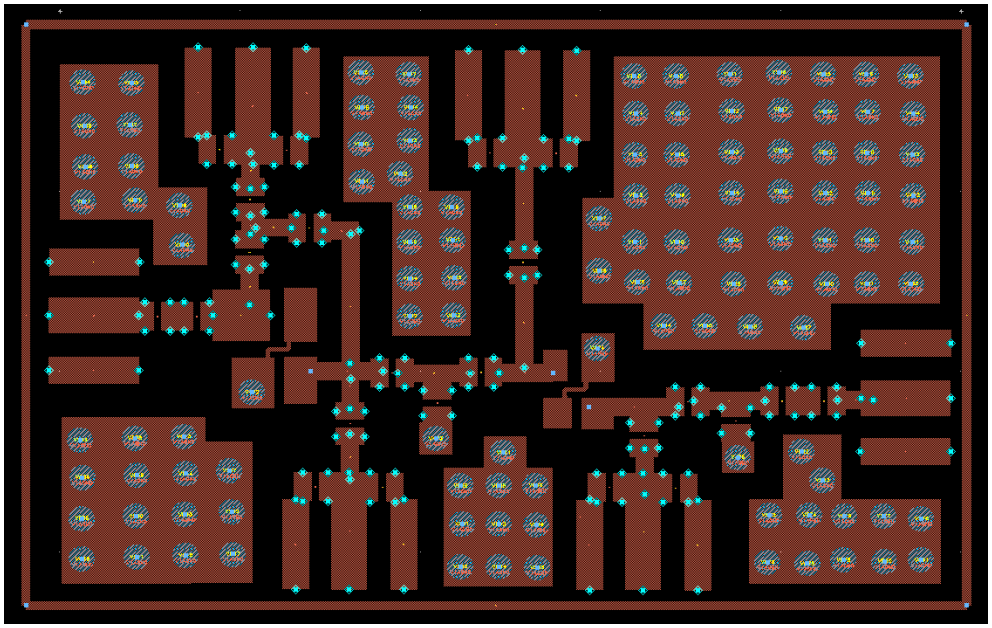

Figure 4.13: Layout of AAmidV1.

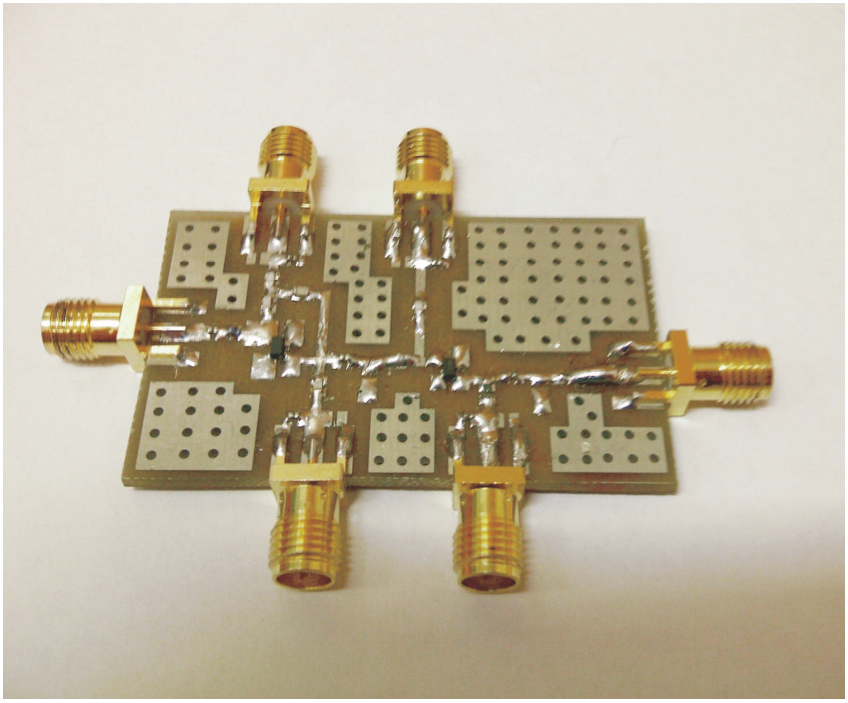

Figure 4.14: Fabricated prototype AAmidV1.

Layout of the AAmidV2 produced in ADS is given in Figure 4.15. Rogers RO4003C substrate with a thickness of 0.51mm, dielectric constant (ϵ_r) of 3.38 and dissipation factor of 0.0022 was used for fabrication of AAmidV2. The LNA dimension was reduced compared to the AAmidV1. The dimension of AAmidV2 is 38mm×28mm. Layout of AAmidV2 is shown in Figure 4.15 with 6 footprints for the coaxial SMA connectors. The RF input is the SMA on the left hand side of the board while the RF output is on the right hand side. The SMA footprints at the top and bottom sides of the board are for supplying the bias voltages to the gates and drains respectively. The via holes on the layout generate good RF ground to the LNA to reduce the oscillation possibilities.

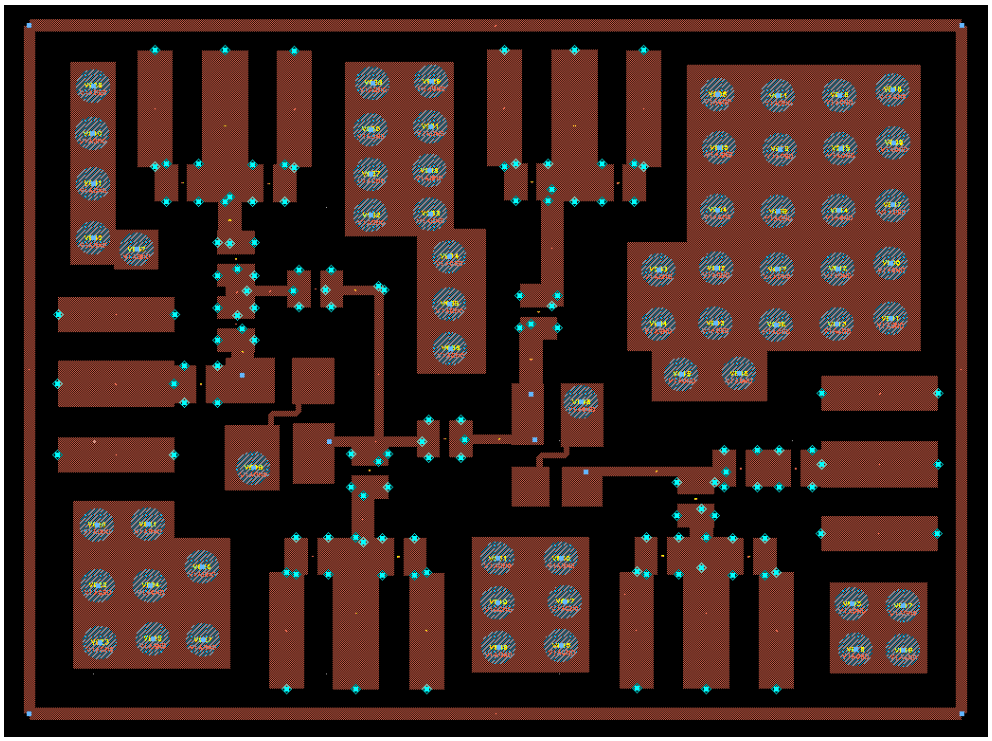

Figure 4.15: Layout of AAmidV2.

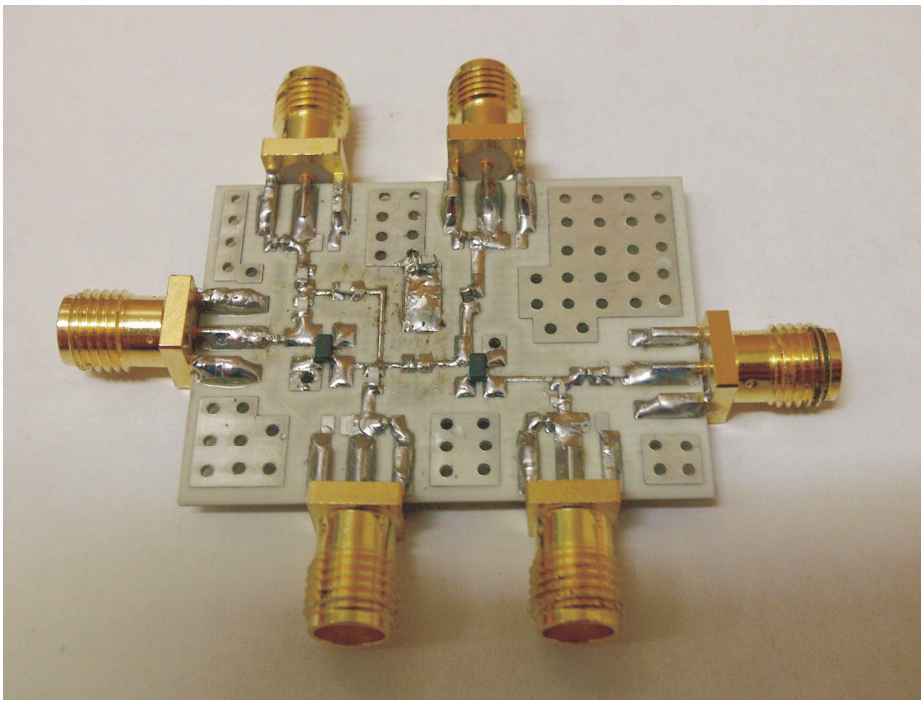

Figure 4.16: Fabricated prototype AAmidV2.

4.5.2 AA-mid LNA Packaging

Figure 4.16 illustrates the fabricated LNA with all passive and active components mounted on to the board. The amplifier housing used for AAmidV1 and AAmidV2 LNAs is shown in Figure 4.17 which is made of brass. The LNA board is attached to the base section of the case with a detachable lid to enclose it. The ground of the LNA was connected to the chassis by soldering the ground of the SMA connectors to it.

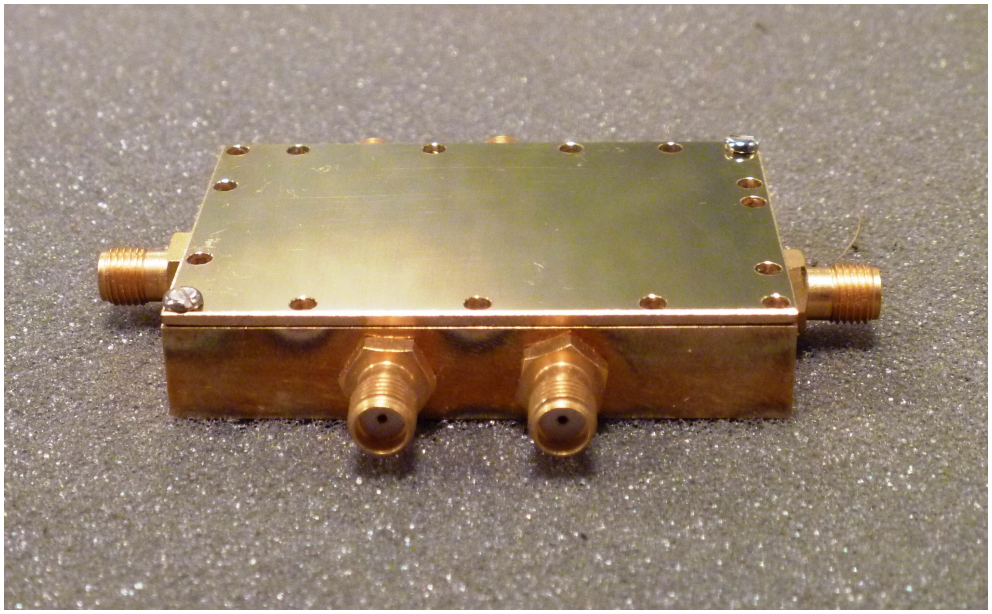

Figure 4.17: Packaged AA-mid LNA.

The LNA housing body has length, width and height of 62.2mm, 42.2mm and 10mm respectively. Two coaxial SMAs were connected at the input and output of the LNAs. The DC power is supplied to the SMAs connected to the gates and drains of each stage through a BNC cables for good RFI shielding purpose. The LNA and the housing body are connected together through the SMAs and therefore they share a well connected common ground.

4.6 MMIC LNAs

A detailed description of 2 MMIC LNAs named as "UMAN-SKAlowV1" and "UMAN8-Xband" using the TQP13N process are explained in this section along with a brief overview of the process library.

4.6.1 TQP13N 130nm pHEMT Library

A comprehensive study and research on all the available components in the process library is vital prior to commencing a MMIC LNA design. TQP13N is a low noise GaAs pHEMT process from TriQuint Semiconductors with a typical cut off frequency of 95GHz. The pHEMTs are in depletion mode with a gate length of 0.13μm. Several combinations of the pHEMTs are available in the TQP13N process by variation of the pHEMT gate width and the number of fingers. The minimum and maximum finger width of the pHEMTs in the process are 10μm and 250μm respectively. TQP13N process permits single finger configuration of pHEMTs. The transistors are constructed of several layers. There are 2 metal layers available in the process. TQP13N process consists of several supported circuit elements that are listed in the following [122]:

- D-mode pHEMT transistors with 0.13μm gate length
- Diodes constructed by connection of drain and source terminals of the FET
- N+ Resistors with value of 105Ω/sq
- Thin Film NiCr Resistors with value of 50Ω/sq
- MIM capacitors with value of 340pF/mm^2
- Inductors and other metal structures

- Substrate vias

The behaviour and performance of the pHEMTs with various gate width dimensions were analysed for the purpose of selecting a suitable pHEMT for the LNA design. The S-parameter responses and noise figure of the transistors were studied by variation of the gate, drain voltages and the frequency. The gate and drain voltages were swept from -0.5V to 0.5V and 0.5V to 2.5V respectively. Figures 4.18 and 4.19 show the plots of S_{21}, R_n and NF_{min} of a 4×50μm pHEMT. One parameter out of V_g, V_d and frequency were kept fixed while the other 2 parameter were varied to obtain the plots shown in Figures 4.18 and 4.19. Figure 4.18 illustrates the performance of the 4×50μm pHEMT with a fixed drain voltage of 2V while the gate voltage varies from -0.5V to 0.5V and frequency varies from 7.5GHz to 12.5GHz respectively. The responses of the 4×50μm pHEMT at frequency of 8.5GHz is illustrated in Figure 4.19 when the gate and drain voltages vary from -0.5V to 0.5V and 0.5V to 2.5V respectively.

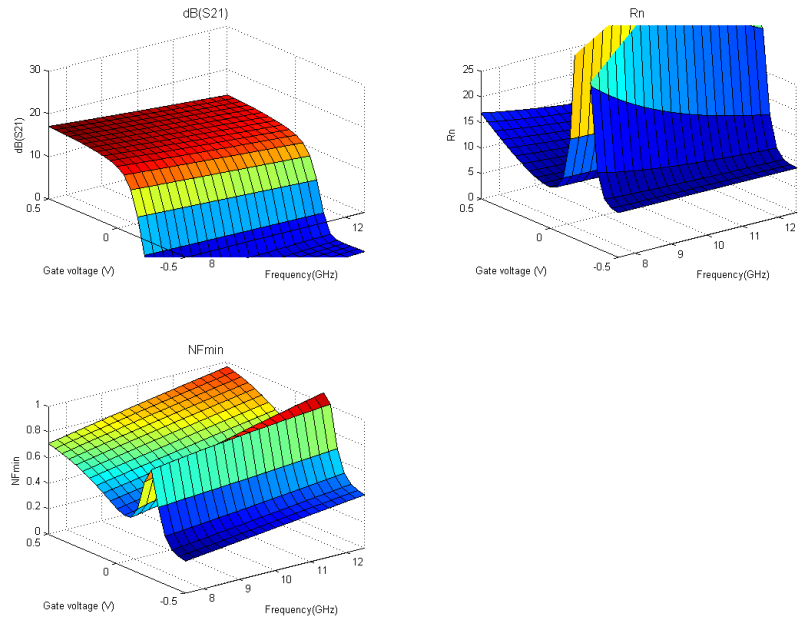

Figure 4.18: Simulated S_{21}, R_n and minimum noise figure performance of the TQP13N 4×50μm pHEMT with variation of V_g and frequency at V_d=2V.

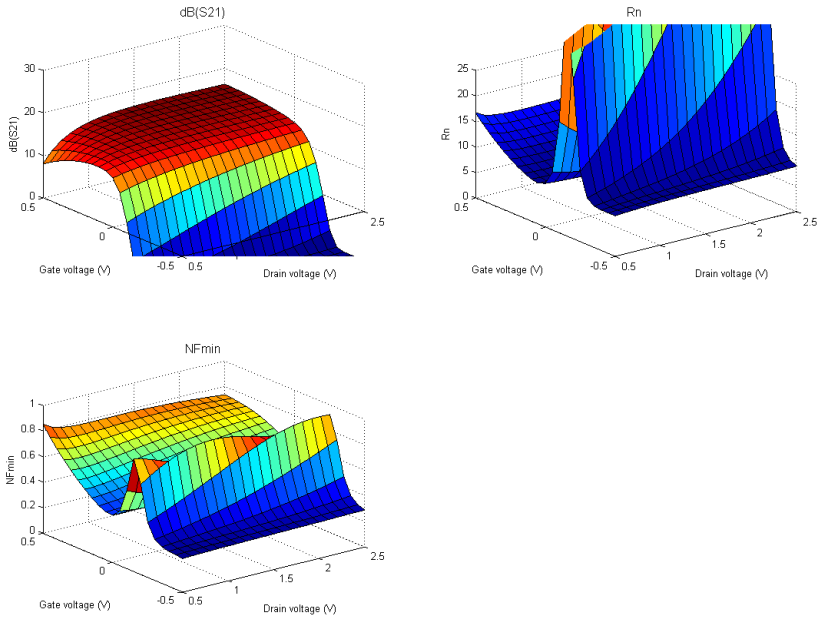

Figure 4.19: Simulated S_{21}, R_n and minimum noise figure performance of the TQP13N 4×50μm pHEMT with variation of V_d and V_g at 8.5GHz.

Two MMIC LNAs were designed using the TQP13N process in ADS software. The details of the design procedure, schematic and layouts of the MMIC LNAs are described in Sections 4.6.2 and 4.6.3. The operation frequency bands of the LNAs are 0.7-1.8GHz and 8-10GHz and are identified as "UMAN-SKAlowV1" and "UMAN8-Xband".

4.6.2 UMAN-SKAlowV1

A single ended MMIC LNA was designed to operate over the frequency range of 0.7-1.8GHz. The LNA consists of 2 stages with input and output impedances of 150Ω and 50Ω respectively. The input impedances of the LNA is determined by the output impedance of the antenna attached to the LNA while the output is connected to the subsequent amplification stages [24].

Design

The circuit design of the LNA is illustrated in Figure 4.20. The gate width dimensions of the transistors in the first and second stages are 50×6μm and 50×8μm respectively. The transistors were chosen based on a trade-off between minimum noise figure and higher gain for the LNA. The primary objective in the first stage was noise figure matching. Hence, the optimum impedance for minimum noise figure of the pHEMT was matched to a 150Ω system. The gain of the first stage was designed to be more than 10dB to minimise the effect of noise from the second stage. Linear noise models of the process were used to attain the noise matching of the LNA. An inductor and a shunt capacitor were used to achieve the noise matching in the first stage. DC block capacitors were used at the input and output of the LNA. A capacitor was used to serve the purpose of interstage decoupling. High value resistors were utilized at the gates

of the pHEMTs in the first and second stages. The high value resistance at the gates of the transistors were used to maintain the gate bias voltage (V_{gs}) and transistor gate protection. Low value resistances were used at the drains of pHEMTs in each stage to reduce the transistor gain and improve the stability in the LNA. The inductors on the DC path of the drains are used for the purpose of DC decoupling from RF path on the LNA. By pass capacitors were employed at the DC biases of the LNA to decouple the DC power supplies from the RF path of the LNA. A resistor was used to improve the output return loss of the LNA. Source inductive feedback on the first stage was used to improve the input return loss of the LNA along with achieving low noise figure by optimum noise figure matching. Source inductive feedback bring the gain and noise circles close to each other without degrading the noise performance significantly. The DC power for the gates and drains of both stages are supplied through separate channels to optimise the noise and bandwidth of the LNA during the characterisation. Functionality of individual components in the design of UMAN-SKAlowV1 is summarised in Table 4.5.

Table 4.5: Description, functions and values of components in UMAN-SKAlowV1 LNA.

Function	Components	Values
Input DC Block	C_1	3pF
Output DC Block	C_{10}	20pF
Interstage Decoupling	C_4	5pF
Noise Matching	L_1, C_2	15nH, 62fF
Impedance Matching	L_4	3nH
By-pass Capacitors	C_5, C_6, C_7, C_8	1pF, 1pF, 1pF, 1pF
Gate Resistor	R_1, R_3	7KΩ, 7KΩ
Drain Resistor	R_2,R_4	50Ω, 10Ω
RF and DC decoupling	L_3,L_5	2nH, 25nH

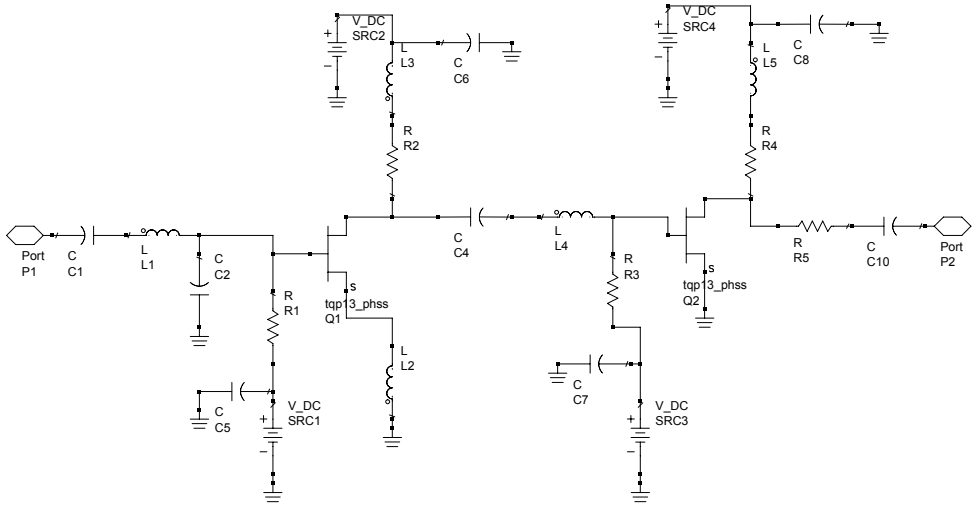

Figure 4.20: Schematic view of the UMAN-SKAlowV1 MMIC LNA.

Layout

Figure 4.21 shows the layout of UMAN-SKAlowV1 LNA with 2 stages. The dimension of the LNA is 2.4mm×1.2mm. The DC probe pads of both stages are placed on the top and bottom of the circuit for the drain and gate respectively. There are 6 probe pads for the gates and drains for on wafer measurements using the existing probe cards.

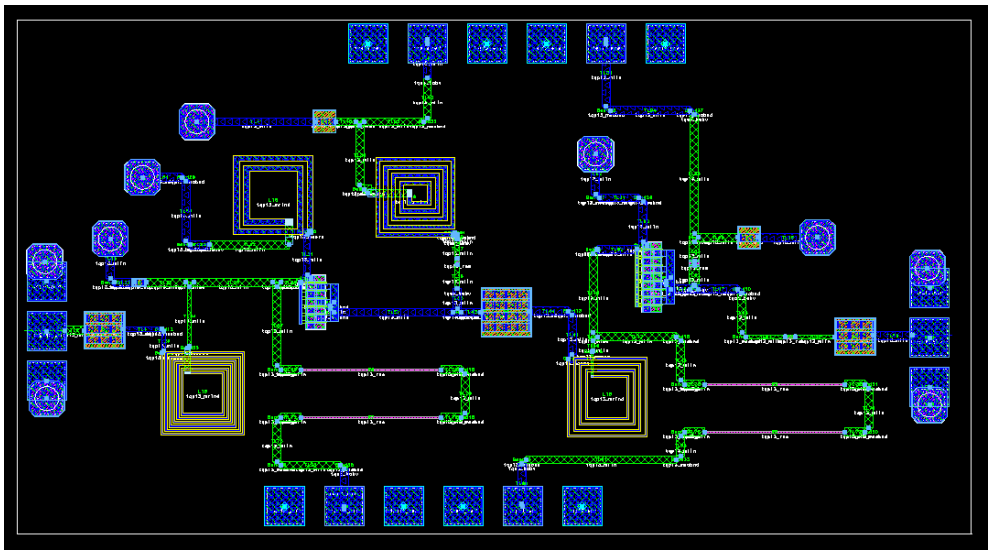

Figure 4.21: Layout of the UMAN-SKAlowV1 LNA.

4.6.3 UMAN8-Xband

Frequencies until 10GHz are covered by the SKA project. Hence a MMIC LNA was designed with TQP13N process to operate over higher frequency end of SKA in the X-band between 8GHz and 10GHz. The LNA was designed to investigate MMIC design approaches and characterisations over higher frequency bands. The wide frequency band of the LNA was selected to develop a multi-purpose LNA. Therefore, the LNA can be employed for various applications including the higher frequency ranges of SKA (8-10GHz), Satellite communications (8-8.5GHz), Radar and deep space communications [6].

The required specification of the LNA design are given in the Table 4.6. The primary objective of the LNA design was to meet and exceed the specified requirements. Hence the frequency bandwidth of the LNA with a flat and high gain was extended until 12GHz.

Table 4.6: LNA design specifications of UMAN8-Xband

Parameter	Specification
Frequency	8-10GHz
Noise Figure in 50 Ω system	<1 dB
Gain	>25 dB
Gain variation	<3 dB pk-pk
Input return loss	<-10 dB
Output return loss	<-10 dB
Nominal input/output impedance	50 Ω

Design

The schematic design of the LNA is illustrated in Figure 4.22. The LNA consists of 3 stages with input and output impedances of 50Ω. In the development of the LNA, the primary aim was to achieve a minimum noise figure with a gain of 30dB. The main objective in the second and third stages was impedance matching in order to enhance the gain of the LNA.

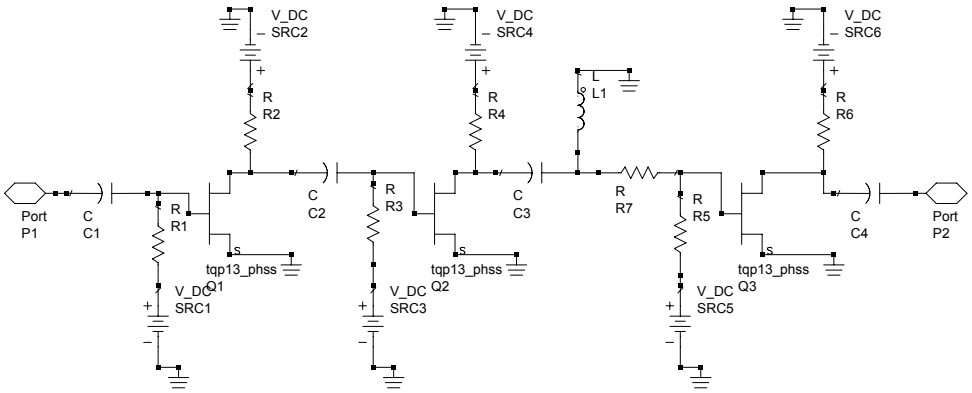

Figure 4.22: The schematic view of the UMAN8-Xband LNA.

The 3 stages of the LNA consist of pHEMTs with gate width of $50\times4\mu$m. The sizes of the transistors were chosen as a reflection between the trade-offs of the low noise, high gain, input and output impedances. In the first stage, the optimum impedance for minimum noise figure of the pHEMT was matched to a 50Ω system using the linear noise models available from the foundry. DC block capacitors were used at the input and output of the LNA. DC block capacitors were used at the input and output in the design process of the LNA. Input, output DC blocks and interstage decoupling capacitors were selected for optimisation and flatness of the gain in the LNA. A low value resistor was employed in the circuit on the RF path for the stability purpose. Resistors with high values were used at the gates of the pHEMTs in each stage of the LNA to get the exact voltage to the gate from the power supply unit and protection of the gates. Low value resistors were used at the drains of each stage. The resistors at the drains were employed to keep the gain down and assist with LNA stability. These resistors also help to achieve a broad-band response across the operational frequency band. Rollet's factor (K-factor) was utilized as an indicator for verification of unconditional stability of the LNA. By-pass capacitors were used to eliminate the feedback through the DC bias lines and maximise the stability. The capacitors are used to decouple the DC supply lines from the RF of the amplifier. Table 4.7, gives a summary of individual components function in the design of UMAN-Xband. The DC power voltages to the gate and drain of each stage was supplied through separate channels. Hence each stage is controlled separately to achieve a desirable S-parameter response and noise figure.

layout

The layout of the LNA was designed in ADS using the TQP13N process library which is illustrated in Figure 4.23. The LNA dimensions are 1.5mm×1.0mm.

Table 4.7: Description of the components, functions and the values in the UMAN8-Xband.

Function	Components	Values
Input DC Block	C_1	2pF
Output DC Block	C_4	2pF
Interstage Decoupling	C_2, C_3	2pF, 2pF
Noise Matching	C_1	2pF
Impedance Matching	L_1, C_3, R_7	0.5nH, 2pF, 15Ω
Gate Resistor	R_1, R_3, R_5	3KΩ, 1KΩ, 1KΩ
Drain Resistor	R_2,R_4, R_6	100Ω, 100Ω, 100Ω

The input and output pads of the LNA are on the left hand side and right hand side of the layout respectively. The drain and gate probe pads of the pHEMTs are located on the upper and lower parts of the LNA chip respectively.

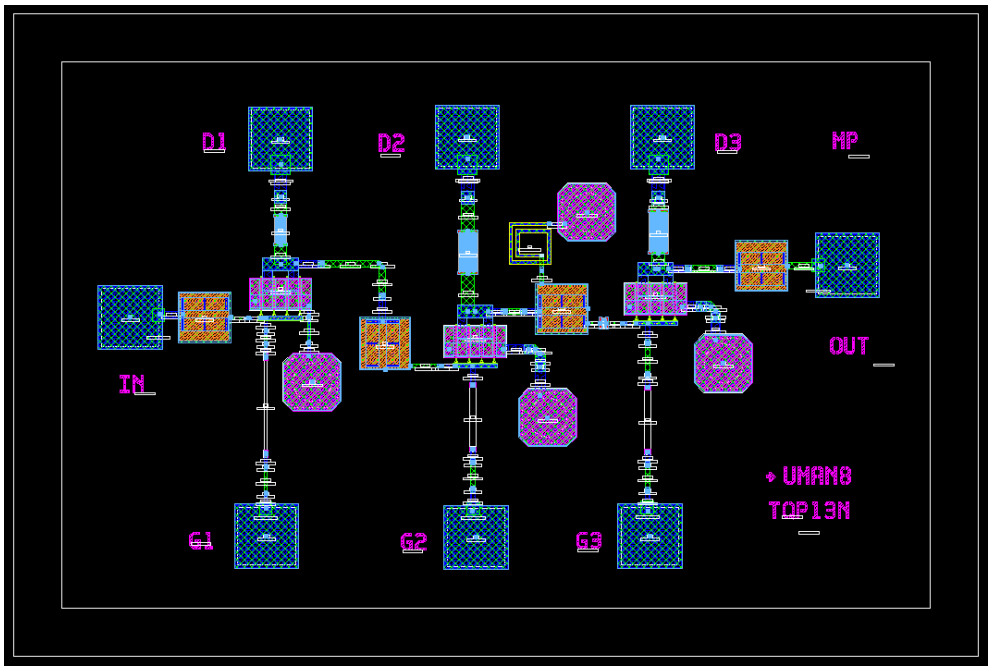

Figure 4.23: The layout of UMAN8-Xband LNA.

4.6.4 MMIC LNA Packaging

Packaging plays an important and vital role in the development of the LNAs. Therefore a complete understanding of LNA packaging aspect is required in order

to deliver a complete LNA. The housing body of the MMIC LNA enables the integration of the MMIC LNAs with other receiver subsystems. The following items must be implemented for the MMIC LNA packaging:

- Placing the Off chip components for both RF and DC
- DC connection interfaces
- Input and output microstrip lines on the the RF path
- Input and output RF interface connections
- Housing the MMIC LNA into the designated area
- Bond wire connections of the LNA with the DC and RF paths
- Gold plated DC and RF paths for the bond wiring purpose

UMAN8-Xband Packaging

An LNA board was designed using Rogers RO 4003C substrate for characterisation of the UMAN8-Xband with dimensions 18mm×22.5mm. Figure 4.24 illustrates the layout of the LNA board. There are 2 footprints for the coaxial SMA connectors on the left and right hand side of the board which include 3 pads. The middle pad of the SMA footprint is for the RF signal and the other 2 pads are connected to the ground of the LNA via the SMA body. The connections of the LNA to the RF and DC paths are through bond wires. Footprints of the bypass capacitors to decouple the DC supply lines from the RF of the amplifier were specified.

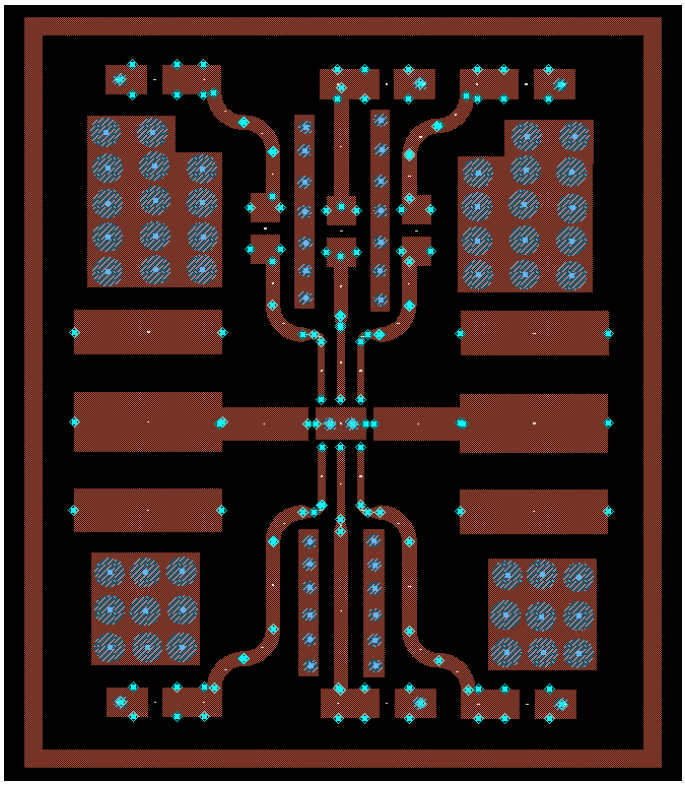

Figure 4.24: The layout of the board designed for measurement of the UMAN8-Xband LNA.

Figure 4.25 shows the designed and fabricated board for characterisation of the UMAN8-Xband. The board was designed to house the MMIC LNA chip, off chip passive components and the by pass capacitors on the DC paths. A small pad with 2 via holes is allocated for the MMIC LNA. The ground connection between the board and MMIC chip are established through the via holes on the pad allocated to the MMIC chip. The MMIC chip would be epoxied to the board using a conductive epoxy. Coaxial SMAs would be used for the RF interface connections of the board. Fifty Ω microstrip lines are used on the board for the RF connection. The DC power for all 3 stages are supplied through wires from the power supply unit. Bondwires are used to connect the RF and DC paths of the MMIC LNA and the board.

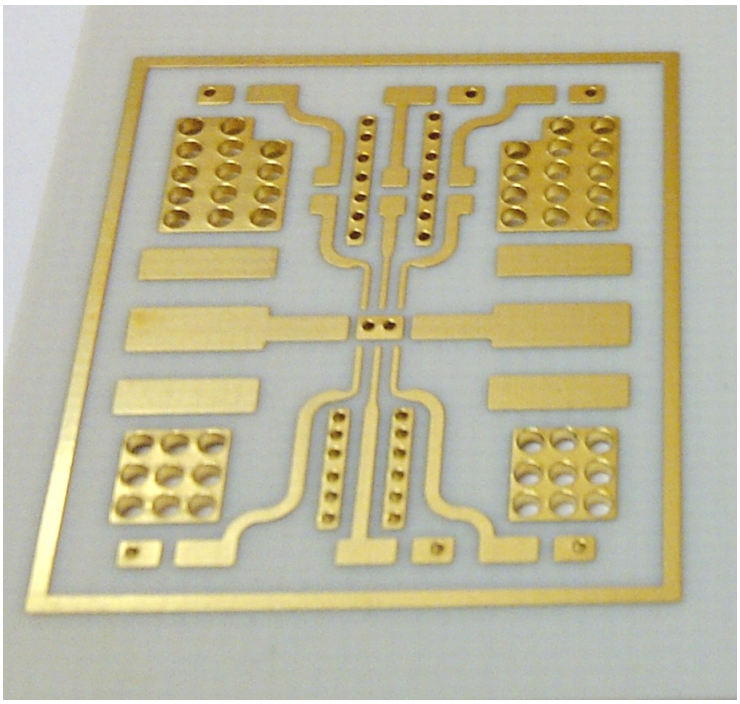

Figure 4.25: Prototype board designed for X-band LNA characterisation.

4.7 DC Bias Networks

The primary focus in the LNA designs is on the RF performance but the DC bias network plays a significant role in the LNA designs. The performance of the transistors in each stage of the LNA depends on the correct gate and drain bias voltages and currents. The bias voltages of the devices affect the S-parameter and noise figure performance in the LNAs. Consequently, the gate and drain bias voltages of each stage can be altered to obtain the optimum biases for a desired S-parameter and noise figure responses.

The DC bias circuit should provide the gate and the drain with the required voltages and the eliminate the possibilities of oscillations. DC block capacitors are implemented at the input and output of the LNAs to prevent any DC signal pass to the transistors. Therefore the DC blocks would filter out any possible DC

offset voltage at the input of the LNA. By pass capacitors are utilised in the DC bias network of the gates and the drains to remove any feedback from the DC to the RF path. The spikes produced by the power supply units are removed by the DC bias network to protect the transistors from permanent damage. Figure 4.26 illustrates the DC bias network for 1 stage in the MIC AA-lo LNA at the gate. The DC bias network of the UMAN8-Xband LNA at the gates is given in Figure 4.27.

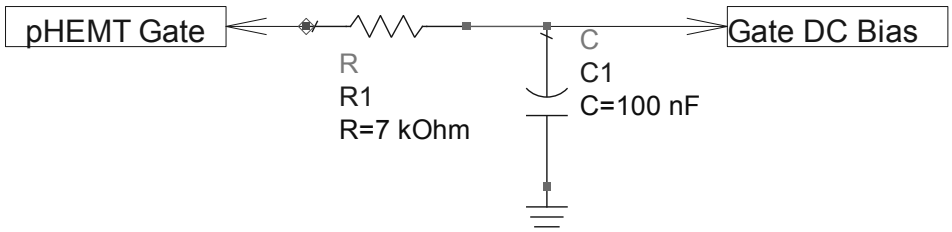

Figure 4.26: The DC bias network used for 1 stage of a MIC AA-lo LNA at the gate.

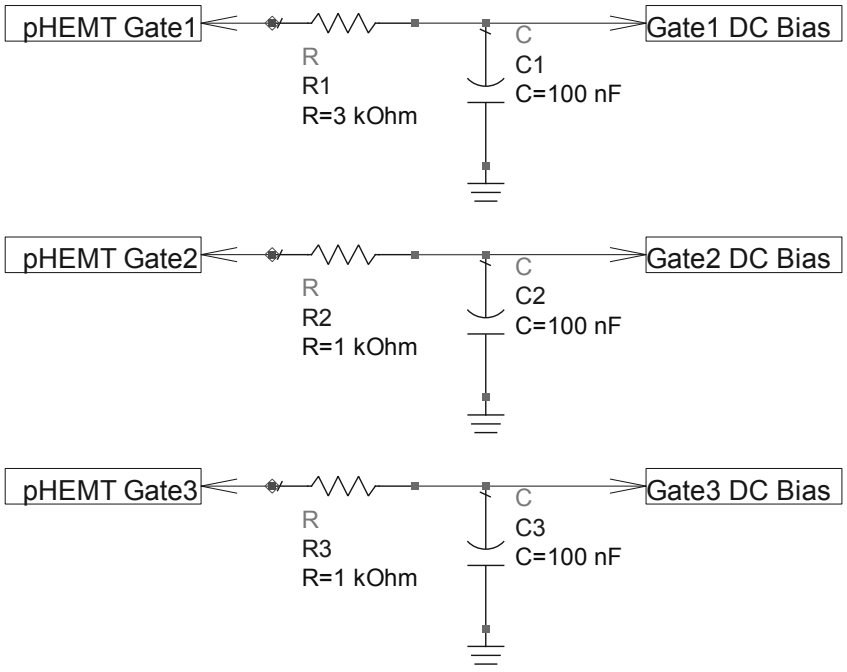

Figure 4.27: The DC bias networks used at the gates of the UMAN8-Xband MMIC LNA with 3 stages.

4.8 Summary

This chapter describes the LNA design procedure, fabrication and packaging processes. A summary of the designed LNAs, their fabrication methods, topologies and operational frequency bands is given in Table 4.8.

The schematic and layout designs of the MIC and MMIC LNAs are illustrated and explained thoroughly. The MIC LNAs were designed, fabricated and characterised for low and high frequency bands of the AA system in the SKA project which cover frequency ranges of 70-450MHz and 400-1400MHz respectively. A number of versions of LNAs were designed and fabricated for the AA system as the design evolved. The subsequent versions of the LNAs were produced not only to maintain the optimum performance parameters but also exceed the requirements where possible.

Table 4.8: Summary of the designed LNAs.

LNA Name	Fabrication technique	Topology	Frequency band
SE-AAloV1	MIC	Single Ended	70-450MHz
SE-AAloV2	MIC	Single Ended	70-450MHz
SE-AAloV3	MIC	Single Ended	70-450MHz
Diff-AAloV1	MIC	Differential input to single ended output	70-450MHz
Diff-AAloV2	MIC	Differential input to single ended output	70-450MHz
AAmidV1	MIC	Single Ended	400-1400MHz
AAmidV2	MIC	Single Ended	400-1400MHz
UMAN-SKAlowV1	MMIC	Single Ended	0.7-1.8GHz
UMAN8-Xband	MMIC	Single Ended	8-10GHz

Detailed description of 2 MMIC LNAs using TQP13N pHEMT process is given in this chapter. UMAN-SKAlowV1 LNA was designed as part of the SKA project to operate over the frequency range of 0.7-1.8GHz while multi-purpose UMAN8-Xband LNA was designed to investigate the LNA design at higher frequency end of the SKA beyond 8GHz.

Chapter 5

Measurement Bench

5.1 Introduction

This chapter describes the experimental and measurement procedures that were used for the work in this thesis. The required arrangements for DC, S-parameter and noise characterisation are explained in further detail. The on-wafer DC and S-parameter measurements of discrete transistors are explained in Section 5.2. A brief description for S-parameter and noise figure characterisation of MIC LNAs is presented in Section 5.3.

5.2 On-Wafer Transistor Measurement

This section describes the process of on-wafer DC and RF characterisation for discrete transistors. Figure 5.1 gives an illustrative view of on-wafer transistors. The RF probes are placed in the middle pad with 2 ground probes on either side. The RF probes carry the signal to the transistors as shown in Figure 5.1. The biases are supplied through the bias tees of the VNA to the RF probes.

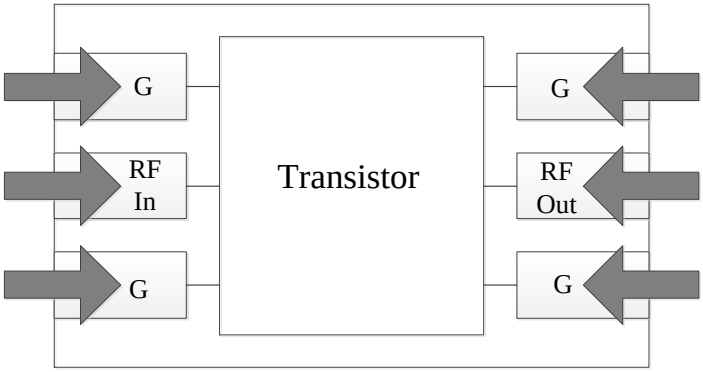

Figure 5.1: An illustrative view of an on-wafer transistor.

The on-wafer measurements of the transistors begins with the DC measurements. A comprehensive overview of all the bias points can be obtained from the DC measurements which assist in choosing the correct bias points for the S-parameter and noise figure measurements. The DC bias is provided at the gate and drain of the transistors through the RF probes at each port from the power supply. The transistors were mounted on a metal plate for the purpose of measurements. A probe station must be utilised for conducting the on-wafer transistor measurements. A wafer probe station from Cascade Microtech was used during the measurements which is compatible with 8510CXF VNA of HP. Figure 5.2 depicts the probe station used for the on-wafer characterisations.

The power is provided through the Power Supply Unit (PSU) 4142B from Agilent Technologies. The power supply is capable of supplying and measuring currents in scale of nA. A computer controls the power supply unit through a

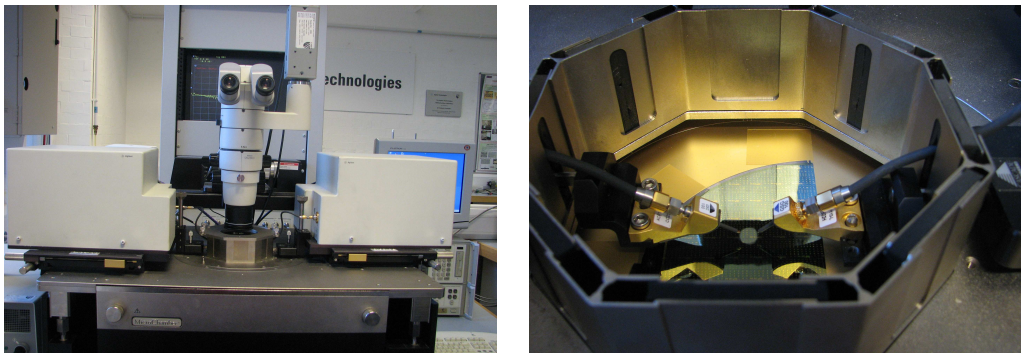

(a) Probe station. (b) Probes and the micro chamber.

Figure 5.2: Probe station for on-wafer transistor characterisation.

software. The software is Integrated Circuit Characterization and Analysis Program (ICCAP) 2009 [123]. The VNA and the power supply units are controlled and driven by ICCAP software to supply the gate and drain biases. A HP 85101C VNA was used for this purpose and it is capable of measurements up to frequency of 110GHz. The computer, VNA and the power supply are connected together via GPIB ports. Current limits were applied to the gate and drain biases to protect the transistors and the measurement devices. The current of the transistors is measured with the same power supply unit. The I-V, transconductance (g_m) curves are produced and extracted through the ICCAP software from the DC measurements. Figure 5.3 illustrates the block diagram of the experimental arrangements for the on-wafer DC and S-parameter measurements.

The experimental set up used for the S-parameter measurements is similar to the DC arrangements. The VNA, RF cables and probes must be calibrated prior to the commencement of the RF measurements. The calibration was performed with the standard LRRM (Line-Reflect-Reflect-Match) techniques by utilising the Cascade Microtech's WinCal software provided in the the computer [124].

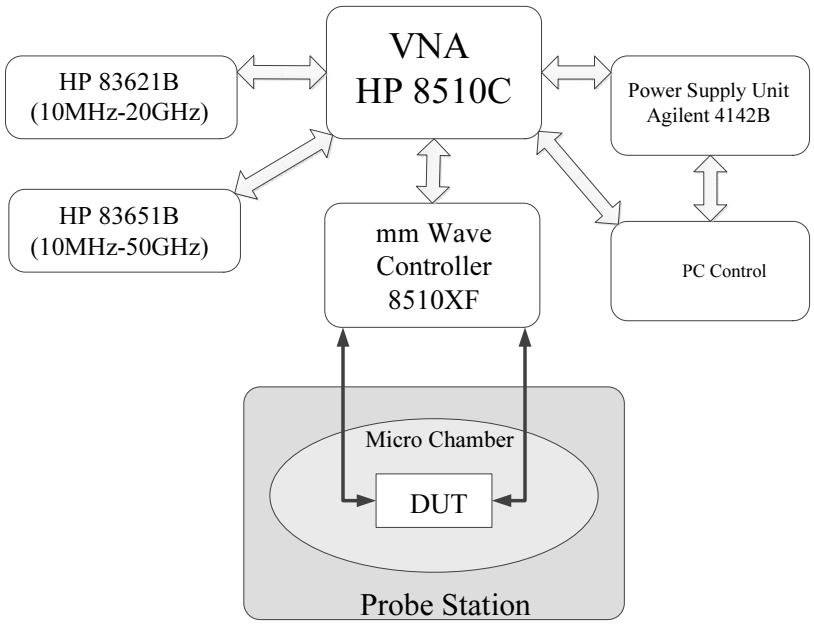

Figure 5.3: Block diagram representation of the DC and S-parameter measurement set-up for on-wafer transistors.

5.3 MIC LNAs Measurements

This section concentrates on the arrangements used for the LNA characterisations. DC and S-parameter measurements of the LNAs are essential for a full characterisation. Therefore, measurement set-up with necessary instrumentations and soft-wares are required for an accurate and repetitive measurements. Comprehensive DC, RF and noise figure measurements of the LNAs were conducted using the set up explained in this section.

5.3.1 S-Parameters

Two-port and 3-port S-parameter responses of the LNAs were measured. Two-port S-parameter measurements were carried out for the single ended input and output LNAs. Three-port mixed mode S-parameters were measured for the LNAs

with differential input and single ended output.

The S-parameters were measured using an Electronic Network Analyser (ENA) E5071B from Agilent Technologies with frequency coverage of 300kHz to 8.5GHz [110]. A picture of the ENA E5071B is presented in Figure 5.4. The ENA has 4 ports and hence multi-port S-parameter measurements are possible. The ENA calibration can be performed with SOLT (Short-Open-Line-Thru) standards or the ECal (Electronic Calibration) module.

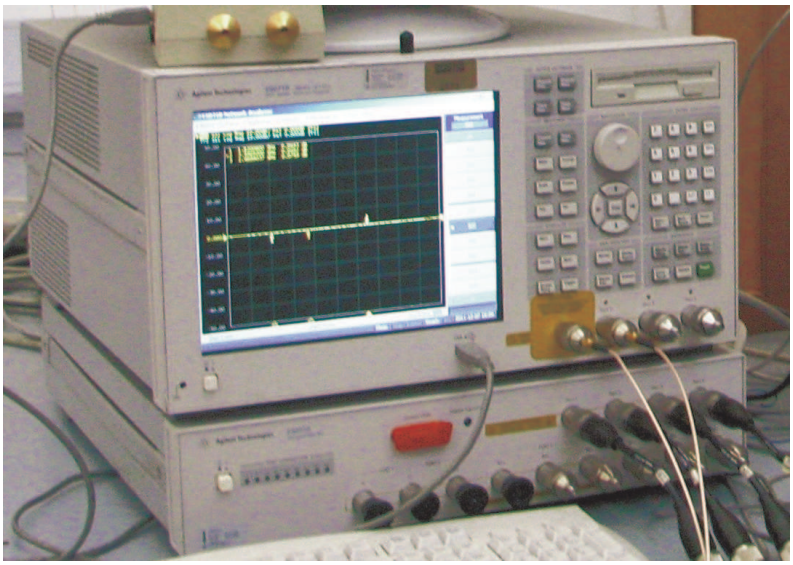

Figure 5.4: Agilent E5071B ENA.

2-Port Measurements

The 2-port S-parameter measurements were carried out for the MIC LNAs with single ended input and output. The block diagram in Figure 5.5 shows the experimental set up used for the RF characterisation of the MIC LNAs. SOLT calibration method is performed on the ENA, RF cables before commencing the measurements. DC power was supplied to the drains and gates of each stage in the LNA by accurate PSUs to ensure the safety of the active devices in the circuit. The current flow in the LNA was checked before connecting the LNA to the VNA

for safety reasons. An s2p file is generated to record the RF characterisation of the single ended LNAs.

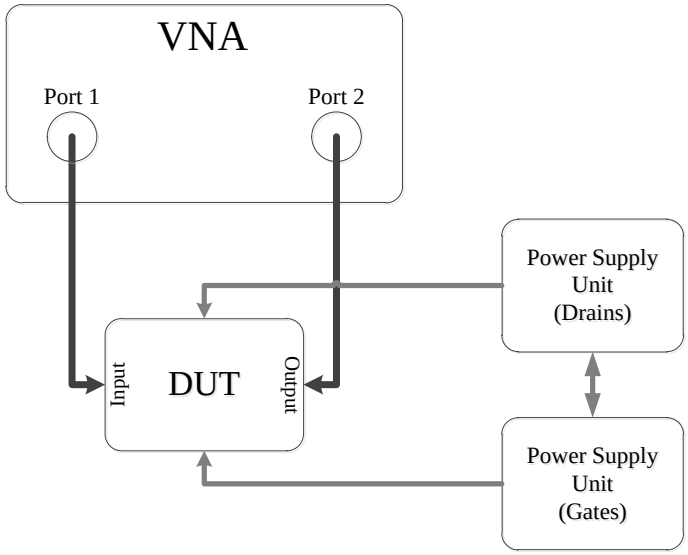

Figure 5.5: Experimental set up for the single ended LNA measurements.

3-Port Measurements

The MIC LNAs with differential input and single ended output are considered as a 3-port device. Therefore, the ENA E5071B with 4 ports must be used for the RF characterisations. Three out of 4 ports in the ENA were used for the measurements. ECal module of the ENA was utilised for the calibration of the ENA and the cables before measuring the LNA. Three-port mixed mode S-parameter measurement tool was activated for measuring the differential LNAs. The block diagram of the experimental arrangements used for conducting the 3-port mixed mode S-parameter measurements are illustrated in Figure 5.6. As shown in Figure 5.6, the gate and drain voltages of each stage in the LNA is supplied through the PSUs. The current flow of the LNAs were checked before

connecting the LNA to the ENA for the purpose of instrument protection.

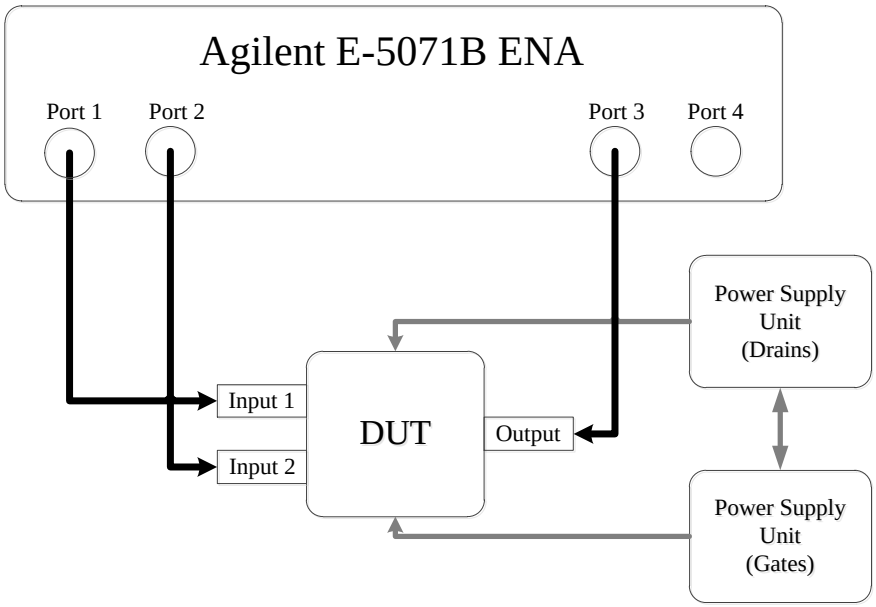

Figure 5.6: Experimental set up for differential to single ended LNA measurements.

5.3.2 Noise Figure Measurement

Figure 5.7 presents the arrangements used for the noise figure measurements of the LNAs. Noise Figure Meter (NFM) HP 8970B was used for the noise characterisation of the MIC LNAs. The NFM operates from frequency of 10MHz to 1600MHz. The NFM can be swept over the whole operating frequency or over a particular frequency range with a desirable frequency step. Noise measurements were performed using 5dB ENR noise source (346A) from Agilent Technology. For noise characterisation of the single ended MIC LNAs, the classical method of noise figure measurement was implemented. The noise figure of the differential to single ended MIC LNAs were measured by attaching the noise source to input1 of the differential inputs and grounding the input2. The measurements were

repeated with similar set-up by swapping the noise source and ground to the input2 and input1 respectively.

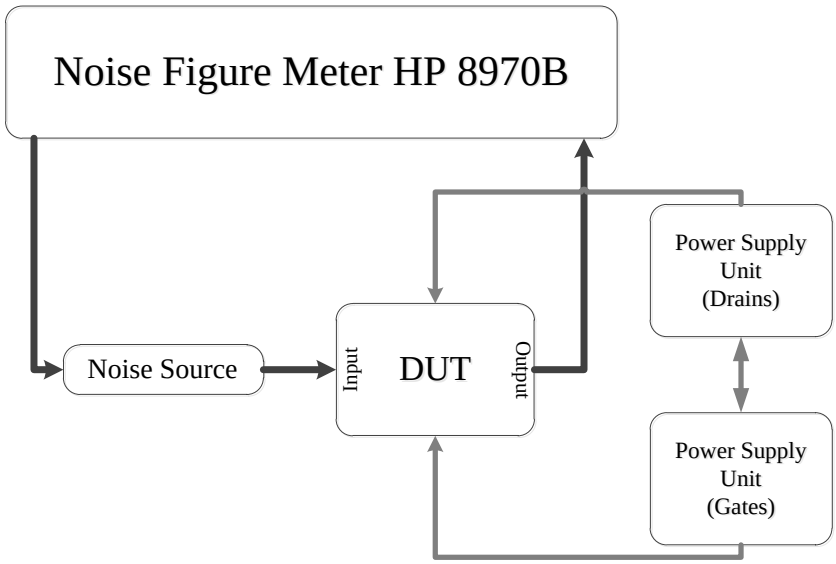

Figure 5.7: Block diagram of the noise figure measurements for MIC LNAs.

5.4 Summary

The details of experimental set up used in the research work presented in the thesis is given in this chapter. A comprehensive description of the instruments and their arrangements for each type of measurement are given in this chapter. The DC and S-parameter measurements set up of the on-wafer transistors and MIC LNAs are explained. The noise figure measurement set up and process is described for the MIC LNAs.

Chapter 6

Results and Analysis

This chapter discusses the performance of TQP13N GaAs pHEMTs of TriQuint Semiconductors. Section 6.1 describes and analyses the simulated and measured DC and S-parameter characteristics of the pHEMTs in detail. A summary of the LNAs, of which the simulated and measured performance explanation and analysis is accounted for in this Chapter is given in Section 6.2. The performance of the LNA includes both the S-parameter and noise figure characterisation. Two MIC LNAs were designed and characterised for operation at frequency ranges of AA-lo and AA-mid in the SKA project which cover the bands of 70-450MHz and 400-1400MHz respectively. Single ended and differential configurations of the AA-lo LNAs are described and analysed in Sections 6.3.1 and 6.3.2 respectively. AA-mid LNAs have single ended configurations and are focused on and studied in detail in Section 6.4. Avago ATF-58143 pHEMTs were used to design and develop the MIC LNAs. The simulated S-parameter and noise figure responses of 2 MMIC LNAs designed using TQP13N process are illustrated in this chapter. The MMIC UMAN-SKAlowV1 LNA was designed to perform over frequency band of 0.7-1.8GHz as part of the MMIC SKA LNA design study which is described and analysed in Section 6.5. UMAN8-Xband is a multi-purpose MMIC LNA designed

for operation at 8-10GHz as part of the LNA design considerations for the SKA high ended frequency band of operation where the analysis and explanation is given in Section 6.6.

6.1 Transistor Measurements

This section focuses on the results obtained from the simulations and measurements of four TQP13N pHEMTs which are discussed in the subsequent subsections.

6.1.1 TQP13 pHEMTs

This section describes the DC characteristics and S-parameter responses of the low noise D-mode GaAs pHEMTs of the TQP13N process of TriQuint Semiconductors. The measured TQP13N pHEMTs have gate length of 130nm and gate widths of $4 \times 25\mu m$, $4 \times 50\mu m$, $4 \times 75\mu m$ and $4 \times 100\mu m$. The room temperature measurements of the pHEMTs were conducted using a HP VNA 8510C and 4200 PSU from Agilent Technology. The drain current (I-V), transconductance (g_m) curves and S-parameter responses of pHEMTs are discussed in more detail in the following sections.

DC characterization of TQP13 D-mode pHEMTs

DC sweeps of V_g and V_d used for TQP13N d-mode pHEMT measurements are given in Table 6.1. The DC characterization of the TQP13N pHEMTs with gate widths of $4 \times 25\mu m$, $4 \times 50\mu m$, $4 \times 75\mu m$ and $4 \times 100\mu m$ were carried out by sweeping V_d and V_g from 0v to 2V and -0.4V to 0.6V respectively for all the pHEMTs. The measured DC characteristics of the devices are presented in the following subsections accompanied with a detailed analysis.

Table 6.1: DC sweeps used for TQP13N pHEMTs characterisation.

pHEMT	V_g	V_d
$4 \times 25\mu m$	(-0.4) to (0.6)V	$0 - 2$V
$4 \times 50\mu m$	(-0.4) to (0.6)V	$0 - 2$V
$4 \times 75\mu m$	(-0.4) to (0.6)V	$0 - 2$V
$4 \times 100\mu m$	(-0.4) to (0.6)V	$0 - 2$V

.

DC characteristics of $4 \times 25\mu m$ pHEMT

The normalised drain current of the device is up to 500mA as shown in Figure 6.1a while the normalised maximum peak g_m of the pHEMT is 823.0mS/mm with V_g of 200mV which is illustrated in Figure 6.1b.

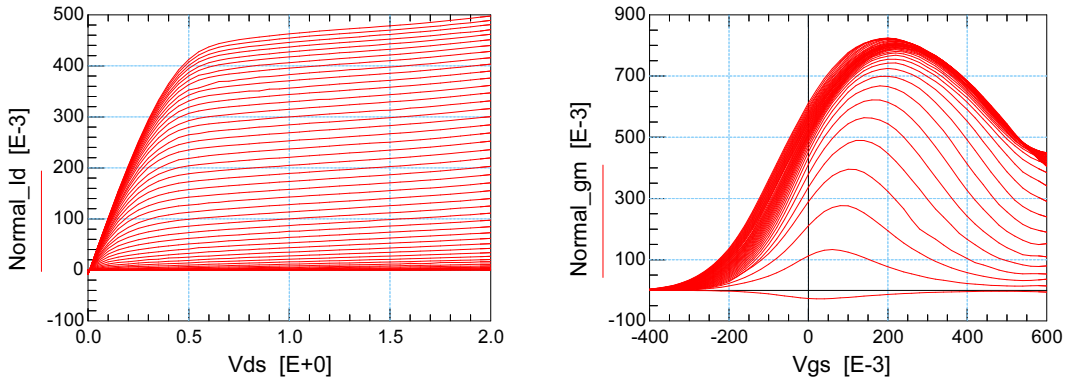

(a) $I_d - V_d$ curve with I_d in mA/mm and V_{ds} in V; V_{gs} from -0.4V to 0.6V.

(b) g_m curve with g_m in mS/mm and V_{gs} in mV; V_{ds} from 0 to 2V.

Figure 6.1: DC measurements of TQP13N pHEMT with gate width of $4 \times 25\mu$m.

DC characteristics of $4 \times 50\mu m$ pHEMT

Figure 6.2a illustrate the normalised I-V curves of the pHEMT with respect to the gate width with drain current variations up to 405mA. The normalised g_m curves are shown in Figure 6.2b where the maximum peak g_m of the device is

668mS/mm with V_g of 200mV.

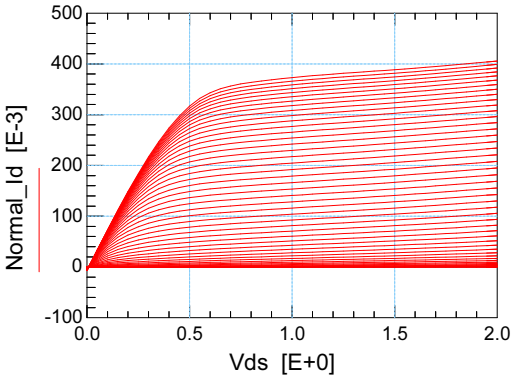

(a) $I_d - V_d$ curve with I_d in mA/mm and V_{ds} in V; V_{gs} from -0.4V to 0.6V.

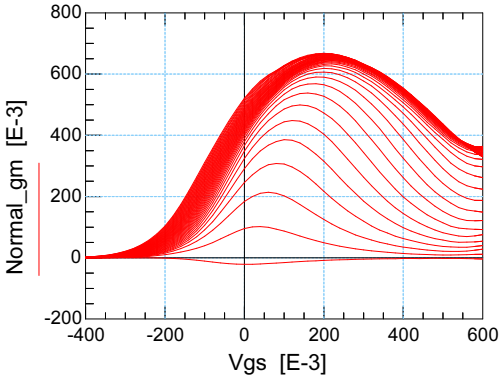

(b) g_m curve with g_m in mS/mm and V_{gs} in mV; V_{ds} varies from 0 to 2V.

Figure 6.2: DC measurements of TQP13N pHEMT with gate width of $4 \times 50\mu$m.

DC Characteristics of $4 \times 75\mu m$ pHEMT

The normalised I-V and g_m curves of the pHEMT with respect to the gate width are illustrated in Figure 6.3a and Figure 6.3b. Maximum peak g_m of the pHEMT is 686.5mS/mm when V_g is 200mV with drain currents of up to 410mA.

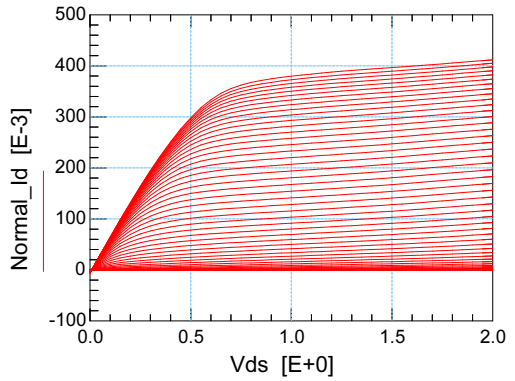

(a) $I_d - V_d$ curve with I_d in mA/mm and V_{ds} in V; V_{gs} from -0.4V to 0.6V.

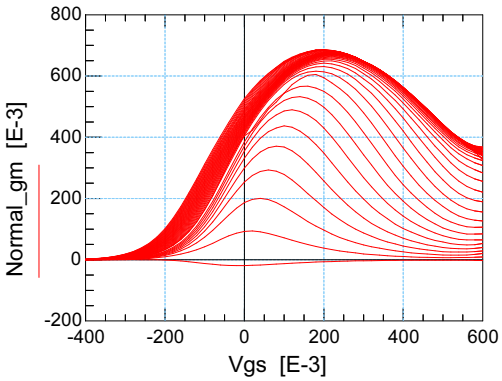

(b) g_m curve with g_m in mS/mm and V_{gs} in mV; V_{ds} from 0 to 2V.

Figure 6.3: DC measurements of TQP13N pHEMT with gate width of $4 \times 75\mu$m.

DC Characteristics of $4 \times 100\mu m$ pHEMT

The measured and normalised I-V curves of the devices which shows drain currents of up to 393mA is shown in Figure 6.4a. The measured g_m curves of the pHEMT are normalized with respect to the gate width and are presented in Figure 6.4b. Maximum peak g_m of the device is 652mS/mm with V_{gs} of 200mV.

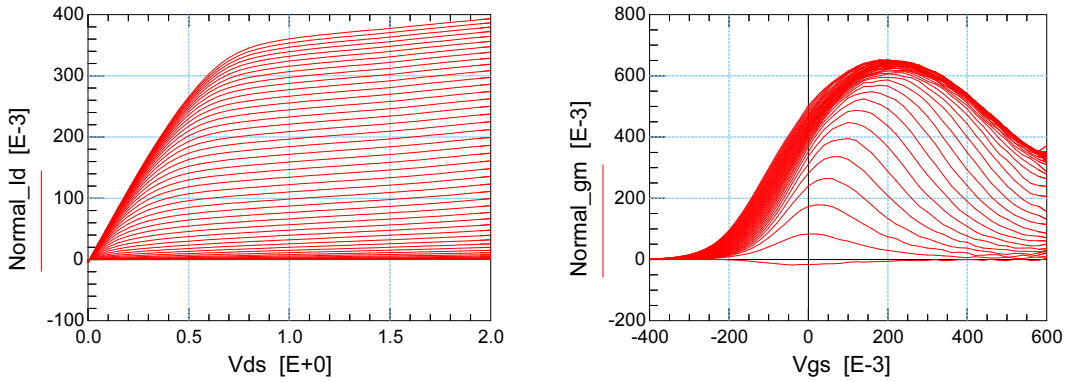

(a) $I_d - V_d$ curve with I_d in mA/mm and V_{ds} in V; V_{gs} from -0.4V to 0.6V.

(b) g_m curve with g_m in mS/mm and V_{gs} in mV; V_{ds} from 0 to 2V.

Figure 6.4: DC measurements of TQP13N pHEMT with gate width of $4 \times 100\mu$m.

Summary of pHEMT DC Characteristics

Table 6.2 summarises peak g_m values of each pHEMT, the corresponding drain voltages, gate voltages and drain currents along with the calculated power consumption of each device. The maximum normalised drain current of the 4×25 μm device is 500mA/mm while that of the rest of the devices is 400mA/mm, which is 25% less. The measured normalised transconductance of pHEMT with gate width dimension of 4×25 μm is 823mS/mm while that of the rest of the devices is about 660mS/mm. This implies that the normalised peak transconductance of the smallest pHEMT is about 25% more than the larger devices. From Tables 6.2 and 6.3, it is also apparent that V_{gs} bias voltages of all the devices are

same to achieve peak g_m. The V_{gs} to achieve minimum noise figure for all the devices are also same. The V_{gs} for minimum noise bias is 0.2V lower than that for peak g_m bias. From the behaviour of the drain current and g_m along with the biases for minimum noise figure it can be inferred that the smaller devices have lower minimum noise figure than the bigger devices. This particular inference from the measured data is very important for LNA designs with TQP13N pHEMTs at different frequency bands because although smaller transistors are suitable for LNA designs at high frequencies they are impractical to implement in a low frequency LNA design. The normalised power consumption decreases from 0.39W to 0.32W for achieving minimum noise figure as the transistors size increases according to Table 6.2 and this aspect can also be verified from the I-V and g_m characteristics. This reduction from data also establishes that for SKA AA system, which range from 70MHz to 1.4GHz, larger transistors can be employed with significant decrease in normalised drain current to bias the transistor for minimum noise figure.

Table 6.2: Summary of the DC characteristics of TQP13 pHEMTs.

pHEMT Size	Normalised Peak g_m	V_g of Peak g_m	V_d of Peak g_m	I_d of Peak g_m	Power
$4 \times 25\mu m$	823.0mS/mm	0.2V	1.75V	226.3mA	0.39W
$4 \times 50\mu m$	668.0mS/mm	0.2V	1.90V	191.8mA	0.36W
$4 \times 75\mu m$	686.0mS/mm	0.2V	1.80V	190.3mA	0.34W
$4 \times 100\mu m$	652.0mS/mm	0.2V	1.80V	180.4mA	0.32W

S-parameter Responses of TQP13 D-mode pHEMTs

The S-parameter responses of TQP13N D-mode pHEMTs at room temperature were measured using a HP 8510A VNA. The S-parameter responses were measured from 0.5GHz to 70GHz. The bias points for S-parameter measurements of

pHEMTs were selected for the lowest minimum noise figure which are outlined in Table. 6.3. The comparative analysis of the simulated and measured S-parameter responses of the pHEMTs are discussed in this section.

Table 6.3: Bias Points of TQP13 D mode pHEMTs for S-Parameter measurement.

pHEMT	V_g	V_d
$4 \times 25\mu m$	0.02V	0.50V
$4 \times 50\mu m$	0V	0.45V
$4 \times 75\mu m$	0V	0.55V
$4 \times 100\mu m$	0V	0.55V

S-parameter Response of $4 \times 25\mu m$ pHEMT

Figure 6.5a and Figure 6.5b show the measured and simulated S-parameter responses of the $4 \times 25\mu m$ pHEMT respectively. As illustrated in Figure 6.5a, the output return loss is lower than -2.5dB over the whole frequency range of measurement while the input return loss is lower than -2dB over frequency range of 20-72.5GHz. The S_{21} is higher than 10dB and 5dB at frequencies of 5GHz and 20GHz respectively. The simulated S-parameter performance of the pHEMT is shown in Figure 6.5b. The S_{21} of the pHEMT is greater than 10dB for frequencies up to 18GHz and more than 5dB between frequencies of 18GHz and 24GHz. The simulated output return loss is less than -10dB from 9GHz to 72.5GHz. The input return loss is lower than -1.5dB over the whole frequency range of simulation. From Figure 6.5a and Figure 6.5b, it is established that the measured S-parameter response of the transistor is not significantly different from the simulated counterpart over the complete frequency band.

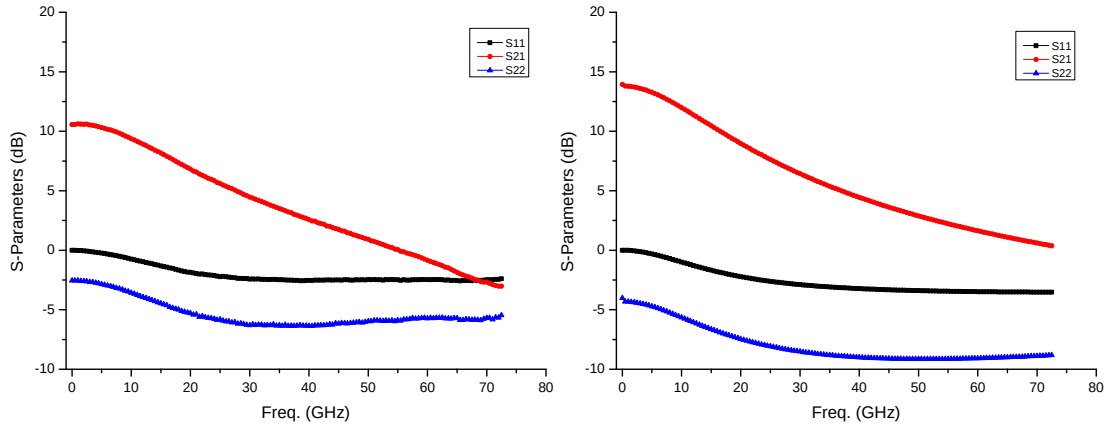

(a) Measured (b) Simulated

Figure 6.5: S-parameter responses of TQP13N pHEMT with gate width of $4 \times 25\mu m$.

S-parameter Responses of $4 \times 50\mu m$ pHEMT

Figure 6.6a and Figure 6.6b illustrate the measured and simulated S-parameter responses of the $4 \times 50\mu m$ pHEMT over the frequency range of 0.5-72.5GHz respectively. As shown in Figure 6.6a, the output return loss of the pHEMT is lower than -4.2dB over the whole frequency range of measurement while the input return loss is less than -2dB from frequency range of 10GHz until 72.5GHz. S_{21} of greater than 18dB and 6dB were measured for frequencies up to 2.5GHz and 20GHz respectively. Figure 6.6b shows the simulated S-parameters of the pHEMT. Simulated output return loss of the pHEMT is lower than -6dB over the whole frequency range. The simulated input return loss is similar to the measured results. Gain of the pHEMT is more than 15dB up to frequency of 6GHz and higher than 23dB at lower frequency ranges as shown in Figure 6.6b. The measured S_{21} at low frequencies is about 5dB lower than that simulated results from the design kit.

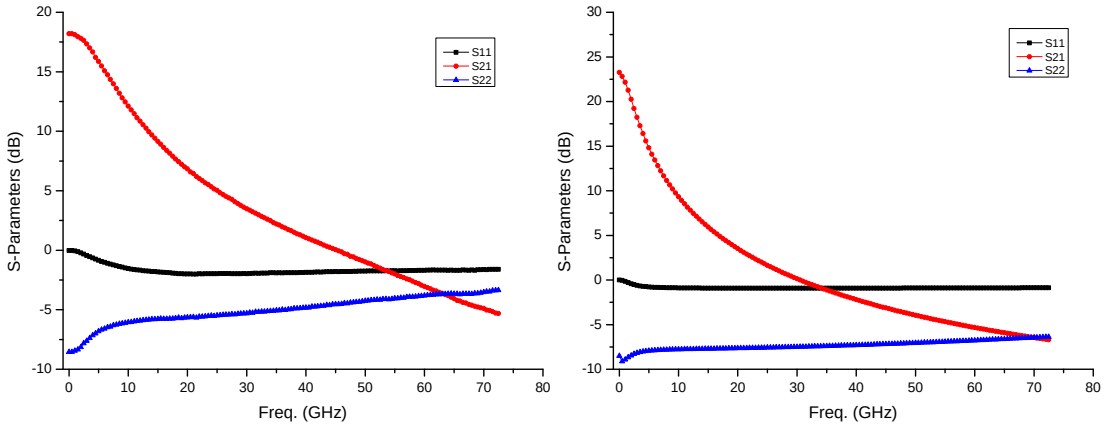

(a) Measured (b) Simulated

Figure 6.6: S-parameter responses of TQP13N pHEMT with gate width of $4 \times 50\mu m$.

S-parameter Response of $4 \times 75\mu m$ pHEMT

Measured and simulated S-parameter responses of a $4 \times 75\mu m$ pHEMT are illustrated in the Figures 6.7a and 6.7b respectively, over the frequency range of 0.5-72.5GHz. The output return loss was measured to be less than -4dB over the whole frequency range while the input return loss of the device is lower than -1.5dB over the frequency range of 5 to 72.5GHz. The S_{21} is greater than 12dB up to frequency of 7.5GHz and more than 4dB up to 20GHz. Figure 6.7b shows the simulated S-parameter responses of the pHEMT with output return loss of lower than -5dB over the whole frequency band. However, the input return loss is consistent with the measured responses and is lower than -1.5dB across the whole frequency band. Gains of more than 10dB were achieved up to 6GHz with high gain of more than 22dB for frequencies up to 2GHz. Like the 4×50 μm device, this device also has a measured S_{21} of 5dB lower than that simulated at low frequencies.

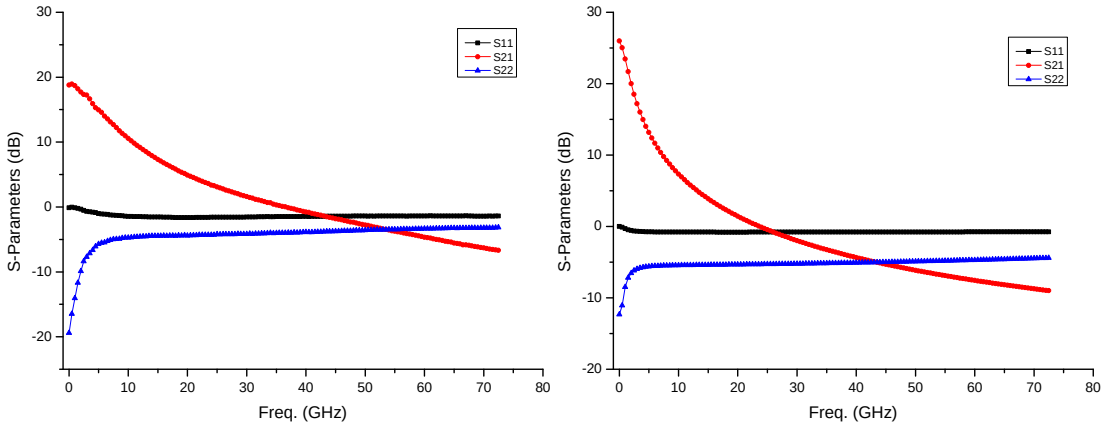

(a) Measured (b) Simulated

Figure 6.7: S-parameter responses of TQP13N pHEMT with gate width of $4 \times 75\mu m$.

S-Parameter Response of $4 \times 100\mu m$ pHEMT

Figures 6.8a and 6.8b illustrate the measured and simulated S-parameter responses of a $4 \times 100\mu m$ device respectively, between frequencies of 0.5GHz and 72.5GHz. The output return loss was measured to be less than -3dB over the whole frequency range while the input return loss is less than -1dB from 5GHz to 72.5GHz. The S_{21} is higher than 16dB and 4dB up to frequencies of 5GHz and 20GHz respectively. The simulated output return loss of the pHEMT is lower than -4dB over the whole frequency band while the input return is -1.5dB as shown in Figure 6.8b. The simulated S_{21} of the pHEMT is greater than 20dB up to frequency of 1.5GHz.

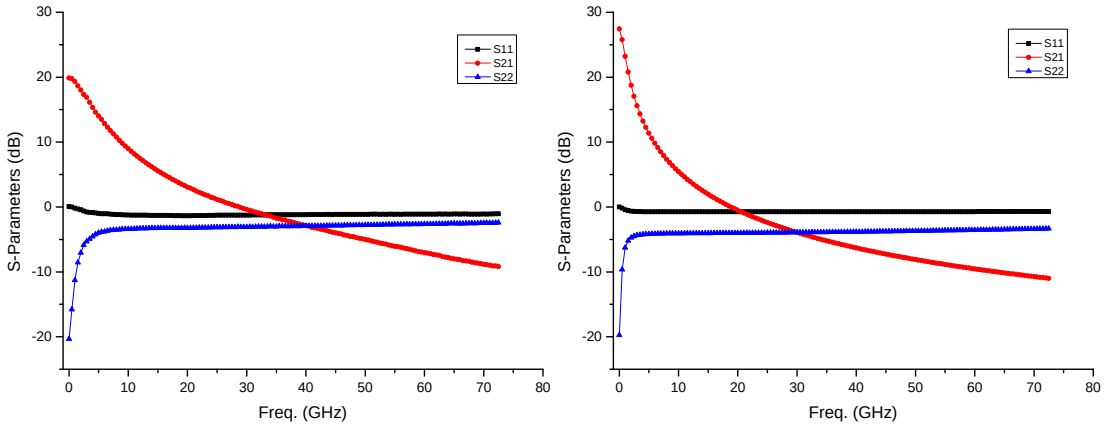

(a) Measured (b) Simulated

Figure 6.8: S-parameter responses of TQP13N pHEMT with gate width of $4 \times 100\mu m$.

TQP13N D-Mode pHEMT Analysis

SKA AA system requires a GaAs HEMT process which does not have only high reliability and repeatability but also is cost effective and low noise. The purpose is to manufacture tens of millions of LNAs with same response which will make the front end and hence the system stable and reliable. This requires a commercial process which has a high volume wafer roll out per annum with very competitive low noise performance. TQP13N is a process which displays very low noise performance with commercial usage and high volume wafer roll out. Thus the transistors of TQP13N process are used for purposes of evaluation and MMIC LNA designs in this thesis.

DC and S-parameter performance of the TQP13-N pHEMTs with gate width dimensions of 100μm, 200μm, 300μm and 400μm are analysed in detail here. The 4×25μm pHEMT has a normalised minimum value of $\sqrt{I_d}/g_m$ parameter of 0.457 at a DC bias of V_{ds}=0.5V and V_{gs}=0.02mV. According to Pospieszalski [96], the pHEMT will have a minimum noise figure at this bias. The corresponding

normalised g_m of the device at this bias is 525mS/mm. The value of peak g_m is 820mS/mm and this occurs at V_{gs} of 0.2V. Thus the transconductance of the pHEMT at minimum noise bias is 64% of peak g_m. The drain current of the transistor at this bias is 5mA which is less than 20% of the saturation current at the same V_{ds}. The minimum noise figure of the pHEMT at minimum noise bias is 0.35dB at 10GHz while at 70GHz it is 1.85dB with maximum stable gain of 16dB and 4dB at 10GHz and 70GHz respectively. This data portray that substantial gain, above 10dB, can be extracted from the pHEMT at 10GHz even at minimum noise figure bias which will ensure the minimisation of noise contribution from the subsequent stages. The maximum stable gain of the pHEMT at peak g_m bias is 25dB at 10GHz and that at 70GHz is 12dB which indicates that more than 30dB stable gain can be obtained from a 3-stage wideband LNA at X-band.

The 4×50μm pHEMT has a normalised minimum value of $\sqrt{I_d}/g_m$ parameter of 0.489 at a DC bias with V_{ds} of 0.45V and V_{gs} of 0V. The value of the parameter for the current device is lower than the $4 \times 25\mu$m device. The corresponding normalised g_m of the device at this bias is 399mS/mm. The value of peak g_m is 668mS/mm with a V_{gs} of 0.2V. Therefore the transconductance value of the pHEMT at minimum noise bias is 60% of the value of peak g_m. The drain current of pHEMT at this bias is 7mA which is less than 16% of the saturation current at the same V_{ds}. The minimum noise figure of the transistor at minimum noise bias is 0.43dB at 10GHz while at 70GHz is 2.25dB with maximum stable gains of 16dB and 4dB at 10GHz and 70GHz respectively. The data show that a substantial gain of above 10dB can be extracted from the HEMT at 10GHz even at minimum noise figure bias which ensures the minimisation of noise contribution from subsequent stages. The maximum stable gain of the pHEMT at peak g_m bias is 28dB at 10GHz and 14dB at 70GHz. This data show that $4 \times 25\mu$m device has less noise figure than a 4×50μm HEMT. Corresponsdingly its normalised peak g_m is also

higher which is also reflected in the maximum stable gain calculated at the bias of peak g_m.

The 4×75μm pHEMT has a normalised minimum value of $\sqrt{I_d}/g_m$ parameter of 0.482 at a DC bias of V_{ds}=0.55V and V_{gs}=0V. The corresponding normalised g_m of the device at this bias is 405.7mS/mm. The peak g_m of the transistors is 686mS/mm occurring at V_{gs} of 0.2V. Thus the transconductance of the pHEMT at minimum noise bias is 60% of peak g_m. The drain current of transistor at this bias is 11mA and that is 15% of the saturation current at the same V_{ds}. The minimum noise figure of the transistor at minimum noise bias is 0.53dB at 10GHz while at 70GHz is 2.75dB with maximum stable gains of 25dB and 10dB at 10GHz and 70GHz respectively. According to this data substantial gain of more than 10dB can be extracted from the pHEMT at 10GHz even at minimum noise figure bias which will minimise the noise contribution from subsequent stages. The maximum stable gain of the HEMT at peak g_m bias is 34dB at 10GHz and 17dB at 70GHz. The minimum noise figure of the device is higher than its smaller counterparts discussed previously with the exception that the value of the parameter postulated by [96] is lower than the 4×50μm HEMT. The maximum stable gain of the device is higher than the previous devices at both 10GHz and 70GHz.

The 4×100μm pHEMT has a normalised minimum value of $\sqrt{I_d}/g_m$ parameter of 0.500 at a DC bias of V_{ds}=0.55V and V_{gs}=0V. The corresponding normalised g_m of the device at this bias is 391mS/mm. The value of peak g_m is 652mS/mm and occurring at a V_{gs} of 0.2V. Hence the transconductance of the transistor at the minimum noise figure bias is 60% of peak g_m value. The drain current of transistor at this bias is 14mA which is less than 16% of the saturation current at the same V_{ds}. The minimum noise figure of the transistor at minimum noise bias is 0.65dB at 10GHz while at 70GHz is 3.33dB with maximum stable gains of 25dB

and 10dB at 10GHz and 70GHz respectively. This data present that substantial gain of above 10dB can be extracted from the HEMT at 10GHz even at minimum noise figure bias which reduces the of noise contribution of the following stages. The maximum stable gain of the HEMT at peak g_m bias is 34dB at 10GHz and at 70GHz is 17dB. The minimum noise figure of this device is higher than the above which shows that the noise figure of the HEMT increases with increase in the finger width for a 4 finger device. The maximum stable gain at peak transconductance bias of the HEMT also increases with bigger gate width at both 10GHz and 70GHz. The above observations are very significant from an LNA designer's perspective as it will serve as guidance to choose the pHEMT with respect to device dimension suitable for a specific frequency of operation.

The work performed on the TQP13N pHEMTs also establishes that although the design kits are fairly accurate at high frequencies, predominantly above 5GHz, their simulated response at low frequencies deviate from the measured response for large gate width devices. TQP13 is a high frequency low noise process targeted for higher frequency LNA development preferably suitable for work above C-band. The implication is that for LNA development, design libraries for TQP13N transistors should be developed independently by the designer. This requirement is necessary for larger gate width devices which is important for SKA LNA designs.

The minimum noise figure values of the pHEMT with gate width dimensions of 4×25μm, 4×50μm, 4×75μm and 4×100μm are illustrated in Figure 6.9 at the minimum noise figure bias. The minimum noise figure of the transistors increases as the dimension of the device increases as illustrated in Figure 6.9. Hence, the size of the transistor and its corresponding noise figure value have significant importance for the minimum noise matching in the LNA design.

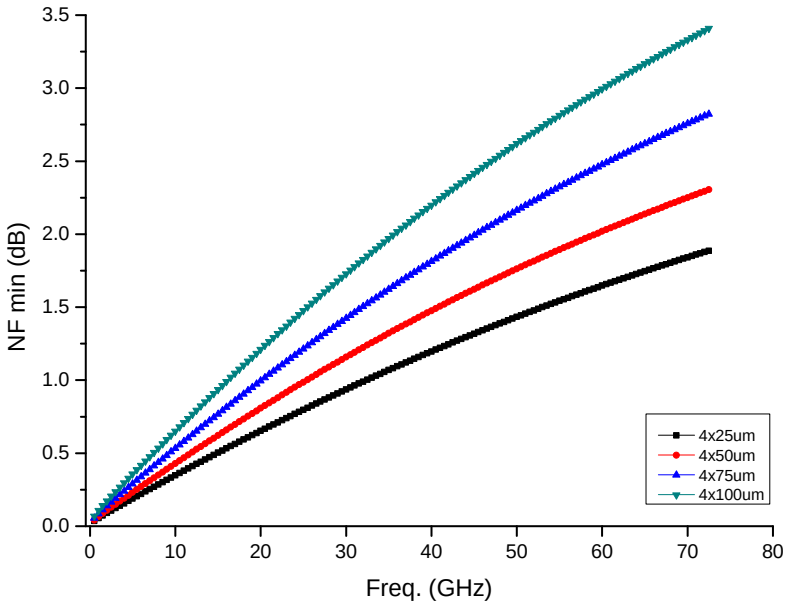

Figure 6.9: Minimum noise figure values of TQP13N pHEMTs with 4 different gate width dimensions.

Figure 6.10 shows the normalised noise resistance (R_n) values of TQP13 pHEMTs for 4 gate width dimensions. The R_n values of 4×50μm, 4×75μm and 4×100μm are less than 0.2Ω from frequency of 2GHz while the 4×25μm pHEMT has R_n values of less than 0.3Ω from frequency of 3GHz. As shown in the Figure 6.10, the normalised R_n values decreases as the sizes increases. The 4×25μm has greater normalised R_n values compared with the 4×100μm pHEMT.

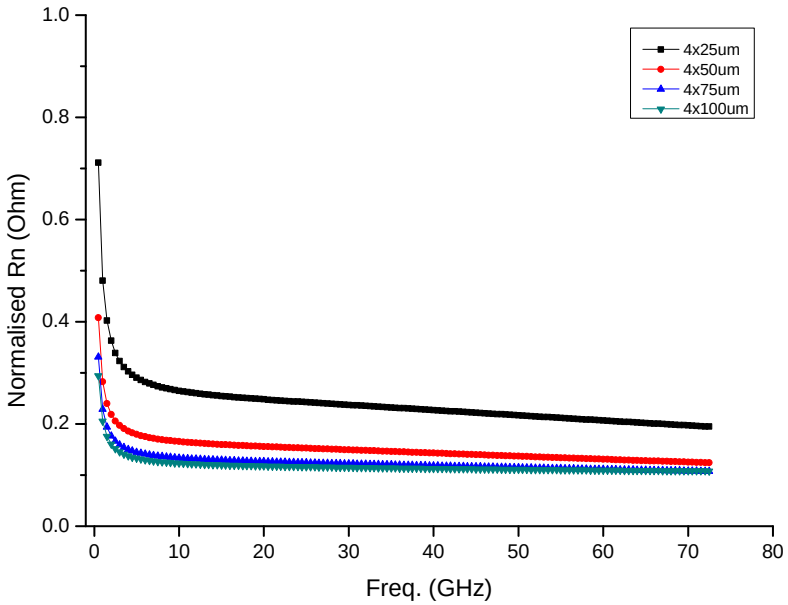

Figure 6.10: Noise resistance values of TQP13N pHEMTs with 4 different gate width dimensions.

Figure 6.11 illustrates the Γ_{opt} of the 4 sizes of the TQP13N pHEMTs from a frequency of 0.5GHz to 70GHz. The transistor sizes in Figure 6.11 are 4×25μm, 4×50μm, 4×75μm and 4×100μm. The Γ_{opt} values at 10GHz and 70GHz of the 4×50μm pHEMT are 50(1.3+j1.6) and 50(0.25+j0.2) respectively. High values of inductances are required to match the noise figure circles to Γ_{opt} at low frequencies while at high frequencies a low value inductor is required.

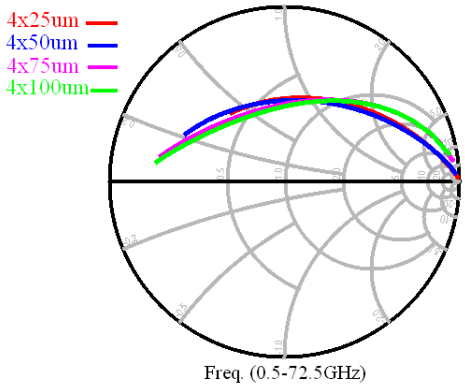

Figure 6.11: Γ_{opt} of TQP13N pHEMTs of 4×25μm, 4×50μm, 4×75μm and 4×100μm.

6.2 LNAs

The diagram depicted in Figure 6.12 is used to demonstrate the LNAs based on the fabrication techniques. The diagram illustrates the names of all the LNA designs described in Chapter 4. As shown in Figure 6.12, the MIC LNAs consist of "AA-lo" and "AA-mid" while the MMIC LNAs include "UMAN-SKAlowV1" and "UMAN8-Xband".

Section 6.3 describes and analyses the AA-lo LNAs S-parameter and noise performances, where Subsections 6.3.1 and 6.3.2 concentrate on single ended and differential LNAs respectively. The explanation of the results and analysis of the AA-mid LNAs are described in Section 6.4. The results and analysis of UMAN-SKAlowV1 and UMAN8-Xband LNAs are given in Sections 6.5 and 6.6 respectively.

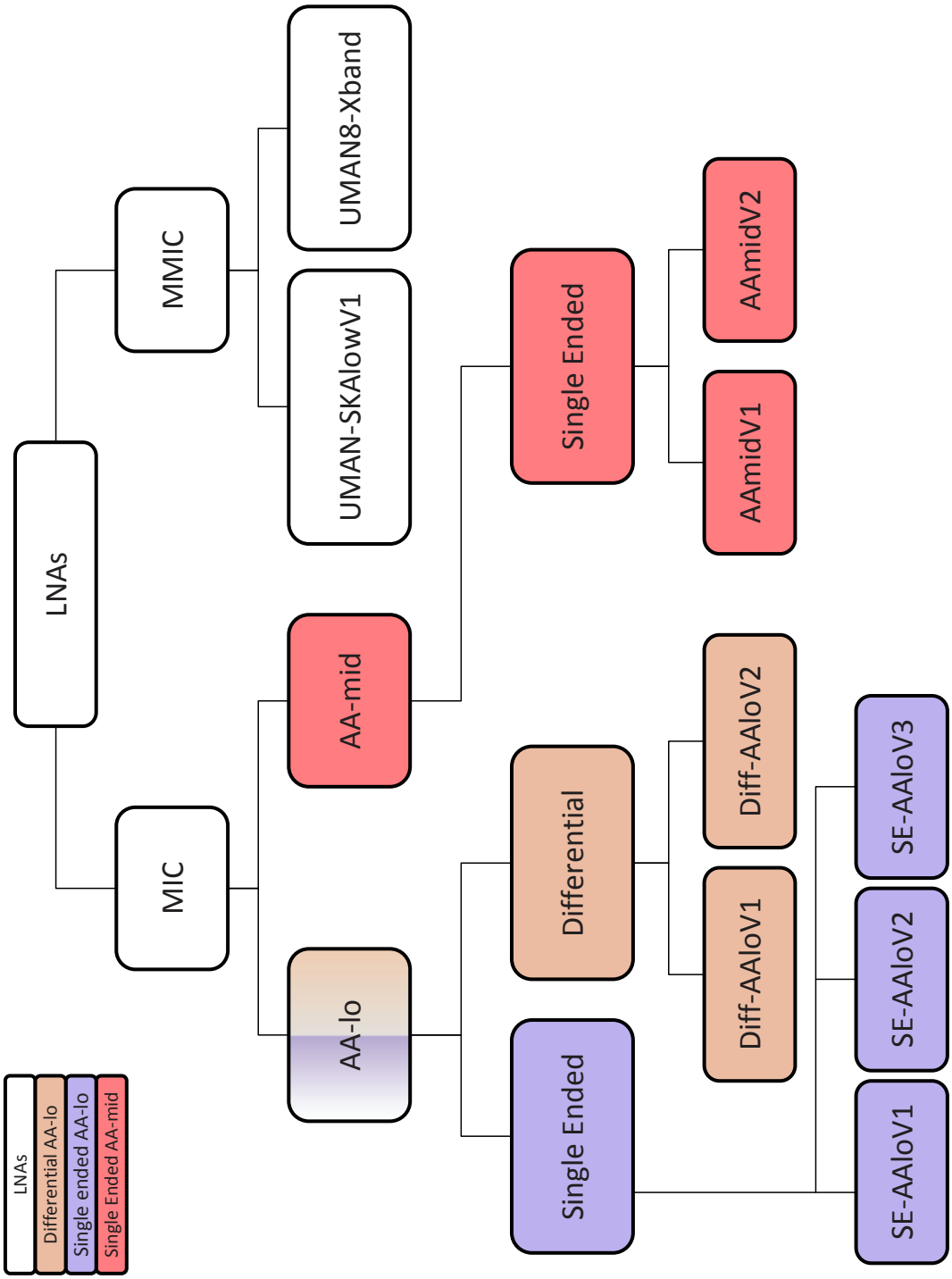

Figure 6.12: Diagram of the designed LNAs.

The noise figure/temperature of an LNA depends on the impedance of the antenna if a linearly polarized antenna is connected directly to the input of the LNA. The LNA noise figure is NF_{min} if the antenna impedance coincides with the Z_{opt} of the LNA and if the antenna impedance differs from Z_{opt}, then the LNA noise figure can be calculated from a knowledge of Z_{opt}, R_n and NF_{min} or their equivalents.

The input impedance of the LNA affects the power transfer from the antenna to the LNA and hence the gain but the signal to noise ratio is not affected which was accounted for in the noise figure described earlier. Isolators are often employed where circular polarization is received to improve the match while they are not necessary for linear polarization. The only problem caused by a poor LNA input match for linear polarization is the gain of the receiver will potentially vary with frequency because the mis-match between the antenna and LNA input varies. Gain ripples will be existent if there is a cable or other transmission lines between the antenna and LNA as the phase shift varies with frequency along the cable. Significant variations in the gain could be a problem for some systems and hence the input impedance of LNA becomes important. The input impedance of the LNA is much more important in the case of a circularly polarized antenna. As any signal from the antenna reflected from the LNA will be re-reflected from the antenna and then it can appear as if it is a signal in the opposite polarization and hence increase the cross-polarised component. In the case of linearly polarised signals, the reflected signals from the LNA can be re-reflected from the antenna contributing to the gain ripple without causing cross-polarization.

6.3 MIC AA-lo LNAs

The simulated and measured performances of 5 LNAs designed for the AA-lo system in the SKA project are discussed in this section as shown in Figure 6.12. The operational frequency band of AA-lo LNAs cover frequencies between 70MHz and 450MHz. Two topologies of single ended input and output and differential input to single ended output of AA-lo LNAs are explained in Sections 6.3.1 and 6.3.2 respectively.

6.3.1 SE-AAlo LNAs

A detailed description of simulated and measured results of SE-AAlo LNAs are given in this section. Design details of the SE-AAlo LNAs are explained in Section 4.4.1. A comprehensive explanation of measured S-parameter and noise figure responses of 3 versions of SE-AAlo LNAs named as SE-AAloV1, SE-AAloV2 and SE-AAloV3 is given in this section followed by an analysis.

SE-AAlo Simulation

The simulated S-parameter performance of the SE-AAlo LNA is shown in Figure 6.13. The output return loss of the LNA, S_{22}, is lower than -10dB over the whole frequency band while it is lower than -15dB beyond 200MHz. Furthermore, the simulations show an input return loss of -4.5dB at 480MHz. The S_{21} of the LNA is greater than 35dB up to frequency of 500MHz with maximum gain values of 38dB over the frequency range of 40MHz to 450MHz. The noise figure of the LNA is less than 0.2dB (noise temperature 14K) from 60MHz to 520MHz with a minimum noise figure of 0.17dB (12K) at 260MHz which is illustrated in Figure 6.14.

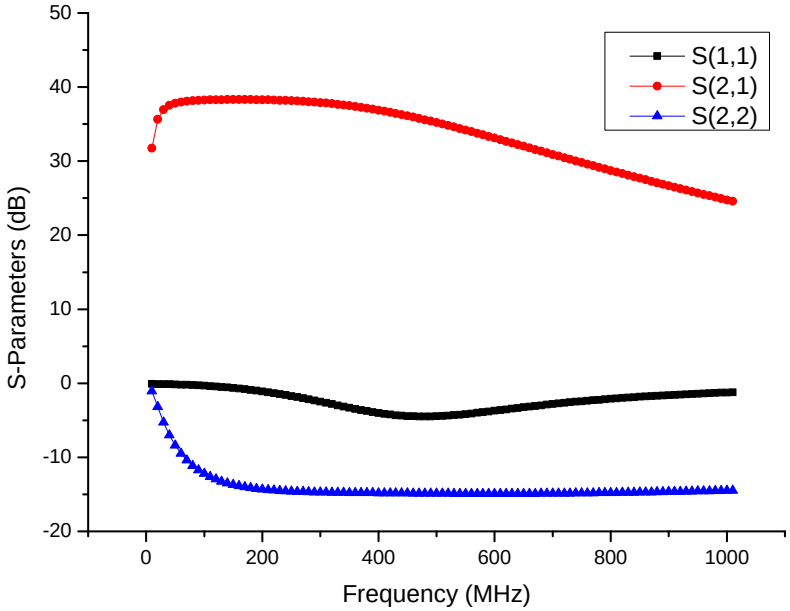

Figure 6.13: Simulated S-parameter responses of SE-AAlo.

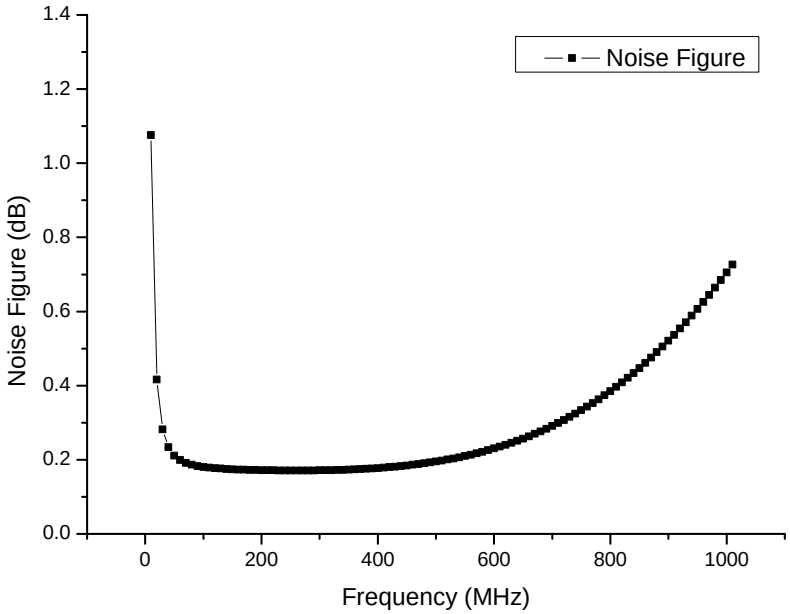

Figure 6.14: Simulated noise figure responses of the SE-AAlo.

SE-AAloV1 Measurement

The measured S-parameter performance of the SE-AAloV1 which was fabricated on a FR4 substrate is presented in Figure 6.15. The S_{21} of the LNA is greater than

20dB with maximum values of 22.5dB over the frequency range of 60-670MHz which rolls off gently from 670MHz. The average input return loss of the LNA is lower than -5dB over the frequency range of 300-650MHz with the lowest input return loss of -15dB at 430MHz. The lower end of the LNA band has high values of input return loss as input return loss was sacrificed in the trade-off for achieving lower and wideband noise figures. However, the output return loss is consistently less than -10dB throughout the frequency range of 140MHz to 710MHz with values of less than -15dB between 550MHz and 680MHz.

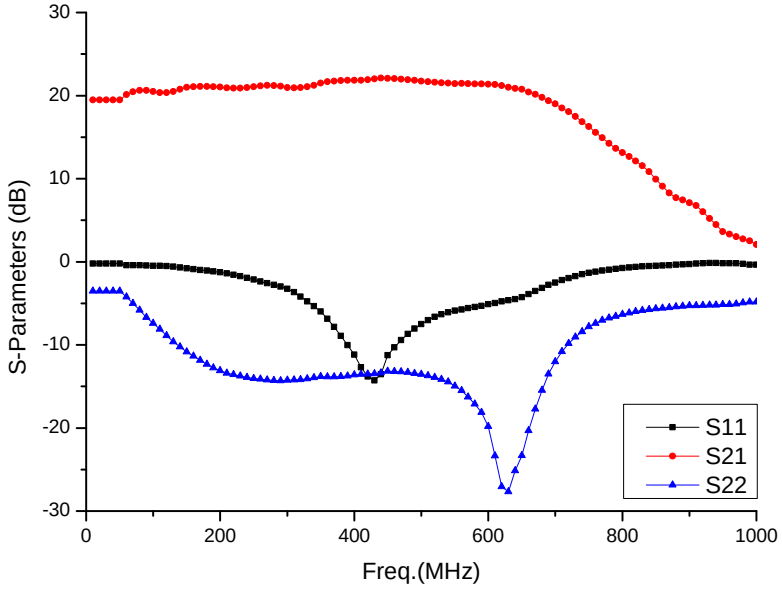

Figure 6.15: Measured S-parameter responses of the SE-AAloV1 LNA.

The power consumption of the SE-AAloV1 at the PSU is summarised in Table 6.4 where the required gate and drain voltages of the optimum performance by the LNA is provided for stage-1 and 2. The LNA consumes 14mA of drain current with 0.9V and 30mA of drain currents with 2V for stage-1 and stage-2 of the LNA respectively. Hence total power consumption of the LNA is 72mW at the PSU.

Table 6.4: Biases for stage-1 and 2 of the SE-AAloV1.

LNA	V_{d1}	V_{g1}	I_{d1}	V_{d2}	V_{g2}	I_{d2}
SE-AAloV1	0.90V	0.46V	14mA	2.0V	0.49V	30mA

The noise figure (noise temperature) of SE-AAloV1 was measured at room temperature and is illustrated in Figure 6.16. The noise figure of the LNA is less than 0.75dB (55K) throughout the frequency range of 160-460MHz with a minimum noise figure of 0.62dB (44.5K) at 160MHz. The AA system has allocated a noise budget of 150K for the receiver temperature. The noise figure values derived from the SE-AAloV1 measurement implies that this LNA is using maximum of 36% of the allocated receiver noise budget over the whole frequency band.

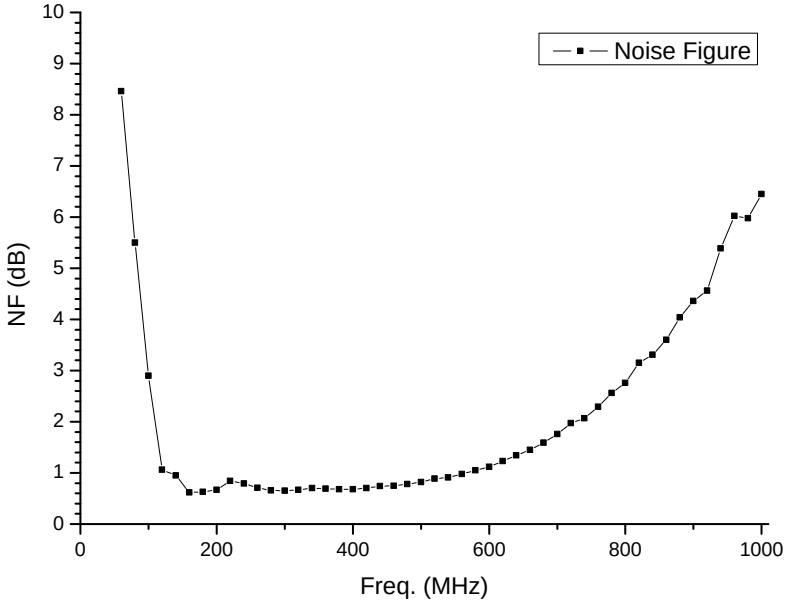

Figure 6.16: Measured noise figure of the SE-AAloV1.

SE-AAloV2 Measurement

The measured S-parameter responses of the SE-AAloV2 which was fabricated on RO4003C substrate are shown in Figure 6.17. Although the average output

return loss of the LNA is lower than -10dB throughout the whole frequencies until 1GHz, the input return loss of the LNA is lower than -10dB over the frequency band of 500-850MHz. Furthermore, the output return loss is less than -20dB between frequencies of 650MHz and 900MHz. The input return loss has higher values in order to achieve lower noise figures. The LNA has performed a flat S_{21} over a very wide frequency band which is more than 330% of the central frequency of AA-lo band. The S_{21} of the LNA is greater than 30dB between from 40MHz until 920MHz with maximum gain of 32dB over frequency range of 40-680MHz.

The measured noise figure (noise temperature) of the SE-AAloV2 at room temperature is less than 0.63dB (45.3K) up to 950MHz which is illustrated in Fig. 6.18. The minimum noise figure of 0.45dB (32K) was measured at frequency of 160MHz. The measured noise (noise temperature) figure of the LNA with an inductor for ESD protection is less than 0.75dB (55K) over the wide frequency range of 20-940MHz as illustrated in Fig. 6.18. The noise figure of the LNA with ESD protection has increased by 20% due to the associated transmission loss of the inductor.

A summary of the required voltages for each stage of the LNA and the corresponding drain currents for the optimum performance of the SE-AAloV2 is given in Table 6.5. The total power consumption of the LNA at PSU is only 25mW by supplying 1V per stage to draw current of 12mA and 13mA in the first and second stage respectively.

Table 6.5: Biases for stage-1 and 2 of the SE-AAloV2.

LNA	V_{d1}	V_{g1}	I_{d1}	V_{d2}	V_{g2}	I_{d2}
SE-AAloV2	1V	0.4V	12mA	1.0V	0.4V	13mA

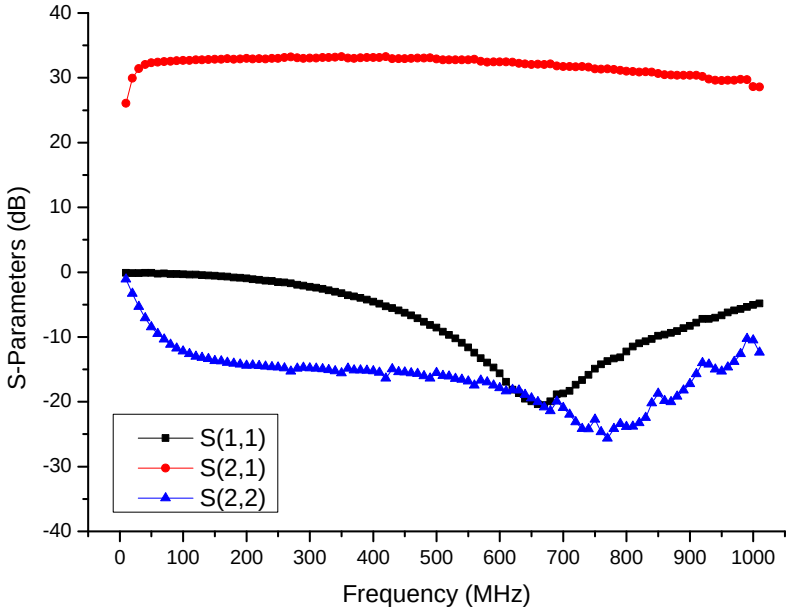

Figure 6.17: Measured S-parameter responses of the SE-AAloV2.

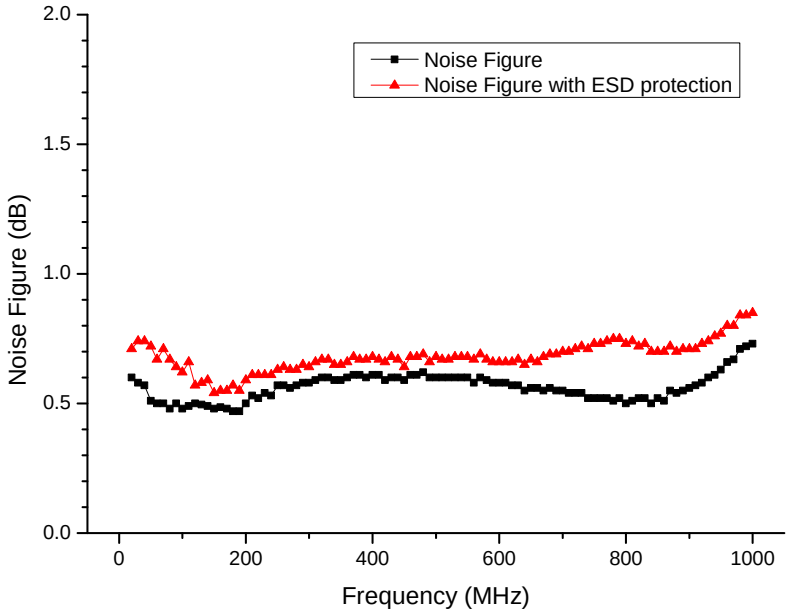

Figure 6.18: Measured noise figure responses of the SE-AAloV2.

SE-AAloV3 Measurement

The S-parameter performance of SE-AAloV3 is illustrated in Figure 6.19 up to frequency of 1GHz. The S_{21} of the LNA is higher than 30dB between frequencies

of 30MHz and 530MHz while the 3-dB roll off the gain occurs at frequency of 710MHz. The average output return loss of the LNA is less than -15dB over the frequency range of 190-930MHz. However, the input return loss of the LNA is -5dB beyond frequency range of 650MHz.

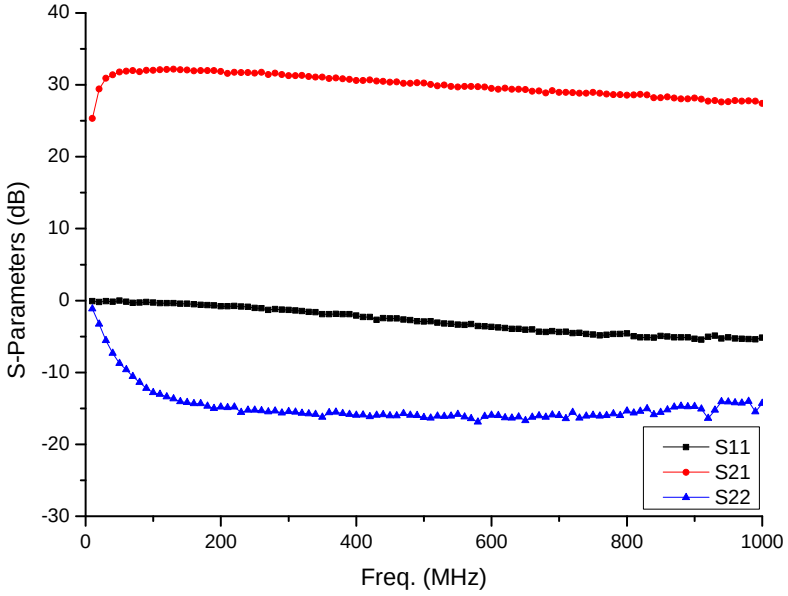

Figure 6.19: Measured S-Parameter responses of SE-AAloV3.

Table 6.6 provides the details of SE-AAloV3 power consumption at the PSU which is 25mW.

Table 6.6: Bias points for stage 1 and 2 of SE-AAloV3.

LNA	V_{d1}	V_{g1}	I_{d1}	V_{d2}	V_{g2}	I_{d2}
SE-AAloV3	1.0V	0.45V	14mA	1.0V	0.42V	11mA

As shown in Figure 6.20, the LNA has noise figures (noise temperatures) of less than 0.7dB (50.7K) over a wide frequency band of 20-1000MHz which is more than 250% of the required bandwidth by AA-lo. The spike observed in the noise figure measurements are due to the RF interferences in the experimental inviroment of the laboratory.

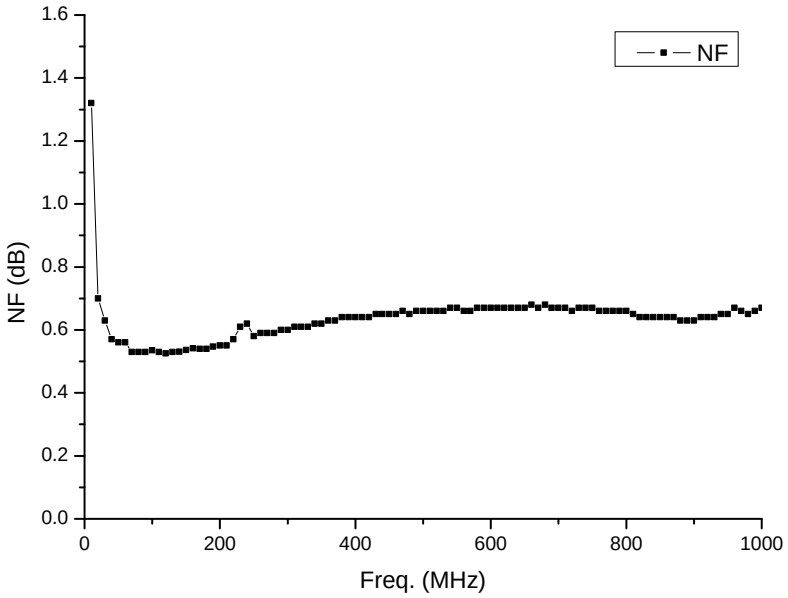

Figure 6.20: Measured noise figure of SE-AAloV3.

Analysis of SE-AAlo LNAs

The AA-lo LNAs were designed to fulfil lower frequency band of the SKA AA system requirements. Each version of AA-lo LNA was designed to improve the performance of the LNAs while the key performance parameters that were focused in the earlier versions are preserved.

SE-AAloV2 has shown significant improvements compared to SE-AAloV1 in terms of the LNA performance parameters. The operational bandwidth of the SE-AAloV2 compared to SE-AAloV1 has improved by 40%. The gain of the SE-AAloV2 has increased to more than 30dB up to 1000GHz while that of SE-AAloV1 was more than 20dB up to 700MHz. In terms of noise figure (noise temperature), SE-AAloV2 has measured values of less than 0.6dB (43K) across the band while it is less than 0.8dB (59K) up to 500MHz. Therefore, the noise figure has reduced by 25% while the corresponding noise bandwidth has doubled. Power consumption of SE-AAloV2 was reduced by more than 40% while there was a 35% reduction in the dimension of the LNA.

The improvements achieved by SE-AAloV2 can be attributed to the change of substrate from FR4 to Rogers 4003C which is thinner (0.5mm) and is low loss in nature. The thin substrate offers less inductive feedback at the source and thus LNAs with a lower noise figure and high gain over a wideband can be designed. DC block capacitor values at the input and output of the LNA were increased to obtain a wider bandwidth. The inductor used in the noise matching network was replaced with a low loss inductor to obtain a wideband low noise figure. The RF width and length of microstrip lines in the first stage were optimised which plays an important role in reducing the LNA noise. The interstage matching circuit was optimised by increasing the value of the interstage capacitor and removing the inductor used for the impedance matching. Ultra wideband capacitors were implemented in the design for the decoupling DC from the RF. The mentioned alteration introduced in the noise and gain matching circuits of the LNAs have improved the response significantly. In the process, the dimension of the LNA was reduced by optimising the layout of the LNAs.

The SE-AAloV2 has met the requirements of the lower frequency band of SKA AA system and has exceeded them in some cases. The power consumption of SE-AAloV2 has exceed the requirements by 17%. The noise temperatures measured for SE-AAloV2 construct only 28% of the allocated noise budget of the T_{sys} in the AA-lo. SE-AAloV3 has maintained primary parameters that were concentrated on in SE-AAloV2 which includes gain, bandwidth, low noise and power consumption while the LNA dimension has reduced by 33%.

Table 6.7 compares the performance obtained from the designed SE-AAlo LNAs with the LNAs designed by research teams in the SKA over AA-lo frequency band along with commercially available LNAs. As mentioned in Section 1.5, the research team at INAF concentrated on design of AA-lo LNAs with the best performance achieved for a single ended LNA named as BEST-3lo [48]. Average

Table 6.7: SKA and commercial LNAs operating over AA-lo frequency band.

LNA	Frequency (MHz)	Gain (dB)	NF (dB)	Power (mW)
SE-AAloV2	10-1000	>31	<0.6	25
SE-AAloV3	10-1000	>29	<0.6	25
[51]	5-4000	> 32.0	<1	33
[50]	5-2000	> 17.0	>1-1.5	18
[56]	50-6000	> 17.5	1.3	270
[55]	50-3000	> 18.8	1.1	350
[125]	50-200	24.0	<0.5	>315
[126]	50-4000	> 19.0	<0.7	450
[48]	130-510	>20	<1.29	510

measured noise figures (temperatures) of SE-AAloV2 and SE-AAloV3 are less than 0.6dB(43K) which is less than half of the measured noise figure values of 1.29dB(100K) for BEST-3lo. Power consumption of the LNA is 510mW which implies that the LNA consumes 20 times more power than the SE-AAloV2 and SE-AAloV3. Therefore, the total power of 2.6MW is reduced for 5,600,000 AA-lo LNAs by utilising the SE-AAloV2 or SE-AAloV3 instead of BEST-3lo. Minimum gain of more than 17.5dB is obtained by [56], [55], [125] and [126] up to 1GHz at an average power consumption of 350mW. However, [50] has lower power consumption than SE-AAloV2 and SE-AAloV3 while the LNA performs 12dB less gain with 2 times more average noise figure values than of SE-AAloV2 and SE-AAloV3. Gain of [51] is comparable with SE-AAloV2 with 32% higher power consumption. The bandwidth achived by SE-AAloV2 and SE-AAloV3 are almost 96% larger than bandwidth of [48]. The bandwidth of [51], [50], [56] and [55] are larger than SE-AAloV2 and SE-AAloV3 while their noise figure performance is at least 0.6dB higher. The noise figure of SE-AAloV2 and SE-AAloV3 are comparable with [125] and [126] while the power consumption is significantly less than by a minimum factor of 92%.

The performance of the LNAs achieved by this work for AA-lo has immense

impact on the overall system performance budgets, specially in terms of noise and power consumption. The LNA performances show that 0.65dB (46.8K) noise figure (noise temperature) LNA can be realised with only 25mW power consumption. This shows an immense improvement in power consumption without any significant penalty on the LNA noise. The large reduction in power consumption of LNAs is highly encouraging and positive for low frequency aperture array SKA as the power is a major issue for the SKA. Moreover, this noise performance has been achieved with an in house LNA assembly and therefore is a fair scope of further improvement in the noise response of the LNA if automated LNA assembly is carried out according to industry standards.

6.3.2 Diff-AAlo LNAs

Simulated and measured S-parameter performance and noise figure results of Diff-AAlo LNAs are described in this section where the LNA design details are given in Section 4.4.2. This section gives and discusses the simulated and measured results achieved for Diff-AAlo LNAs. The measured data of Diff-AAloV1 and Diff-AAloV2 are explained in details with a complete analysis.

Diff-AAlo Simulation

Figure 6.21 shows the simulated mixed mode S-parameter responses of Diff-AAlo LNA which is designed to adopt the special topology of differential input and single ended output based on the required condition of the AA system. The differential gain of the LNA, S_{sd} is higher than 36dB with 1dB ripple over the frequency band of 50-620MHz. However, the common mode gain of the LNA, S_{sc}, is less than 14.4dB over a wide frequency range of 50MHz to 620MHz. The return losses of the LNA is also presented in Figure 6.21. The LNA has demonstrated a

differential input return loss (S_{dd}) of less than -2dB between 190MHz and 670MHz while the lowest value of S_{dd} is -4.6dB at frequency of 490MHz. The output return loss (S_{ss}) is lower than -10dB from 120MHz while for the frequency range of 270-620MHz, it is less than -15dB. Common mode return loss of the LNA, S_{cc}, is lower than -1.2dB over the whole operational frequency band of the LNA. The noise figure (noise temperature) of the LNA is less than 0.63dB (45.3K) over the operational frequency band with minimum noise figure (noise temperature) of 0.54dB (38.4K) at 100MHz which is illustrated in Figure 6.22. The noise figure of the AA-lo LNAs are effected by the sky noise which is dominant at lower frequency end of AA-lo. The common mode rejection ratio (CMRR) of the LNA is more than 22dB up to the frequency of 1GHz as shown in Figure 6.23. The simulated results of the single ended and differential AA-lo LNAs show promising performance which exceed that achieved by LNA designers in SKA. The measured performance of the LNAs are discussed in the following sections.

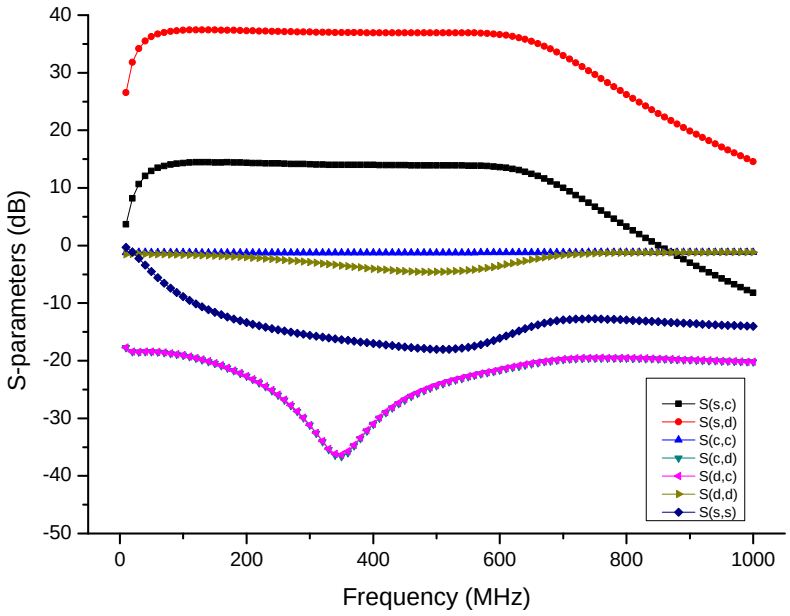

Figure 6.21: Simulated mixed mode S-parameter responses of the Diff-AAlo.

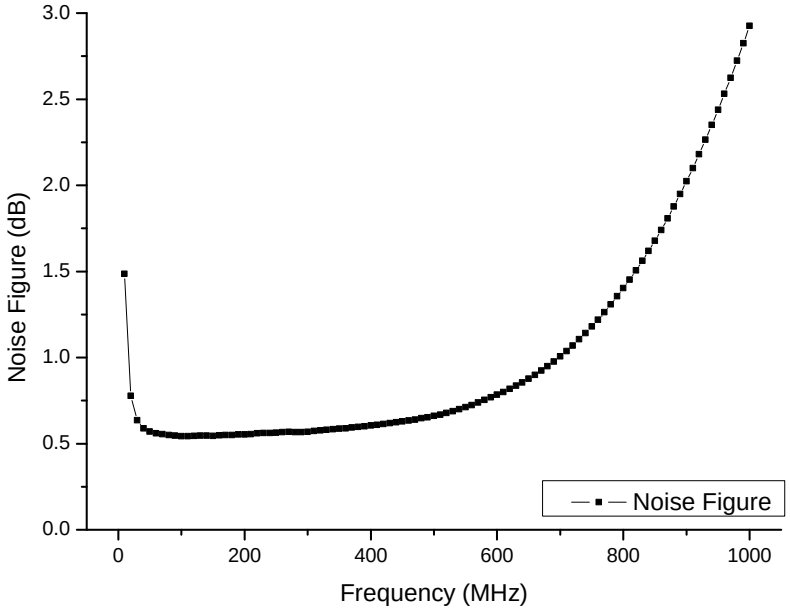

Figure 6.22: Simulated noise figure responses of the Diff-AAlo.

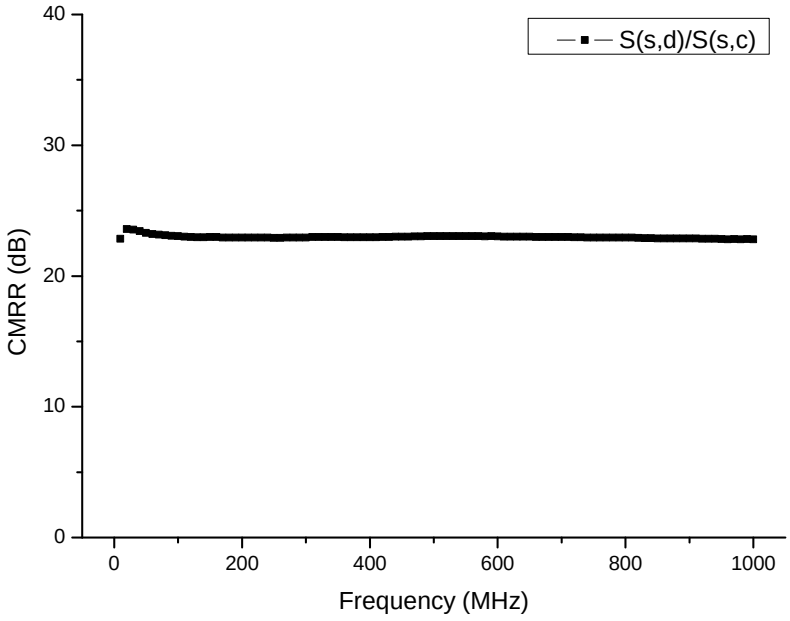

Figure 6.23: Simulated common mode rejection ratio of the Diff-AAlo.

Diff-AAloV1 Measurement

Mixed mode S-parameter performance of the Diff-AAloV1 is presented in Figure 6.24 which was fabricated on a FR4 substrate. AA-lo LNAs have a wide

operational frequency band which is 146% of the central frequency. The differential gain (S_{sd}) of the LNA is higher than 23dB over the frequency band of 40-640MHz which is 230% of the AA-lo central frequency and the gain rolls off gently from 640MHz. The common mode gain (S_{sc}) of the LNA is less than 1.1dB over the whole frequency band of operation. The differential input return loss (S_{dd}) of the LNA is lower than -10dB over the frequency range of 420-640MHz whilst the output return loss (S_{ss}) is below -10dB between 170MHz and 710MHz.

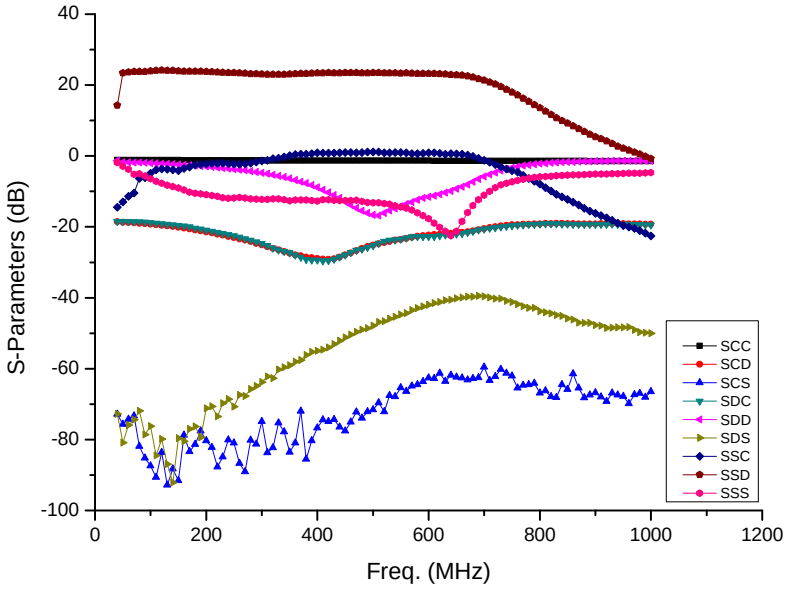

Figure 6.24: Measured mixed mode S-parameter responses of the Diff-AAloV1.

Table 6.8 outlines the necessary gate and drain voltages for obtaining the optimum performance of Diff-AAloV1. Subsequently the total power consumption of the LNA at the PSU is calculated to be 44.18mW.

Table 6.8: Biasing points for stage-1 and 2 of the Diff-AAloV1.

LNA	V_{d1}	V_{g1}	I_{d1}	V_{d2}	V_{g2}	I_{d2}
Diff-AAloV1	0.87V	0.46V	14mA	1.6V	0.41V	20mA

The measured noise figures (temperatures) of Diff-AAloV1 at room temperature are given in Figure 6.25 which demonstrates values less than 1dB (75K)

over the frequency band of 120-380MHz with a minimum noise figure of 0.63dB (45K)at 160MHz. The data indicate Diff-AAloV1 contribution to the receiver noise budget of AA-lo is 50%.

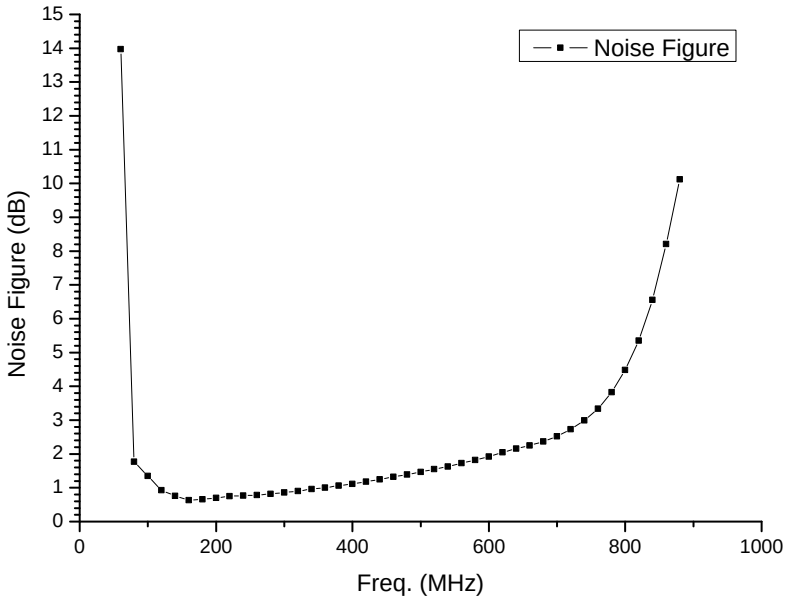

Figure 6.25: Measured noise figure of Diff-AAloV1.

Diff-AAloV2 Measurement

Figure 6.26 shows the measured return losses of the transformer which has been used in the design of Diff-AAloV2 LNA. Both input and output VSWRs of the balun are better than 1.25:1 and hence has little impact on the return losses of the LNA.

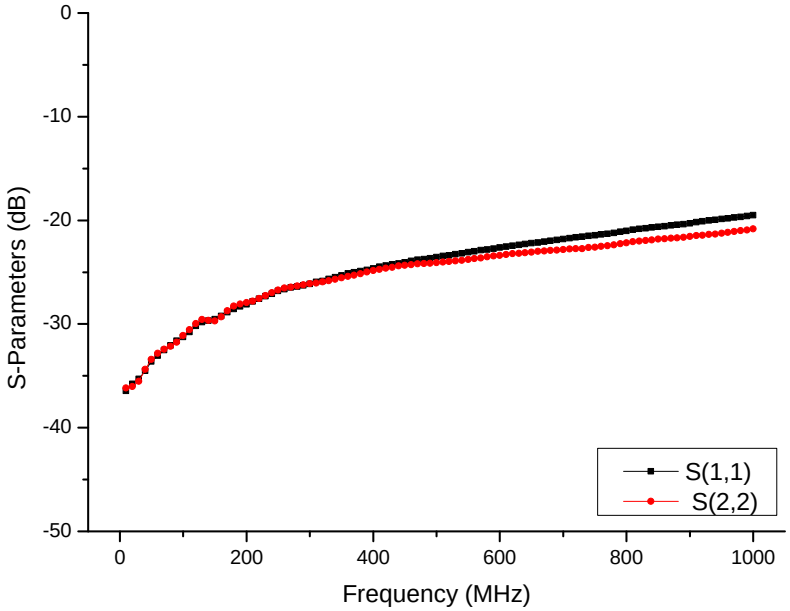

Figure 6.26: Measured input and output return losses of the transformer used in Diff-AAloV1 and Diff-AAloV2 LNAs [13].

The mixed mode S-parameter responses of Diff-AAloV2 LNA are measured at 3 different bias points. The bias points are identified as Bias1, Bias2 and Bias3 and the details of all 3 biases are given in Table 6.9. The mixed mode S-parameter and noise figure performances of the Diff-AAloV2 are characterised at each bias point separately. The total power consumption of the Diff-AAloV2 at the PSU for Bias 1, 2 and 3 is 23mW, 22.5mW and 15mW respectively. Total power consumption of all 3 biases of Diff-AAloV2 prove that not only power budget of AA-lo has been met but it has also exceed the requirements by 23%, 25% and 50% at Bias1, 2 and 3 respectively.

Figure 6.27 and Figure 6.28 show the measured differential and common mode gains of all 3 biases for Diff-AAloV2 respectively.

Differential gain, S_{sd}, of the LNA is greater than 31dB with 2dB roll off over the frequency range of 70MHz to 450MHz for Bias 1. However, the LNA performs well beyond the frequency band of operation as the differential gain

Table 6.9: Bias points of the Diff-AAloV2.

Diff-AAloV2	Bias1	Bias2	Bias3
V_{d1} (V)	1.00	1.50	1.50
V_{g1} (V)	0.40	0.35	0.33
I_{d1} (mA)	12.0	8.00	5.00
V_{d2} (V)	1.00	1.50	1.50
V_{g2} (V)	0.40	0.35	0.33
I_{d2} (mA)	11.0	7.00	5.00

of the LNA at Bias 1 is higher than 30dB over a very wide frequency range of 20-910MHz with 4dB roll off. This implies that at Bias 1, the LNA is operational over a frequency band which is more than 340% of the AA-lo central frequency. Bias 2 measurements show S_{sd} of higher than 30dB with a 2dB roll off between frequencies of 20MHz and 760MHz while that is higher than 26dB at 20-1000MHz by applying Bias 3. It can be concluded that as the differential gain of the Diff-AAloV2 decreases, the common mode gain decreases and this is relevant to the amount of total power consumption of the LNA.

The measured common mode gains (S_{sc}) of Diff-AAloV2 are illustrated in Figure 6.28 with values of less than 11dB, 9dB and 4dB over the LNA operational frequency at Bias 1, 2 and 3 respectively. As expected, the common mode gain of the LNA is relatively low. It is apparent that between the differential and common mode gains of Diff-AAloV2 shown in Figures 6.27 and 6.28, for all 3 biases a minimum 20dB difference exists.

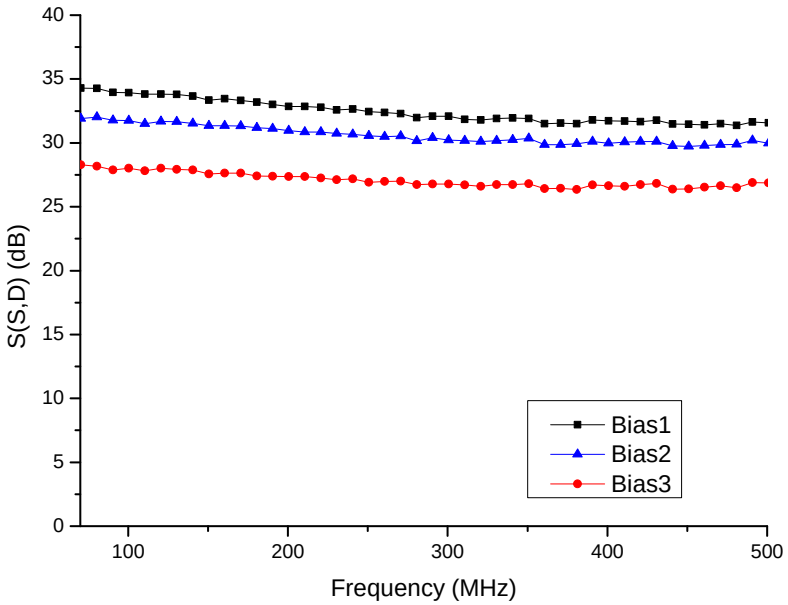

Figure 6.27: Measured differential mode gain of Diff-AAloV2.

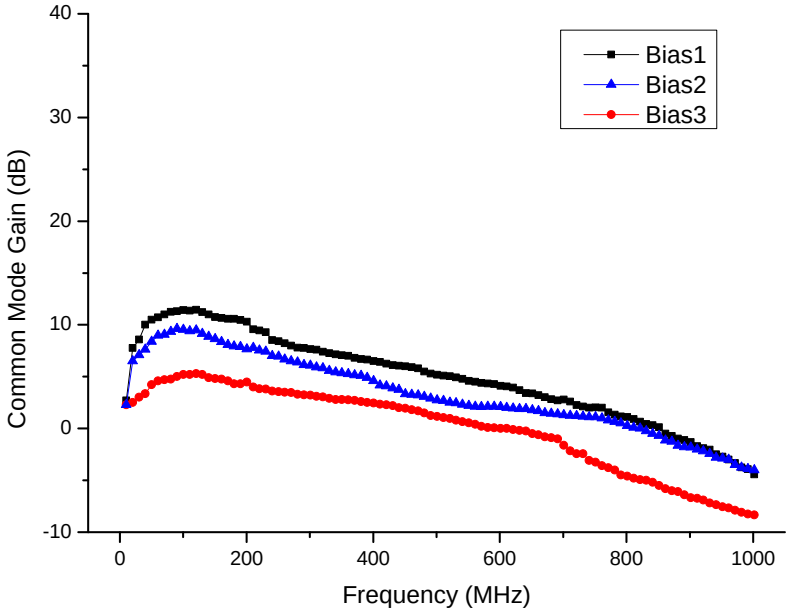

Figure 6.28: Measured common mode gain of the Diff-AAloV2.

The measured return losses of Diff-AAloV2 at Bias 1, 2 and 3 are illustrated in Figures 6.29, 6.30 and 6.31 up to a frequency of 1GHz. The single ended output return loss (S_{ss}) of the LNA for all the biases is better than -15dB throughout the whole frequency band of the LNA operation until 1GHz. The average differential

input return loss (S_{dd}) of the LNA for all 3 biases beyond 600MHz is less than -10dB. The primary reason of higher input return losses at lower frequency ranges can be attributed to the sacrifice of input return loss of lower noise figures. The common mode return loss of the LNA (S_{cc}) for all 3 biases is less than -1dB over the whole LNA frequency band of operation.

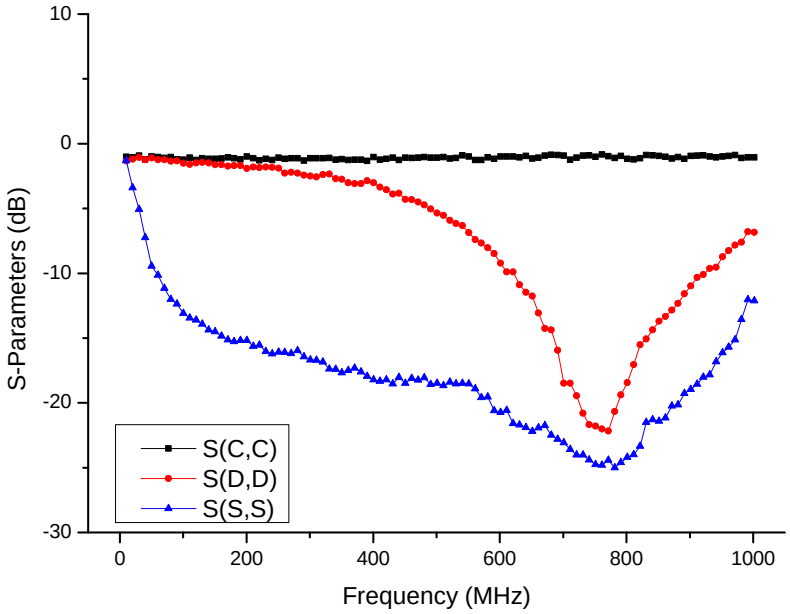

Figure 6.29: Measured differential, common and single mode return losses of the Diff-AAloV2 at Bias1.

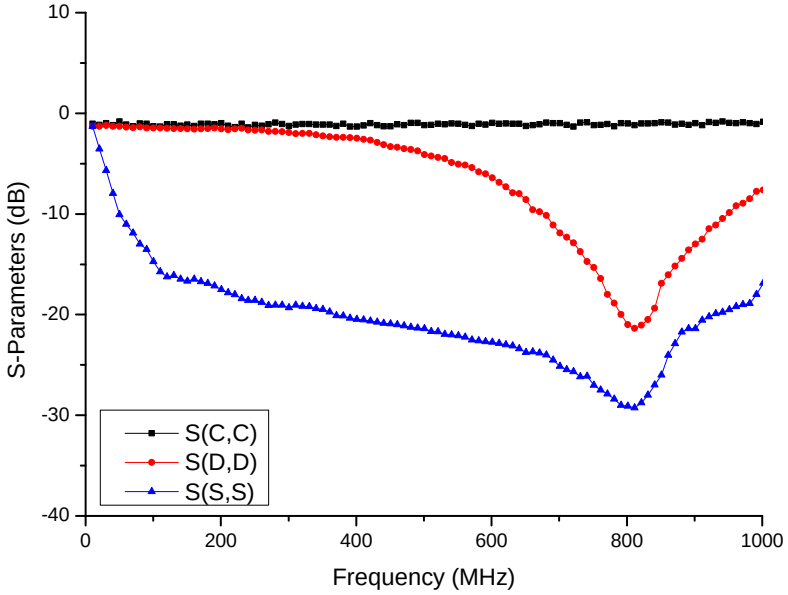

Figure 6.30: Measured differential, common and single mode return losses of Diff-AAloV2 at Bias2.

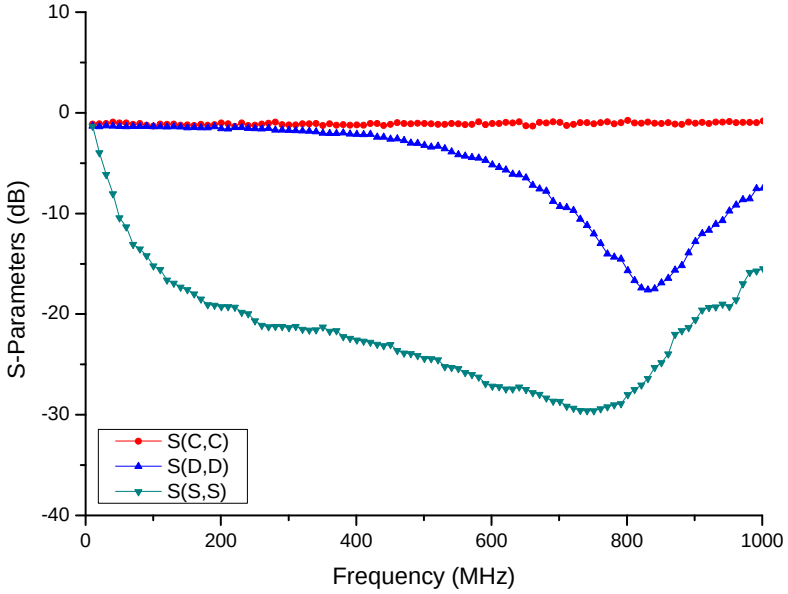

Figure 6.31: Measured differential, common and single mode return losses of Diff-AAloV2 at Bias3.

Noise figure measurements of Diff-AAloV2 for all the bias points are illustrated in Figure 6.32 along with the insertion loss of the transformer used in Diff-AAloV2. At Bias 1, minimum noise figure (noise temperature) of Diff-AAloV2 is

0.52dB (37K) at 170MHz while the noise figure of the LNA is less than 1dB (75K) up to frequency of 450MHz. The average noise figure of the LNA at Bias 1, is below 0.75dB (54.7K) for 60% of the AA-lo bandwidth. Noise figure of the Diff-AAloV2 is less than 1.1dB (83.6K) over the whole frequency band of operation at Biases 2 and 3. Noise figures (temperatures) of Diff-AAloV2 for all 3 biases are highly influenced by the loss of the transformer. The loss of transformer increases significantly beyond 300MHz and hence dominates the noise figure of the LNA which is apparent in Figure 6.32

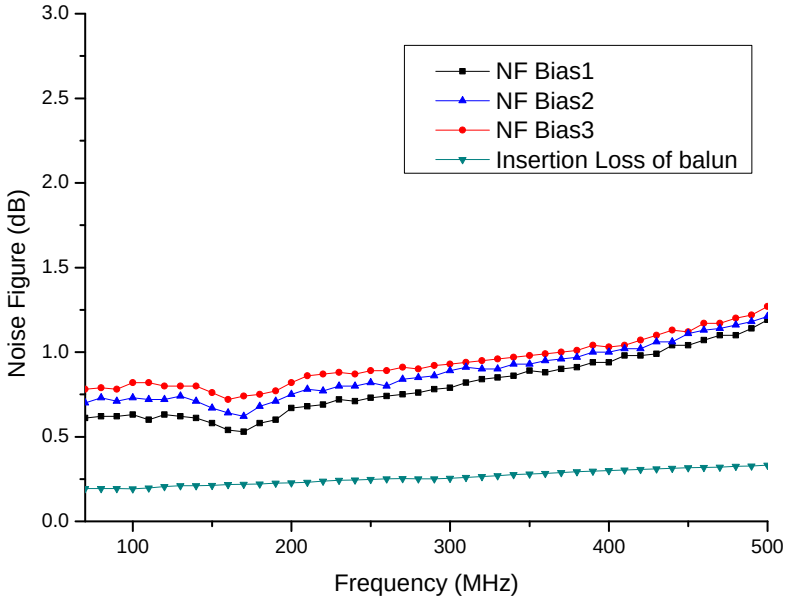

Figure 6.32: Measured noise figure responses of the Diff-AAloV2 LNA at 3 separate biases and the loss of the balun used in the LNA.

The measured Common Mode Rejection Ratio (CMRR) of the LNA for all 3 biases are illustrated in Figure 6.33. For frequencies up to 1GHz, the CMRR is more than 20dB. The transformer has a significant contribution in achieving the high CMRR values. The responses of the balun were taken into account in the design stage in order to obtain a wideband CMRR response. The measured value of the CMRR is comparable to that of the simulations.

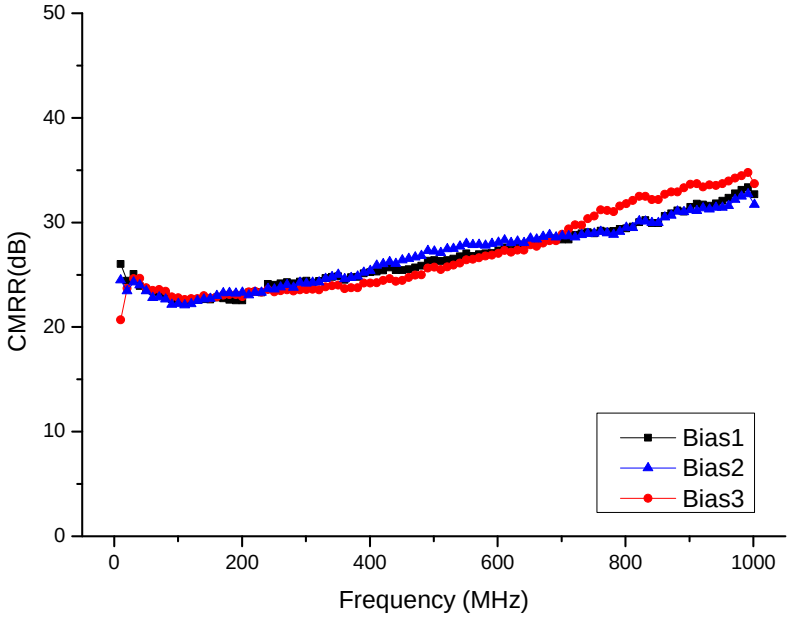

Figure 6.33: Measured common mode rejection ratio of the LNA2.

Table 6.10 gives a summary of the Diff-AAloV2 performance in terms of S-parameter and noise figure characterisation at Biases 1, 2 and 3.

Table 6.10: Summary of Diff-AAloV2 Measurements

LNA Diff-AAloV2	Flat Gain BW(MHz)	Gain (dB)	Power (mW)	NF minima (dB)@(MHz)	Typical CMRR(dB)
Bias 1	$20-910$	>30	23	0.52 @ 170	25
Bias 2	$20-760$	>30	22	0.61 @ 170	25
Bias 3	$20-1000$	>26	15	0.71 @ 170	25

Analysis of Diff-AAlo LNAs

The Diff-AAlo LNAs were designed to meet the required LNA configuration of differential input and single ended output in the AA-lo system as well as the specified requirements of the AA-lo LNAs. Each version was designed to improve the performance while the key performance parameters that were focused in the earlier versions are preserved.

Characterisation of Diff-AAloV2 establishes a substantial improvement from Diff-AAloV1 in the terms of primary performance parameters. The optimum performance of Diff-AAloV2 is derived by Bias 1 and hence this bias is used for the purpose of comparison with Diff-AAloV1. The noise measurements demonstrate a noise reduction of 25% for Diff-AAloV2 for frequencies up to 300MHz. The frequency band of Diff-AAloV2 was increased by 30% while the gain enhanced by at least 10dB. Furthermore, the total power consumption of Diff-AAloV2 has decreased to a great extent of almost half the initial result. The optimisation of the Diff-AAloV2 has reduced the LNA dimension by a factor of at least 30%.

The primary difference between the Diff-AAlo LNAs and SE-AAlo LNAs are the use of a transformer in front of the SE-AAlo LNA to convert the balanced signal to an unbalanced signal. Therefore, the improvements achieved by Diff-AAloV2 compared to Diff-AAloV1 can be attributed to the improvement applied to SE-AAloV2 from SE-AAloV1 which are explained in detail in Section 6.3.1 in the Analysis subdivision.

The Diff-AAloV1 and Diff-AAloV2 are the only differential LNAs available for operation over the AA-lo band amongst the SKA LNA research teams. Therefore, Diff-AAloV2 performance is compared with commercially available balanced LNAs or fully differential LNAs in terms of power consumption, bandwidth, gain and noise figure in Table 6.11. The frequency range of Diff-AAloV2 is comparable with [127] while the power consumption of the Diff-AAlo at Bias1 is 66% less and the noise figure is 4dB less over the whole frequency band of operation. Althought, the frequency bands are different, the gain and noise figure performance of [128] is close to Diff-AAloV2 whilst the power consumption is 500mA which is significantly higher than Diff-AAloV2. Diff-AAloV2 is a suitable LNA choice for the AA-lo system in the SKA as it can be integrated to the differential output antenna directly and its performance meets the required criteria of the

AA-lo system.

Table 6.11: Commercially available LNAs for Diff-AAlo LNAs.

LNA	Frequency(MHz)	Gain(dB)	Noise Figure(dB)	Power(mW)
Diff-AAloV2	70-1000	32	<1	23
[128]	1800-2200	29.9	0.6	500
[127]	1-2700	>17.0	<5	69

Diff-AAloV2 LNA performances implies that a differential LNA with a very low power consumption of 23mW can be realised to achieve low noise figures (temperatures) of less than 0.75dB (55K) up to 300MHz. Characterisation of a differential LNA with an extremely low power consumption is a huge step forward towards producing cost effective LNAs as the power consumption is reduced by 23% from the minimum requirements.

6.4 MIC AA-mid LNAs

This section describes the simulated and measured performances of the designed MIC AA-mid LNAs operational from 400MHz to 1400MHz with single ended input and output topology. The measured performance of 2 fabricated versions of AA-mid LNAs named as AAmidV1 and AAmidV2 are explained in detail in this section. The AAmidV1 and AAmidV2 analysis is accompanied by a comparison of the current SKA LNAs designs at AA-mid frequency band.

AA-mid Simulation

Figure 6.34 shows the simulated S-parameter responses of the LNA designed for the AA-mid. The LNA has S_{21} of greater than 25dB over the whole operational frequency band. The input return loss of the LNA is better than -5dB over the frequency range of 400-1400MHz while it is less than -9dB between frequency of

580MHz and 900MHz. Simulated output return loss of the LNA is lower than -10dB and -8dB over the frequency ranges of 400-800MHz and 810-1400MHz respectively. Simulated noise figure of AA-mid LNA illustrated in Figure 6.35 shows a noise figure (noise temperature) of less than 0.4dB (28K) up to 1GHz while the noise figure (noise temperature) is less than 0.67dB (48.5K) over the entire frequency band of interest. The minimum noise figure of the LNA is 0.25dB (17.2K) at 450MHz. Rollet's factor (K-factor) simulation of the LNA is presented in Figure 6.36 up to frequency of 2GHz. The simulations prove that the LNA is unconditionally stable with the lowest K-factor of 32.8 at frequency of 1570MHz.

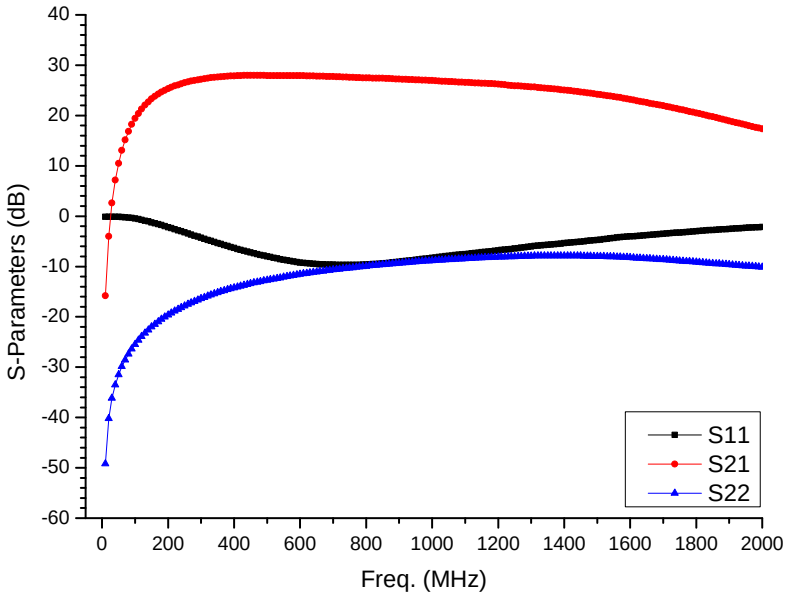

Figure 6.34: Simulated S-Parameter responses of the AA-mid LNA.

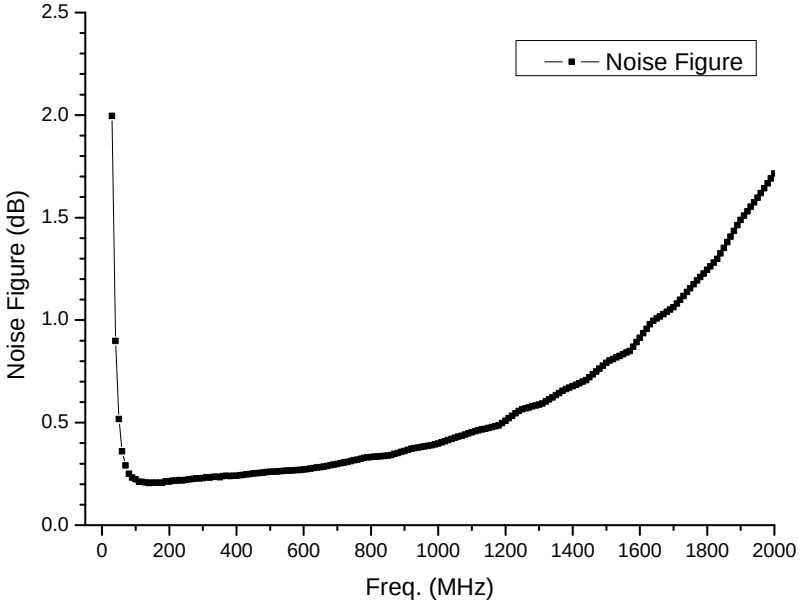

Figure 6.35: Simulated noise figure responses of the AA-mid LNA.

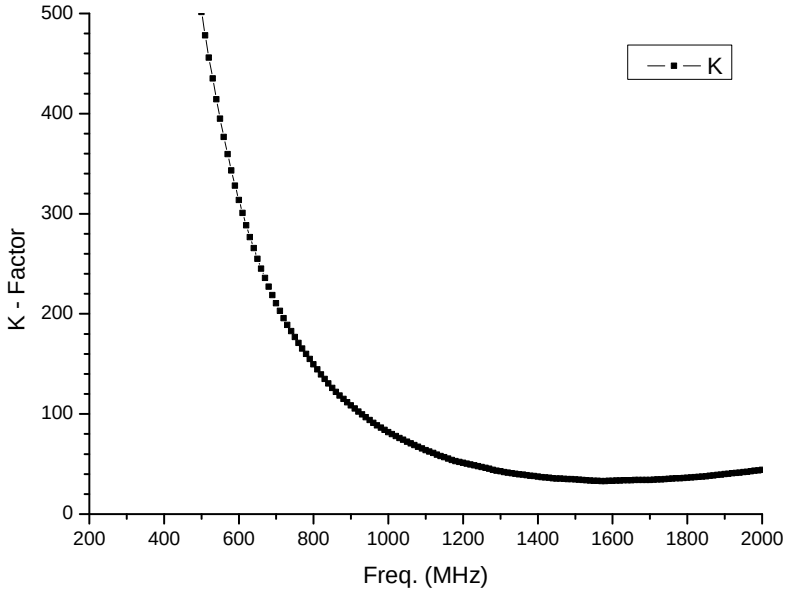

Figure 6.36: Simulated K-factors of the AA-mid LNA.

AAmidV1 Measurements

The measured S-parameter responses of AAmidV1 which was fabricated on a FR4 substrate is illustrated in Figure 6.37. The average output return loss of the LNA was measured to be -10dB throughout the whole frequency band of operation. The S_{21} of the LNA is greater than 20dB up to the frequency of 1400MHz whilst over the frequency range of 400-1010MHz, the S_{21} is higher than 23dB. The average input return loss of the LNA is better than -5dB from the frequency of 600MHz. Over the frequency range of 700-900MHz, the average input return loss is better than -10dB with -12dB at 800MHz. The input return loss of the LNA at the low end of the band was sacrificed for a wideband noise figure response over the complete frequency band of interest.

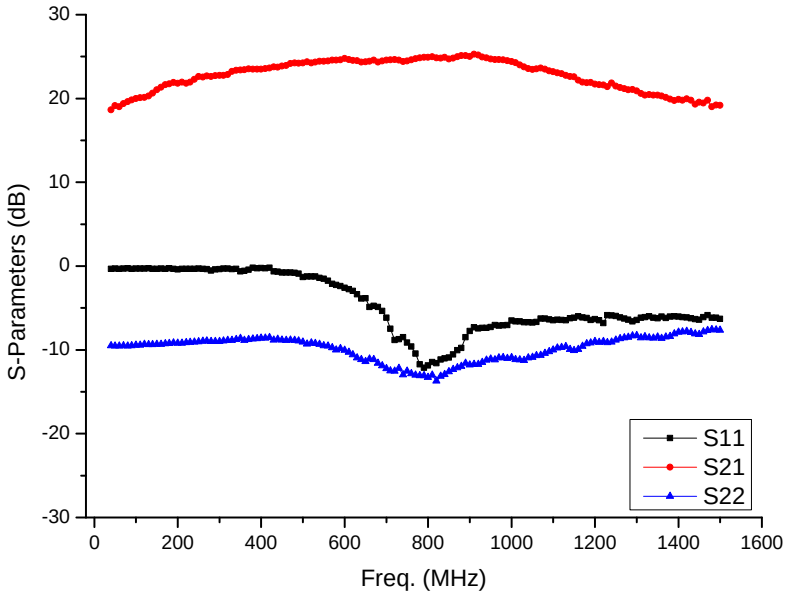

Figure 6.37: Measured S-Parameter responses of AAmidV1 .

Table 6.12 shows that the total power consumption of the AAmidV1 LNA at the power supply unit for an optimum performance is 56.25mW.

The LNA has noise figures (temperatures) of less than 0.6dB (43K) over the

Table 6.12: Bias points for stage 1 and 2 of the AAmidV1 LNA.

LNA	V_{d1}	V_{g1}	I_{d1}	V_{d2}	V_{g2}	I_{d2}
AAmidV1	1.25V	0.70V	35mA	1.25V	0.43V	10mA

entire frequency band of 400-1400MHz with a minimum noise figure (noise temperatures) of 0.5dB (35K) between 800MHz and 1000MHz as illustrated in Figure 6.38. The slight increase observed in the noise figure of the LNA at frequencies of 1GHz, 1.15GHz and 1.3GHz are due to the interferences at these frequencies in the laboratory.

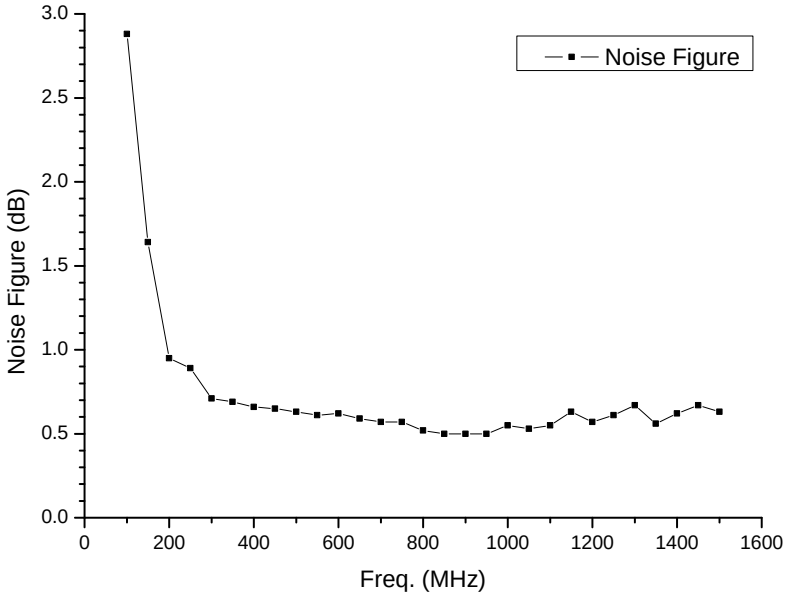

Figure 6.38: Measured noise figure of the AAmidV1 .

AAmidV2 Measurements

The measured S-parameter and noise figure responses of AAmidV2 fabricated on Rogers substrate (RO4003C) at room temperature is described in this section. Figure 6.39 illustrates the measured S-parameter performance of the LNA. The S_{21} of the LNA is higher than 25dB over the operational frequency band with the maximum gain of 29dB between 800MHz to 1100MHz. The input return loss

of the LNA is high up to frequency of 900MHz while the average input return loss is better than -6dB beyond 900MHz. Achieving lower noise figures over a wide frequency band were selected in the trade-off between noise figure and input return loss in the design stage. The output return loss is less than -10dB over the frequency range of 400-800MHz while it is less than -5dB over the complete frequency range.

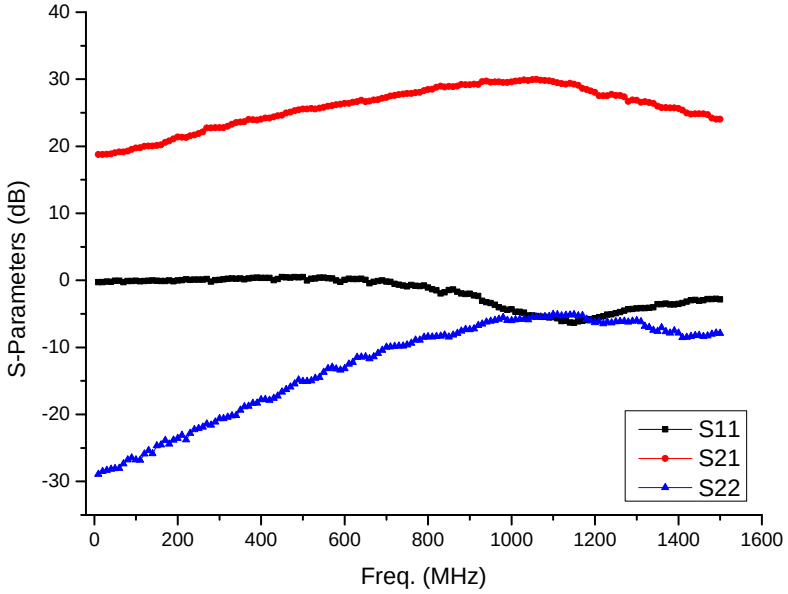

Figure 6.39: Measured S-Parameter responses of the AAmidV2 LNA.

The necessary drain voltages, gate voltages and currents are summarised in Table 6.13 to achieve an optimal performance for AAmidV2. Subsequently 28mW is the total power consumption of AAmidV2 at the PSU.

Table 6.13: Bias points for stage 1 and 2 of AAmidV2.

LNA	V_{d1}	V_{g1}	I_{d1}	V_{d2}	V_{g2}	I_{d2}
AAmidV2	0.70V	0.40V	30mA	1.0V	0.40V	7mA

The measured noise figure (noise temperature) of the AAmidV2 is shown in Figure. 6.40, where the average noise figure (noise temperature) of the LNA is

0.45dB (32K) with a minimum value of 0.41dB (29K) at 900MHz. The noise figure of the LNA is less than 0.48dB (34K) beyond frequency of 550MHz.

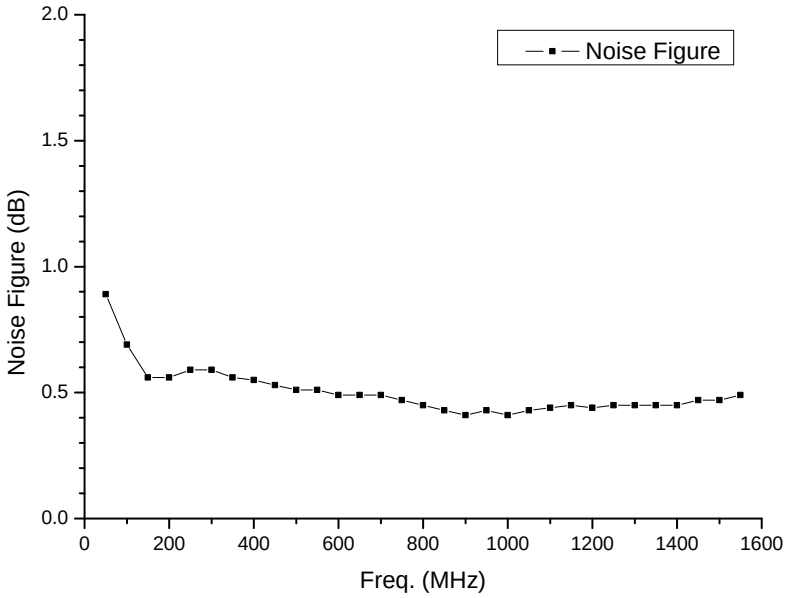

Figure 6.40: Measured noise figure responses of the AAmidV2.

Analysis of AA-mid LNAs

The AA-mid LNAs were designed to meet the requirements of the higher frequency band of AA system. The S-parameter, noise figure and power consumption of AAmidV2 were improved significantly compared to the AAmidV1 LNA. Both AAmidV1 and AAmidV2 have bandwidth of 400MHz-1400MHz which is more than 110% of the central frequency of 900MHz.

The measured noise figure of AAmidV2 was improved by a factor of 30% in comparison with that of AAmidV1. The improvement in the noise figure of the LNA can be attributed to the removal of a passive component and RF path optimisation in the first stage of the amplifier. The removal of stage-1 inductor along with reduction in value of shunt feedback resistor play a role in decreasing the noise figure over the complete bandwidth. The input return loss of the LNA was sacrificed for wideband low noise matching over the wideband frequency

range.

Total power consumption of AAmidV2 at PSU was reduced by 50%. This significant reduction in the total power consumption is due to employment of Rogers substrate instead of FR4, because of the low loss, thinner substrate and high permittivity of RO4003C with which a wideband high gain and low loss response has been achieved with low power. This substantial reduction in the power consumption has exceeded the requirement set by the AA system and has a magnificent impact in terms of power consumption of the whole AA front-end subsystem and makes the system power efficient and cost effective.

The S_{21} of AAmidV2 is 20% more than of the achieved gain for AAmidV1 over the frequency range of 400-1400MHz. However the gain is not as flat as the gain of AAmidV1. This discrepency is caused due to the reduction in inductive feedback of the LNA.

Table 6.14 gives a summary of LNAs operating over the higher frequency band of SKA developed by research teams involved in SKA and the state of art commercial LNAs. The most updated single ended LNAs measured at room temperature are used for the purpose of comparison and analysis. The measured average noise figure of AAmidV2 is less than 32K which is lower than 35K obtained by [129] and [35]. The LNA [35] operating at 0.3-1GHz has noise temperatures of 56K which is 37% higher than that of AAmidV2. Whilst the power consumption obtained by the LNA operating over 0.3-1GHz was 69.3mW which is lower than the other SKA LNAs by [35], [44] and [129], it consumes 60% more power than AAmidV2. At a power consumption of 340mW, a noise figure of less than 25K was measured by [44] over the frequency range of 0.6-1.6GHz whilst that is 7K less than the acheived average noise temperatures by AAmidV2 at 28mW. The gain performance of the AAmidV2 is greater than LNAs operating over 0.3-1GHz and 0.7-4GHzby [35] while it is lower than [44] and [129]. The lower gain performance

is the result of a trade off for the lower power consumption while achieving considerably high enough gain to minimise the noise contributions from the subsequent stages in the system. Although gain of [130] is comparable with AAmidV2 but noise figures are higher and power consumption is 28 times more than AAmidV2. Despite of achieving noise figures lower than 0.6 by [131], gain is 10dB less while the power consumption is 37% higher than AAmidV2. The gain performances of [132] and [133] are higher than AAmidV2 while the noise figure is twice of that for AAmidV2 with a significant power consumption of 275mW. [133] has 4dB more gain than AAmidV2 with a higher noise figure values, and significant power consumption of more than 200mW. Therefore it can be concluded that the AAmidV2 is the most power efficient LNA in the SKA with a comparatively low noise figures.

Table 6.14: SKA and commercially available LNAs for AA-mid band.

LNA	Frequency (GHz)	Gain (dB)	NF (dB)	Power (mW)
AAmidV2	0.4-1.4	26	0.45	28
[129]	1-1.8	40	0.5	-
[35]	0.3-1.0	24	0.8	69.3
[35]	0.7-4	25	0.5	300
[44]	0.6-1.6	37	<0.4	340
[132]	0.4-1.5	30	<0.9	275
[130]	0.4-2.2	>26	<1.2	790
[131]	0.45-6	>16 (up to 2GHz)	0.6 (up to 2GHz)	45
[133]	0.6-2.5	30	1	250

Achievement of the AAmidV2 S-parameter and noise figure performance at a very low power consumption of 28mW at the PSU demonstrates a significant step in the LNA designs for the high frequency band of the AA system in SKA. As mentioned in Table 1.1, the required number of the LNAs for AA-mid is 55,000,000. Consequently by using AAmidV2 instead of [44] the total power consumption of the LNAs are reduced by 17.2MW. The S-parameter and power

consumption of AAmidV2 has met and exceeded the requirements of the AA system. These LNAs have demonstrated unconditionally stable LNAs with low noise figures by using inexpensive commercially available pHEMTs fabricated on commercially available microwave substrates.

6.5 MMIC UMAN-SKAlowV1 LNA

The simulated performance of an LNA designed for the SKA project to operate between frequencies of 0.7GHz and 1.8GHz is described in this section. The LNA was designed by using TQP13N pHEMT process and is explained in Section 4.6.2. Figure 6.41 illustrates the simulated S-parameter responses of the LNA over the frequency range of 0.5-3.0GHz. The output return loss of the LNA is consistently less than -5dB over whole frequency band whilst the input return loss is lower than -5dB from frequencies of 1.15GHz. However the input return loss is better than -10dB beyond the frequency of 1.6GHz. The S_{21} is more than 26dB from frequency of 0.7GHz to 2.4GHz which is more than 154% of the LNA required bandwidth. Figure 6.42 shows that the noise figure of the LNA is below 0.9dB (67K) over the frequency range of 0.75-2.1GHz with minimum noise figures (temperatures) of 0.85dB (63K) from 1.1GHz to 1.45GHz. The Rollet's factor (K-factor) of the LNA is illustrated in Figure 6.43 which shows the K-factor is greater than 8.7 within the operational frequency band of the LNA. The minimum K-factor of the LNA is 3.8 within the frequency band of 2.65-2.85GHz which is above 1. This indicates the LNA is unconditionally stable and hence there should not be any issues with the stability.

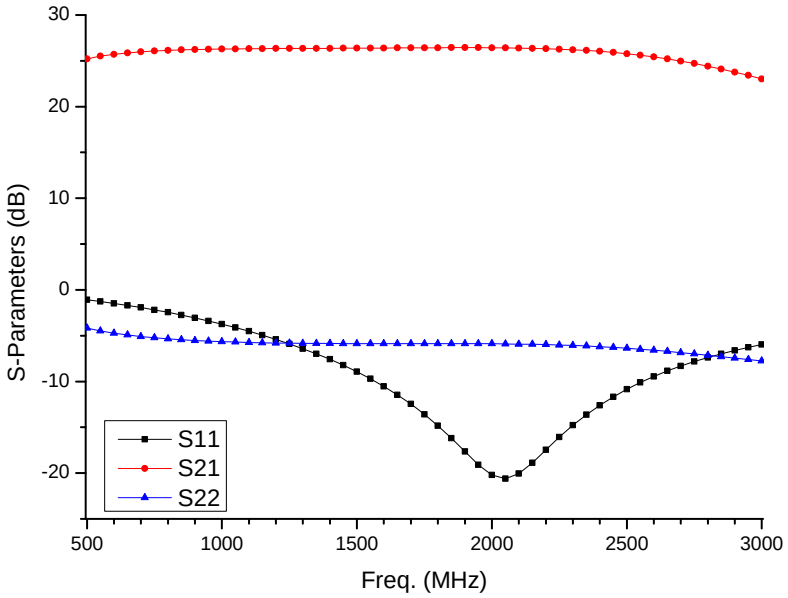

Figure 6.41: Simulated S-parameter responses of UMAN-SKAlowV1.

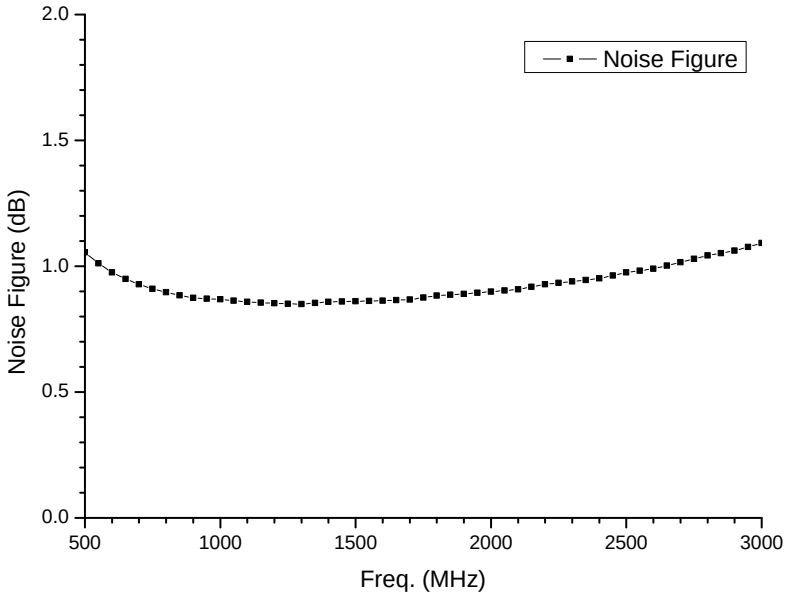

Figure 6.42: Simulated Noise Figure of UMAN-SKAlowV1.

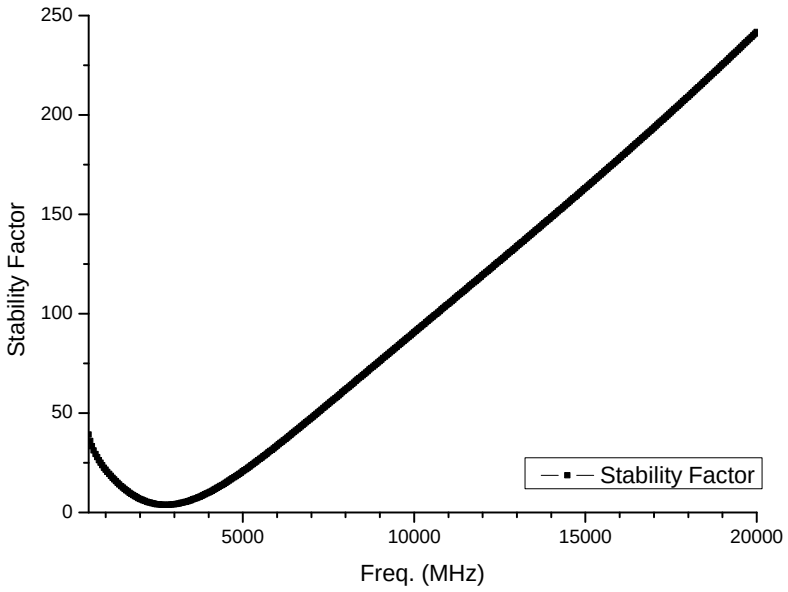

Figure 6.43: Simulated K-factor values for UMAN-SKAlowV1.

Table 6.15 gives the key parameter performances obtained by various LNAs operating over frequency bands similar to 0.7-1.8GHz. UMAN-SKAlowV1 achieved 34% higher gain and 18% lower noise figures compared with [134] over a wider bandwidth. UMAN-SKAlowV1 performs at a wider bandwidth than [135] while the noise figure values are comparable. While gain and noise performances of [136] exceed the performance obtained by UMAN-SKAlowV1, the bandwidth is narrower and covers frequencies below the central frequency of UMAN-SKAlowV1.

Table 6.15: Comparison of commercially available LNAs with UMAN-SKAlowV1.

LNA	Frequency (GHz)	Gain (dB)	NF (dB)
UMAN-SKAlowV1	0.5-2.5	26	<0.9
[134]	0.7-2.0	17	1.1
[135]	0.65-1.4	32	0.9
[136]	0.7-1.1	29	<0.7

6.6 MMIC UMAN8-Xband LNA

The simulated performance of UMAN8-Xband LNA using TQP13N process is described in this section. Details of the UMAN8-Xband design is given in Section 4.6.3. Figure 6.44 shows the simulated S-parameter responses of the LNA over the frequency range of 8-12GHz. The gain of the LNA is greater than 30 dB up to frequency of 10GHz while that is higher than 28dB over frequency range of 8-12GHz. The measurement of the TQP13N $4 \times 50\mu m$ pHEMT over the frequency range of 8-12GHz has an average gain of 10dB at the central frequency of 10GHz. Therefore, the data from pHEMT measurements confirm the possibility of obtaining 30dB gain from UMAN8-Xband which consists of 3 stages using pHEMTs with gate width dimension of $4 \times 50\mu m$. The input return loss of the LNA is lower than -11dB over entire band of 8-12GHz. The output return loss of the LNA is below -12dB from 8GHz to 10.2GHz with a minimum value of -15dB at 8.9GHz and 9GHz. Noise figure over frequency range of 8-12GHz is shown in Figure 6.45 with an average noise figures (temperatures) of 1dB(75K) over the whole operational frequency band. The stability factor (K-factor) of the LNA up to frequency of 40GHz is illustrated in Figure 6.46 with values of more than 12.2 within the frequency band of operation. The simulated results of the designed LNA exhibits a promising and stable performance from the fabricated LNA as K-factors are more than 10 up to frequency of 16GHz. The LNA S-parameter and noise figure responses present that the minimum requirements of the X-band LNA stated in Table 4.6 has been met and exceeded. The gain of LNA was exceeded by a factor of 20% and the frequency band of the LNA was extended until 12GHz.

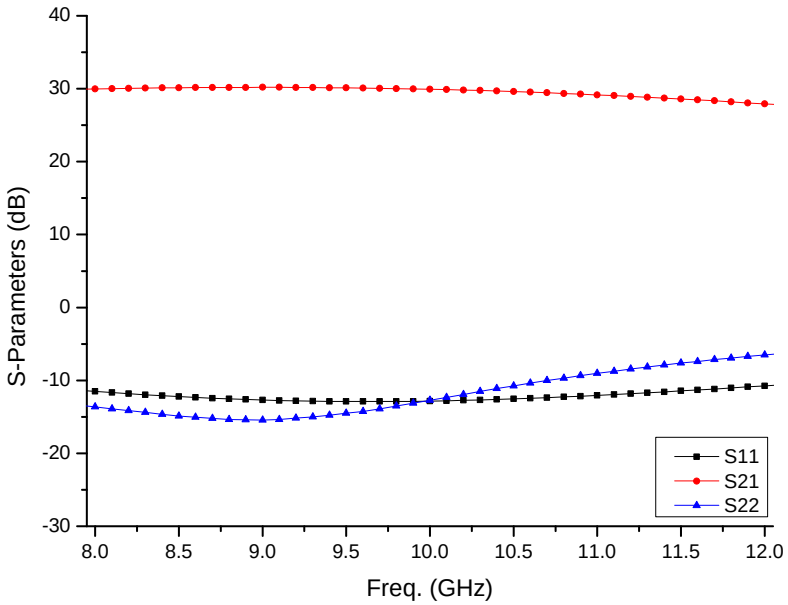

Figure 6.44: Simulated S-parameter responses of UMAN8-Xband.

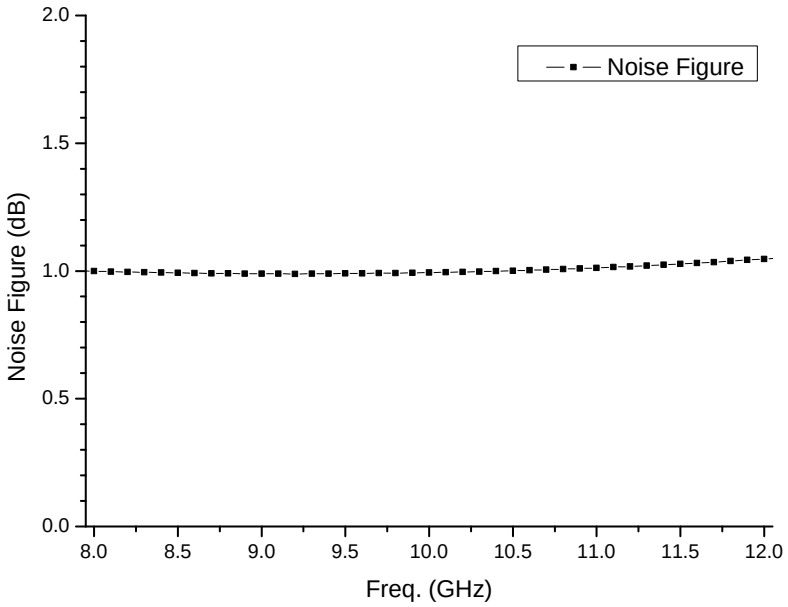

Figure 6.45: Simulated noise figure of UMAN8-Xband.

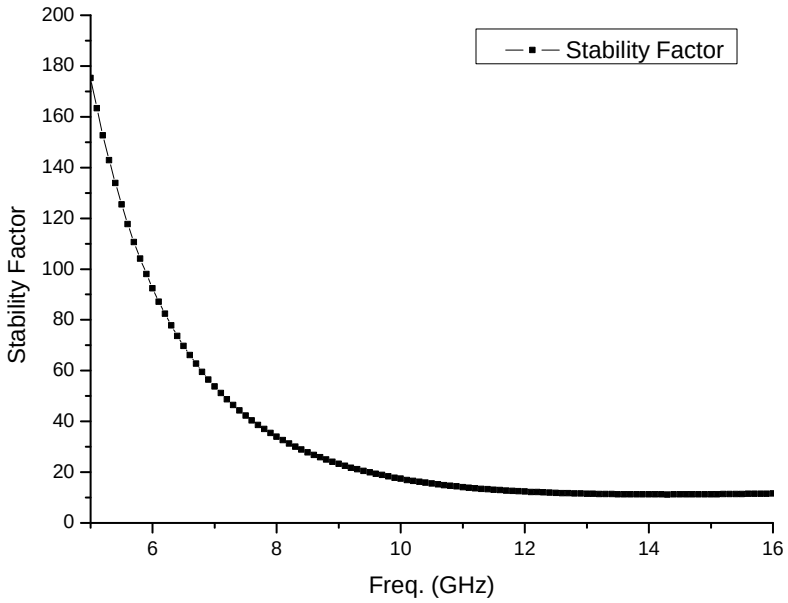

Figure 6.46: Simulated K-factor of UMAN8-Xband.

The performance obtained from UMAN8-Xband simulation is compared with 2 commercially available LNAs operating at X-band. The gain obtained from UMAN8-Xband is 10dB higher than [137] over the frequency band of 8-12GHz. Whilst the operation bandwidth of UMAN8-Xband is 80% larger than [138], it exhibits lower gain. The simulated noise performance of UMAN8-Xband illustrates 23% lower noise figures in comparison with [137] and 150% less than [138]. Return losses of the LNAs are comparable over the frequency band of interest for each of the LNAs. Table 6.16 summaries the performance of the LNAs.

Table 6.16: LNAs operating at X-band.

LNA	Frequency (GHz)	Gain (dB)	NF (dB)
UMAN8-Xband	8-12	30	1
[137]	6-14	20	1.3
[138]	7.7-8.5	48	2.5

6.7 Summary

The DC and S-parameter characterisation of four TQP13N pHEMTs of TriQuint Semiconductors with gate width dimension of $4 \times 25\mu m$, $4 \times 50\mu m$, $4 \times 75\mu m$ and $4 \times 100\mu m$ are explained in this chapter along with an analysis of pHEMT DC and RF performances. The measurements were carried out to evaluate the process for the SKA LNA designs and potential mass production of the SKA LNAs.

The simulated and measured S-parameter and noise figure performances of 9 LNA are given and analysed in this chapter. Figure 6.12 illustrates a diagram of all the designed LNAs that were accounted for in this chapter. Both MIC and MMIC fabrication techniques are used in the development of the LNAs. Table 6.17 gives a summary of the LNA names along with the gain and noise figure performances over their operational frequency bands. Detailed discussion and analysis of the LNAs are given within this chapter.

Table 6.17: Summary of LNAs performances over the bandwidth.

LNA	Fabrication Technique	Bandwidth	Average Gain(dB)	Average NF(dB)
SE-AAloV1	MIC	70-450MHz	>20	<0.8
SE-AAloV2	MIC	70-450MHz	>32	<0.6
SE-AAloV3	MIC	70-450MHz	>32	<0.6
Diff-AAloV1	MIC	70-450MHz	>22	<1.0
Diff-AAloV2	MIC	70-450MHz	>32	<0.75
AAmidV1	MIC	400-1400MHz	>22	<0.6
AAmidV2	MIC	400-1400MHz	>25	<0.5
UMAN-SKAlowV1	MMIC	0.7-1.8GHz	>26	<0.85
UMAN8-Xband	MMIC	8-12GHz	>30	<1.0

The primary focus of the MIC LNAs are on the LNAs designed for the lower and higher frequency bands of the SKA AA system. The main objectives of the SKA LNAs were concentrated on obtaining lowest power consumption and

noise figure at the same time. A number of versions were developed for the MIC LNAs as the designs and measurements evolved to meet the key performance parameters required by the AA system. SE-AAloV1, SE-AAloV2, SE-AAloV3, Diff-AAloV1 and Diff-AAloV2 were designed and characterised for operation in the AA-lo band while AAmidV1 and AAmidV2 were characterised to cover the AA-mid.

The UMAN-SKAlowV1 LNA was designed for operation in the lower frequency band of the SKA while the UMAN8-Xband LNA was an attempt to investigate the LNA design at the high frequency end of SKA. However, UMAN8-Xband LNA was designed to be applicable for multiple applications including satellite communication.

Table 6.18: LNAs designed for SKA AA system.

LNA	Bandwidth	Gain	Noise	Power	Size	Total
SE-AAloV1						
SE-AAloV2						
SE-AAloV3						
Diff-AAloV1						
Diff-AAloV2						
AAmidV1						
AAmidV2						

Table 6.18 uses the traffic light system to illustrate the success of the LNAs designed for SKA AA system. Each cell is filled with traffic light colours of green, amber and red to demonstrate the level of achievements in each prototype. Green cells show either satisfaction or exceeding the minimum requirements while amber cells show further improvements to be implemented. Furthermore, the red coloured cells mean the requirements of the system are not fully met. Consequently the LNAs success level are determined based on the dominant colour. Hence, it is noticeable that majority of key performance parameters are met by SE-AAloV2, SE-AAloV3, Diff-AAloV2 and AAmidV2.

The SE-AAloV2 and SE-AAloV3 have achieved low noise figures (temperatures) of less than 0.6dB (43K) across the band at a very low power consumption of 25mW at the PSU while the gains of more than 30dB are derived by the LNA to minimise the noise contribution of the subsequent amplification system in the front-end. AAmidV2 LNA has achieved average noise figures (temperature) of 0.45dB (32K) at power consumption of 28mW with gains of more than 25dB. The SE-AAloV2/SE-AAloV3 and AAmidV2 LNAs have achieved very good gain and noise performances at power consumptions that exceeds the requirements by 17% and 7% respectively. A total power of 2.7MW and 17.2MW can be saved in the LNA section just by employing SE-AAloV2/SE-AAloV3 and AAmidV2 for AA-lo and AA-mid respectively when compared with [48, 44].

Chapter 7

Conclusion and Future Work

This chapter summaries the research efforts which have been described in the previous chapters. The results and outcomes of the work are evaluated in this chapter. The success and novelty of the work, contextual with the projects, have also been analysed in Section 7.1. The possible scopes of future work and further developments in the research based on the work presented in this thesis is discussed in Section 7.2.

7.1 Conclusion

The research objectives which have been achieved can be broadly summarised as follows;

- MIC and MMIC LNA designs and developments for the SKA AA system.
- Single ended and differential MIC LNA designs and characterisation for AA-lo frequency band (70-450MHz) consisting of SE-AAloV1, SE-AAloV2, SE-AAloV3, Diff-AAloV1 and Diff-AAloV2.
- Single ended MIC LNAs characterisation for AA-mid frequency range of

400-1400MHz consisting of AAmidV1 and AAmidV2.

- Evaluation of the low noise 130nm gate length TQP13N GaAs pHEMT process of TriQuint Semiconductors for the SKA MMIC design.
- MMIC LNA design of UMAN-SKAlowV1 based on TQP13N pHEMT process.
- MMIC LNA design of UMAN8-Xband using TQP13N pHEMT process.

This thesis has explained the design, realisation and measurements of 7 MIC LNAs for the SKA AA system operating between 70MHz to 1.4GHz. The frequency band of SKA is divided into 2 main bands of lower and higher AA which are defined as AA-lo and AA-mid respectively. The SKA AA system requires ten of millions of LNAs to increase the sensitivity of the telescope. For this unprecedented number of LNAs in radio astronomy receivers, design focus lies not only on low noise but also on lowest possible power consumption with substantial gain to suppress the noise of subsequent stages. The RF and noise figure measurements at room temperature were carried out for characterisation purpose of the SKA AA LNAs. Throughout the research work, a number of LNA version were designed and characterised to satisfy and exceed the key performance parameters necessary for the SKA AA system. The antennas designed for the SKA system have either differential or single ended outputs and hence design of differential inputs are essential. However, the subsequent amplification stages in the front end have balanced configuration which implies a single ended configuration at the output of the LNAs. The significant contributions of this thesis towards the SKA project is the design and realisation of LNAs with both single ended and differential input to single ended output configurations which are suitable for the SKA AA system.

The AA-lo LNA designs include a single ended input and output and the other with differential input and single ended output. Consequently, 2 configurations have been investigated and characterised for the AA-lo system including one single ended and the other differential input to singled ended output. SE-AAloV2 has exhibited a flat gain of higher than 30dB over a wide frequency band until 920MHz which is more than 330% of the central frequency of AA-lo band. The output return loss of the SE-AAloV2 was better than -10dB over the frequency band of 70-1000MHz while the input return loss of is lower than -5dB beyond 420MHz. The average noise figure (temperature) of the LNA was measured to be less than 0.6dB (43K) over a wide frequency band of 40-950MHz. The high gain and low noise performance of both SE-AAloV2 and SE-AAloV3 were attained at a very low power consumption of only 25mW at the PSU which is a significant achievement as it exceeds the requirements by a factor of 17% . The comparative analysis of the SE-AAloV2 and SE-AAloV3 LNAs with the current LNA research work for the AA-lo [48] shows a total power saving of 2.7MW for the AA-lo LNAs while the noise figure is reduced by a factor of 2 and higher gain is obtained from the amplifier. The achieved good performance of the AA-lo LNAs at an exteremly low power consumption means the entire power consumption of the system is reduced and subsequently the the cost of the project is decreased significantly. The performance obtained from the Diff-AAloV2 at the optimum bias shows differential gain (S_{sd}) of greater than 30dB over frequency range of 20-910MHz with 4dB roll off. The differential input return loss of the LNA (S_{dd}) is lower than -5dB above frequency of 490MHz while the single ended output return loss (S_{ss}) is less than -10dB beyond 60MHz. The measured noise figure (temperature) of Diff-AAloV2 was less than 0.75dB (55K) up to 270MHz which forms 30% of the noise budget of the receiver system for AA-lo. The performance of Diff-AAloV2 achieved a good performance at a very low power consumption of 23mW at

PSU. The measured data show that the key performance parameters of the LNA was exceeded while the LNA offers a differential input to single ended output configuration which is required for the AA system.

The AA-mid system requires single ended LNAs and hence one configuration was utilised in the design of AA-mid LNA. This work demonstrates the performance achieved by AAmidV2 with an average noise figure (temperature) of 0.45dB (32K) at a very low power consumption of 28mW for AA-mid frequency band. The bandwidth of AAmidV2 is from 0.4GHz to 1.4GHz which is more than 110% of its central frequency with a an average gain of more than 26dB. The power requirements of the LNA was exceeded by a factor of 7%. This data implies that a total power of 17.2MW can be reduced by implementation of AAmidV2 for the AAmidV2 system when compared with the most updated LNA work by [44] as it consumes 12 times more power than AAmidV2.

The implication of these achievements is a significant step forward with a far reaching effects on SKA front end as significant amount of gain and low noise figures are achieved at a very low power consumption. This performance not only meets the target for maximum power consumption of 30mW for SKA AA system LNAs but also attains a gain of over 25 and 30dB which ensures less noise figure contribution from the second stage of the LNAs.

Two MMIC LNAs of UMAN-SKAlowV1 and UMAN8-Xband were designed to compare and contrast MIC and MMIC technologies and their suitability to the SKA. The TQP13N pHEMT process with 130nm gate length of TriQuint Semiconductors were used for MMIC LNA designs. TQP13N pHEMT low noise process of TriQuint Semiconductors was chosen for MMIC LNA development based on the evaluation performed in [139].

A promising and stable simulated performance was obtained from UMAN-SKAlowV1 over its frequency band of operation which is 0.7-1.8GHz. The LNA

was designed to investigate the MMIC LNA designs of the SKA at the low end frequency range of operation. The LNA has more than 25dB gain over an extended frequency range of 0.5-2.5GHz with noise figures (temperatures) of less than 0.9dB (67K).

UMAN8-Xband LNA was designed for exploring the MMIC LNA designs over the high frequency end of SKA project as it is operational until 10GHz. The simulations proved the UMAN8-Xband LNA is unconditionally stable with a flat average gain of 30dB across the frequency band of 8-12GHz. The average simulated noise figure (temperature) of the LNA is 1dB (75K).

The LNAs designed and characterised as part of this thesis investigated both MIC and MMIC LNA fabrication techniques for the SKA project. SKA project involves in design and installation of tens of millions of LNAs for the full uninterrupted operation of the SKA as the largest and most sensitive telescope in the world. Therefore parameters of low power consumption, high reliability and repeatability and mass production of the designed LNAs play important role in the SKA LNA design as well as the high gain and low noise factors that are required for all the radio astronomy receivers. The designed LNAs assist to achieve higher sensitivity with attaining high gains over a large bandwidth along with achieving lower noise figures across the band. The power consumption of the MIC LNAs are extremely low and hence less power is consumed resulting in a cost effective system. The MMIC LNA designs and fabrication will help the system in terms of repeatability, mass production of LNA and reducing the fabrication costs of the LNAs.

7.2 Future Work

This section identifies and describes the scope of future work based on the research work presented in this thesis. The MIC SKA AA LNAs RF and noise performance can be continued by the LNA measurement at cryogenic temperatures to study the LNA performances at cryogenic temperatures.

Further improvements and optimisation in the layout design of the MIC LNAs for the SKA AA system can be implemented with automated fabrication of the LNAs with standards of the industry can reduce the noise performance.

MMIC version of AA-lo and AA-mid LNAs can be designed and fabricated since the MIC LNA designs techniques were successfully evaluated and characterised. Further investigation on the available foundries and processes are required to select the best candidate in terms of requirements of the SKA LNAs as the project progresses.

The RF and noise characterisation of the MMIC UMAN8-Xband LNA at room and cryogenic temperatures are required as it was designed for the high end frequency band of operation in the SKA. The cryogenic measurements of the LNA can be implemented to check the suitability of the LNA for space and satellite communications applications as it covers frequency band of 8 to 12GHz.

The UMAN-SKAlowV1 MMIC LNA described in this thesis can be fabricated and characterised at both room and cryogenic temperatures.

Bibliography

[1] B. Chenggang, "Design of Differential Low Noise Amplifier for the Square Kilometer Array," *MSc Thesis submitted to the University of Manchester*, 2008.

[2] C. A. Balanis, *Antenna Theory Analysis and Design.* John Wiley and Sons, 1997.

[3] J. Kraus and R. J. Marhefka, *Antenna For All Applications.* McGraw Hill, 2002.

[4] M. Panahi, B. Bhaumik, and D. George, "Power-efficient ultra wideband lnas for the world's largest radio telescope," *Submitted to Review of Scientific Instruments,*, 2012.

[5] P. Dewdney, P. Hall, R. Schilizzi, and T. Lazio, "The square kilometre array," *Proceedings of the IEEE*, vol. 97, no. 8, pp. 1482 –1496, aug. 2009.

[6] A. Faulkner *et al.* (April 2010) The Aperture Arrays for the SKA: the SKADS White Paper. [Online]. Available: http://www.skatelescope.org/uploaded/5367_122_Memo_Faulkner.pdf

[7] P. Dewdney *et al.* (November 2010) SKA Phase 1: Preliminary System Description. [Online]. Available: http://www.skatelescope.org/uploaded/21705_130_Memo_Dewdney.pdf

[8] S. Bhaumik, "MMIC Design of Ultra Low Noise Amplifiers," *PhD Thesis submitted to the University of Manchester*, 2010.

[9] S. Marsh, *Practical MMIC Design.* Artech House, 2006.

[10] J. Bij de Vaate *et al.* (April 2011) AA Concept Descriptions (SKA Document Number WP-2-010.020.010-TD-001).

[11] D. G. S. Bhaumik. (2010) AA-lo AA-mid LNA Designs. [Online]. Available: http://www2.skatelescope.org/indico/getFile.py/access?contribId=81&sessionId=11&resId=0&materialId=0&confId=3

[12] W. Bakalski, W. Simburger, H. Knapp, H.-D. Wohlmuth, and A. Scholtz, "Lumped and distributed lattice-type lc-baluns," in *Microwave Symposium Digest, 2002 IEEE MTT-S International*, vol. 1, 2002, pp. 209 –212.

[13] TC1-1-13MG2+ Data, Surface Mount RF Transformer. Minicircuits. [Online]. Available: http://www.minicircuits.com/MCLStore/ModelInfoDisplay?13258466461260.\411376292829466

[14] B. F. Burke and F. Graham Smith, *An Introduction to Radio Astronomy.* Cambridge University Press, 2002.

[15] D. A. Kettle, "Characterisation of low noise devices for radio astronomy applications," *PhD Thesis submitted to the University of Manchester*, 2006.

[16] R. T. Schilizzi *et al.* (Dec. 2007) Preliminary Specifications for the Square Kilometre Array. [Online]. Available: http://www.skatelescope.org/PDF/memos/100_Memo_Schilizzi.pdf

[17] G. Hampson, B. Smolders, and A. Joseph, "One Square Metre of a Million," in *29th European Microwave Conf.*, vol. 1, Oct. 1999, pp. 111 –114.

[18] A. Van Ardenne, "Concepts of the Square Kilometre Array; toward the new generation radio telescopes," in *IEEE Int. Symp. Antennas and Propagation Soc.*, vol. 1, Jul. 2000, pp. 158 –161 vol.1.

[19] A. Faulkner *et al.* (2010) Aperture Arrays for the SKA: the SKADS White Paper. [Online]. Available: http://www.skatelescope.org

[20] B. Gaensler, "The Square Kilometre Array: An international radio telescope for the 21st century," in *IEEE Int. Frequency Control Symp., Joint with the 22nd European Frequency and Time forum*, Apr. 2009.

[21] W. Imbriale, "The square kilometre array: Engineering opportunities," in *Wireless Information Technology and Systems (ICWITS), 2010 IEEE International Conference on*, 28 2010-sept. 3 2010, p. 1.

[22] M. A. Garrett *et al.* (August 2010) A Concept Design for SKA Phase 1 (SKA1) . [Online]. Available: http://www.skatelescope.org/uploaded/27414_125_Memo_Garrett.pdf

[23] A. Brown, Y. Zhang, D. Kant, and J. de Vaate, "Wideband planar phased arrays for the square kilometre array," in *Phased Array Systems and Technology (ARRAY), 2010 IEEE International Symposium on*, oct. 2010, pp. 616 –623.

[24] Y. Zhang and A. Brown, "Bunny ear combline antennas for compact wideband dual-polarized aperture array," *Antennas and Propagation, IEEE Transactions on*, vol. 59, no. 8, pp. 3071 –3075, aug. 2011.

[25] N.-T. Huang, R. Mittra, R. Maaskant, and W. Yu, "Investigation of the vivaldi array for square kilometer array (ska) application using the parallelized fdtd code gems on the lofar blue gene/l supercomputer," in *Antennas*

and Propagation Society International Symposium, 2007 IEEE, june 2007, pp. 2341 –2344.

[26] K. D. Palmer and S. J. Marais, "Baluns for Feeding Ultra Wideband Antennas," in *The European Conference on Antennas and Propagation: EuCAP 2006*, ser. ESA Special Publication, vol. 626, Oct. 2006.

[27] S. Bhaumik, M. Panahi, and D. Kettle, "Differential lna considerations for the square kilometer array," in *Antenna Technology and Applied Electromagnetics and the Canadian Radio Science Meeting, 2009. ANTEM/URSI 2009. 13th International Symposium on*, feb. 2009, pp. 1 –4.

[28] D. M. Pozar, *Microwave Engineering.* John Wiley and Sons, Inc., 2005.

[29] R. E. Collin, *Foundations for Microwave Engineering.* McGraw Hill Inc., 1992.

[30] AAVP2011 workshop in Netherlands December 2011. [Online]. Available: http://www.astron.nl/aavp2011/documents.php

[31] Conical log spiral antennas for SKAlow? The Path to SKA-low Workshop ICRAR/CIRA in Perth 8 September 2011. [Online]. Available: http://ict.icrar.org/store/Presentations/skalow/Jiwani_A_Conical_spiral.pdf

[32] E. de Lera Acedo, E. Garcia, V. Gonzalez-Posadas, J. Vazquez-Roy, R. Maaskant, and D. Segovia, "Study and design of a differentially-fed tapered slot antenna array," *Antennas and Propagation, IEEE Transactions on*, vol. 58, no. 1, pp. 68 –78, jan. 2010.

[33] Y. Zhang and A. Brown, "Octagonal ring antenna for a compact dual-polarized aperture array," *Antennas and Propagation, IEEE Transactions on*, vol. 59, no. 10, pp. 3927 –3932, oct. 2011.

[34] G. Kant, P. Patel, S. Wijnholds, M. Ruiter, and E. van der Wal, "Embrace: A multi-beam 20,000-element radio astronomical phased array antenna demonstrator," *Antennas and Propagation, IEEE Transactions on*, vol. 59, no. 6, pp. 1990 –2003, june 2011.

[35] S. Bhaumik and D. George, "Review of square kilometre array lna technologies and topologies," *Widefield Science and Technology for the SKA*, November 2009.

[36] "Astron website," December 2011. [Online]. Available: http://www.astron.nl/

[37] "Apertif," December 2011. [Online]. Available: http://www.astron.nl/general/apertif/apertif

[38] J. Bij de Vaate, "Active antenna design and characterization," *Wide Field Science and Technology for the SKA in Limelette, Belgium*, 2010.

[39] O. Garcia-Perez, "Fida3: A novel active array design for the mid-frequency range of the ska," 2010.

[40] L. Belostotski and J. Haslett, "Sub-0.2 db noise figure wideband room-temperature cmos lna with non-50ohm; signal-source impedance," *Solid-State Circuits, IEEE Journal of*, vol. 42, no. 11, pp. 2492 –2502, nov. 2007.

[41] ——, "A technique for differential noise figure measurement of differential lnas," *Instrumentation and Measurement, IEEE Transactions on*, vol. 57, no. 7, pp. 1298 –1303, july 2008.

[42] S. Weinreb, J. Bardin, H. Mani, and G. Jones, "Matched wideband low-noise amplifiers for radio astronomy," *Review of Scientific Instruments*, vol. 80, no. 4, pp. 044 702 –044 702–5, apr 2009.

[43] J. Pandian, L. Baker, G. Cortes, P. Goldsmith, A. Deshpande, R. Ganesan, J. Hagen, L. Locke, N. Wadefalk, and S. Weinreb, "Low-noise 6-8 ghz receiver," *Microwave Magazine, IEEE*, vol. 7, no. 6, pp. 74 –84, dec. 2006.

[44] S. Weinreb. (Dec. 2011) Very Low Noise Ambient Temperature Amplifiers for the 0.6 to 1.6 GHz Range. [Online]. Available: http://www.skatelescope.org/uploaded/41805_137_Memo_Weinreb.pdf

[45] M. Panahi and D. George, "Verification of differential low noise amplifier measurement," *Widefield Science and Technology for the SKA*.

[46] S. Boulay et al, "Novel ultra low noise amplifiers based on ingaas/inalas phemts," *Wide Field Science and Technology for the SKA,*, 2010.

[47] N. Ahmad, S. Arshad, and M. Missous, "New inp based phemt double stage differential to single-ended mmic low noise amplifiers for ska," in *Advanced Semiconductor Devices Microsystems (ASDAM), 2010 8th International Conference on*, oct. 2010, pp. 305 –308.

[48] J. M. Federico Perini, "Aalo cots lna (istituto di radioastronomia inaf bologna)."

[49] S.-F. Chao, J.-J. Kuo, C.-L. Lin, M.-D. Tsai, and H. Wang, "A dc-11.5 ghz low-power, wideband amplifier using splitting-load inductive peaking technique," *Microwave and Wireless Components Letters, IEEE*, vol. 18, no. 7, pp. 482 –484, july 2008.

[50] SGL0363Z LNA, Datasheet. RFMD. [Online]. Available: http://www.rfmd.com/CS/Documents/SGL-0363ZDS.pdf,October2011

[51] SGL0622Z LNA Datasheet. RFMD. [Online]. Available: http://www.rfmd.com/CS/Documents/SGL0622ZDS.pdf,October2011

[52] M. El-Nozahi, A. Helmy, E. Sa andnchez Sinencio, and K. Entesari, "A 2-1100 mhz wideband low noise amplifier with 1.43 db minimum noise figure," in *Radio Frequency Integrated Circuits Symposium (RFIC), 2010 IEEE*, may 2010, pp. 119 –122.

[53] Y. Liao, Z. Tang, and H. Min, "A cmos wide-band low-noise amplifier with balun-based noise-canceling technique," in *Solid-State Circuits Conference, 2007. ASSCC '07. IEEE Asian*, nov. 2007, pp. 91 –94.

[54] Y.-H. Yu, Y.-S. Yang, and Y.-J. Chen, "A compact wideband cmos low noise amplifier with gain flatness enhancement," *Solid-State Circuits, IEEE Journal of*, vol. 45, no. 3, pp. 502 –509, march 2010.

[55] ZX60-33LN LNA, Datasheet. Mini-Circuits. [Online]. Available: http://www.minicircuits.com/pdfs/ZX60-33LN+.pdf,October2011

[56] MGA-53543 LNA Datasheet. Avago Technologies. [Online]. Available: http://www.avagotech.com/pages/en/rf_microwave/amplifiers/low_noise_\amplifiers/mga-53543/,October2011

[57] D. Im, I. Nam, and K. Lee, "A low power broadband differential low noise amplifier employing noise and im3 distortion cancellation for mobile broadcast receivers," *Microwave and Wireless Components Letters, IEEE*, vol. 20, no. 10, pp. 566 –568, oct. 2010.

[58] T. Chang, J. Chen, L. Rigge, and J. Lin, "Esd-protected wideband cmos lnas using modified resistive feedback techniques with chip-on-board packaging," *Microwave Theory and Techniques, IEEE Transactions on*, vol. 56, no. 8, pp. 1817 –1826, aug. 2008.

[59] O. Garcia Perez, D. Segovia-Vargas, L. Garcia Munoz, J. Jimenez-Martin, and V. Gonzalez-Posadas, "Broadband differential low-noise amplifier for active differential arrays," *Microwave Theory and Techniques, IEEE Transactions on*, vol. 59, no. 1, pp. 108 –115, jan. 2011.

[60] S.-E. Shih, W. Deal, D. Yamauchi, W. Sutton, W.-B. Luo, Y. Chen, I. Smorchkova, B. Heying, M. Wojtowicz, and M. Siddiqui, "Design and analysis of ultra wideband gan dual-gate hemt low-noise amplifiers," *Microwave Theory and Techniques, IEEE Transactions on*, vol. 57, no. 12, pp. 3270 –3277, dec. 2009.

[61] K.-H. Chen, J.-H. Lu, B.-J. Chen, and S.-I. Liu, "An ultra-wide-band 0.4 ndash;10-ghz lna in 0.18-um cmos," *Circuits and Systems II: Express Briefs, IEEE Transactions on*, vol. 54, no. 3, pp. 217 –221, march 2007.

[62] X. Ma, G. Chen, and Y. Feng, "A cmos low-noise amplifier for spectral sensing in cognitive radios," in *Microelectronics Electronics, 2009. PrimeAsia 2009. Asia Pacific Conference on Postgraduate Research in*, jan. 2009, pp. 37 –40.

[63] Q.-T. Lai and J.-F. Mao, "A 0.5-11 ghz cmos low noise amplifier using dual-channel shunt technique," *Microwave and Wireless Components Letters, IEEE*, vol. 20, no. 5, pp. 280 –282, may 2010.

[64] J. Bij de Vaate, R. Witvers, and E. Woestenburg, "Front-end integration requirements for the square kilometre array radio telescope," in *Compound Semiconductor Integrated Circuit Symposium (CSICS), 2010 IEEE*, oct. 2010, pp. 1 –3.

[65] H. P. Le, K. Shah, and J. Singh, "A fully-on-chip wideband low noise amplifier for radio telescope applications," in *Circuits and Systems, 2009. ISCAS 2009. IEEE International Symposium on*, may 2009, pp. 1941–1944.

[66] H.-H. Roh, K.-T. Park, H.-R. Oh, Y.-R. Seong, J.-S. Park, and M.-S. Kang, "A common gate low noise amplifier with high linearity over uhf rfid bands," in *Electromagnetic Compatibility and 19th International Zurich Symposium on Electromagnetic Compatibility, 2008. APEMC 2008. Asia-Pacific Symposium on*, may 2008, pp. 88 –91.

[67] M. Nakatsugawa, Y. Yamaguchi, and M. Muraguchi, "An l-band ultra-low-power-consumption monolithic low-noise amplifier," *Microwave Theory and Techniques, IEEE Transactions on*, vol. 43, no. 7, pp. 1745 –1750, jul 1995.

[68] D. North and W. Ferris, "Fluctuations induced in vacuum-tube grids at high frequencies," *Proceedings of the IRE*, vol. 29, no. 2, pp. 49 – 50, feb. 1941.

[69] S. Ballantine, "Schrot-effect in high-frequency circuits," *Journal of the Franklin Institute*, vol. 206, no. 2, pp. 159 – 167, 1928. [Online]. Available: http://www.sciencedirect.com/science/article/B6V04-49WWYXT-1V/2/2245504283e3b0caea5309031559741d

[70] D. NORTH, "The absolute sensitivity of radio receivers," *R.C.A. Review,*, vol. 6, p. 332, october 1942.

[71] W. Lewis, "Radar receivers," *Electrical Engineers - Part I: General, Journal of the Institution of*, vol. 93, no. 70, pp. 467 –469, october 1946.

[72] L. Moxon, "The noise characteristics of radar receivers," *Electrical Engineers - Part IIIA: Radiolocation, Journal of the Institution of*, vol. 93, no. 1, p. 288, 1946.

[73] E. Herold and L. Malter, "Some aspects of radio reception at ultra-high frequency: Part iii. the signal-to-noise ratio of radio receivers," *Proceedings of the IRE*, vol. 31, no. 9, pp. 501 – 510, sept. 1943.

[74] ——, "Some aspects of radio reception at ultra-high frequency: Part iv. general superheterodyne considerations at ultra-high frequencies," *Proceedings of the IRE*, vol. 31, no. 10, pp. 567 – 575, oct. 1943.

[75] ——, "Some aspects of radio reception at ultra-high frequencies: Part v. frequency mixing in diodes," *Proceedings of the IRE*, vol. 31, no. 10, pp. 575 – 582, oct. 1943.

[76] ——, "Some aspects of radio reception at ultra-high frequency: Part i. the antenna and the-receiver input circuits," *Proceedings of the IRE*, vol. 31, no. 8, pp. 423 – 438, aug. 1943.

[77] H. Rothe and W. Dahlke, "Theory of noisy fourpoles," *Proceedings of the IRE*, vol. 44, no. 6, pp. 811 –818, june 1956.

[78] H. Friis, "Noise Figures of Radio Receivers," *IRE Proc.*, vol. 32, no. 7, pp. 419 – 422, Jul. 1944.

[79] H. Wallman, A. Macnee, and C. Gadsden, "A low-noise amplifier," *Proceedings of the IRE*, vol. 36, no. 6, pp. 700 – 708, june 1948.

[80] M. Lebenbaum, "Design factors in low-noise figure input circuits," *Proceedings of the IRE*, vol. 38, no. 1, pp. 75 – 80, jan. 1950.

[81] M. Currie and D. Forster, "Low noise tunable preamplifiers for microwave receivers," *Proceedings of the IRE*, vol. 46, no. 3, pp. 570 –579, march 1958.

[82] R. Rockwell, "Low-noise klystron amplifiers," *Electron Devices, IRE Transactions on*, vol. 6, no. 4, pp. 428 –437, oct. 1959.

[83] R. Weglein and F. Keywell, "A low-noise x-band parametric amplifier using a silicon mesa diode," *Microwave Theory and Techniques, IRE Transactions on*, vol. 9, no. 1, pp. 39 –43, january 1961.

[84] R. Hearn, R. Bennett, and B. Wind, "Some types of low noise amplifier," *Radio Engineers, Journal of the British Institution of*, vol. 22, no. 5, pp. 393 –403, november 1961.

[85] P. Lauritzen and J. Leistiko, O., "Field-effect transistors as low-noise amplifiers," in *Solid-State Circuits Conference. Digest of Technical Papers. 1962 IEEE International*, vol. V, feb 1962, pp. 62 – 63.

[86] S. F. T. Mimura, T. Hiyamizu and K. Nanbu, "A new field-effect transistor with selectively doped GaAs/n-$Al_xGa_{1-x}As$ heterojunctions," *Japanese Journal of Applied Physics*, vol. 19, no. 5, pp. 225 – 227, May 1980.

[87] T. Mimura, "The early history of the high electron mobility transistor (hemt)," *Microwave Theory and Techniques, IEEE Transactions on*, vol. 50, no. 3, pp. 780 –782, mar 2002.

[88] M. Pospieszalski, "Modeling of noise parameters of MESFETs and MODFETs and their frequency and temperature dependence," *IEEE Trans. Microw. Theory Tech.*, vol. 37, no. 9, pp. 1340 –1350, Sep. 1989.

[89] S. Okwit, "An Historical View of the Evolution of Low-Noise Concepts and

Techniques," *IEEE Trans. Microw. Theory Tech.*, vol. 32, no. 9, pp. 1068 – 1082, Sep. 1984.

[90] M. Pospieszalski, "Extremely low-noise amplification with cryogenic FETs and HFETs: 1970-2004," *IEEE Microwave*, vol. 6, no. 3, pp. 62 – 75, Sep. 2005.

[91] R. S. Pengelly, *Microwave Field-Effect Transistors-Theory, Design and Application.* Research Studies Press, 1984.

[92] I. D. Robertson, *MMIC Design.* London: The Institute of Electrical Engineers, 1995.

[93] F. Ali and A. Gupta, *HEMTs and HBTs: Devices, Fabrication, and Circuits.* London: Artech House, 1991.

[94] J. M. Golio, *Microwave MESFETs and HEMTs.* Norwood, MA: Artech House, 1970.

[95] M. Roy, "Front-End Considerations for Next Generation Communication Receivers," *PhD Thesis submitted to the University of Manchester*, 2011.

[96] M. Pospieszalski, "Extremely low-noise amplification with cryogenic fets and hfets: 1970-2004," *Microwave Magazine, IEEE*, vol. 6, no. 3, pp. 62 – 75, sept. 2005.

[97] A. Van der Ziel, *Noise in Solid State Devices and Circuits.* New York John Wiley and Sons, 1986.

[98] J. Engberg and T. Larsen, *Noise Theory of Linear and Nonlinear Circuits.* Wiley, 1995.

[99] A. van der Ziel, *Noise: Sources, Characterisation, Measurement*. Prentice-Hall, Inc., 1970.

[100] F. Hooge, "1/f noise," *Physica*, vol. 83B, p. 14, 1976.

[101] T. H. Lee, *Planar Microwave Engineering, A practical Guide to Theory, Measurement and Circuits*. Cambridge University Press, 2004.

[102] K. Kurokawa, "Power waves and the scattering matrix," *IEEE Trans. Microw. Theory Tech.*, vol. 13, no. 2, pp. 194 – 202, Mar. 1965.

[103] A. M. P. G. D. Vendeli and U. L. Rohde, *Microwave Circuit Design Using Linear and Nonlinear Techniques*. John Wiley and Sons, 1990.

[104] E. Matthews, "The use of scattering matrices in microwave circuits," *Microwave Theory and Techniques, IRE Transactions on*, vol. 3, no. 3, pp. 21 –26, april 1955.

[105] D. Bockelman and W. Eisenstadt, "Combined differential and common-mode scattering parameters: theory and simulation," *Microwave Theory and Techniques, IEEE Transactions on*, vol. 43, no. 7, pp. 1530–1539, Jul 1995.

[106] ——, "Combined differential and common-mode analysis of power splitters and combiners," *Microwave Theory and Techniques, IEEE Transactions on*, vol. 43, no. 11, pp. 2627–2632, Nov 1995.

[107] ——, "Pure-mode network analyzer for on-wafer measurements of mixed-mode s-parameters of differential circuits," *Microwave Theory and Techniques, IEEE Transactions on*, vol. 45, no. 7, pp. 1071–1077, Jul 1997.

[108] L. Sun, Z. Wang, and J. Gao, "A method for on-wafer s-parameter measurement of a differential amplifier by using two-port network analyzer," *Microwave Conference Proceedings, 2005. APMC 2005. Asia-Pacific Conference Proceedings*, vol. 5, pp. 4 pp.–, Dec. 2005.

[109] A. S. Sedra and K. C. Smith, *Microelectronic Circuits*. Oxford University Press, 1998.

[110] A. Technologies, *Agilent E5070B/E5071B ENA Series RF Network Analyzers: User Guide*, June 2007.

[111] Advanced Design System (Version 2009). Agilent Technologies. [Online]. Available: http://www.home.agilent.com/agilent/product.jspx?nid=-34346.0.00&lc=eng&cc=GB&pselect=SR.Looking

[112] G. Gonzalez, *Microwave Transistor Amplifiers Analysis and Design*. Prentice Hall, 1997.

[113] J. Rollett, "Stability and power-gain invariants of linear twoports," *Circuit Theory, IRE Transactions on*, vol. 9, no. 1, pp. 29 – 32, mar 1962.

[114] ——, "Correction to stability and power-gain invariants of linear twoports," *Circuit Theory, IEEE Transactions on*, vol. 10, no. 1, p. 107, mar 1963.

[115] S. A. Maas, *The RF and Mircrowave Circuit Design Cookbook*. Artech House Publisher, 1998.

[116] Application Note on Transformers. Mini Circuits. [Online]. Available: http://www.minicircuits.com/app/AN20-002.pdf

[117] Balun Transformers. Mini Circuits. [Online]. Available: http://www.minicircuits.com/pages/BalunApplicationNote.htm

[118] N. Marchand, "Transmission-line conversion transformer," *Electronics*, vol. 17, pp. 142–145, Dec. 1944.

[119] P. H. Ladbrooke, *MMIC Design: GaAs FETs and HEMTs.* Artech House, 1943.

[120] Agilent ATF-58143 Low Noise Enhancement Mode Pseudomorphic HEMT in a Surface Mount Plastic Package Data Sheet. Avago Technologies. [Online]. Available: http://www.datasheetcatalog.org/datasheets2/15/153214_1.pdf

[121] TC1-1-13MG2+ Datasheet, Surface Mount RF Transformer. Minicircuits. [Online]. Available: http://www.minicircuits.com/pdfs/TC1-1-13MG2+.pdf

[122] (Dec 2011) . TriQuint Semiconductors. [Online]. Available: http://www.triquint.com/prodserv/foundry/docs/TQP13-N.pdf

[123] Integrated Circuit Characterization and Analysis Program 2009. Agilent Technologies. [Online]. Available: http://www.home.agilent.com/agilent/product.jspx?cc=GB&lc=eng&ckey\=1297149&nid=-34268.0.00&id=1297149

[124] Wincal. Cascade Microtech. [Online]. Available: http://www.cmicro.com/products/probes/wincal-xe

[125] WCA05300A LNA Datasheet. WanTcom. [Online]. Available: http://www.rell.com/resources/RellDocuments/SYS_25/WCA05300A.pdf

[126] SPF5122Z LNA Datasheet. RFMD. [Online]. Available: http://www.rfmd.com/CS/Documents/SPF-5122ZDS.pdf,January2012

[127] AD8354ACPZ Datasheet. ANALOG DEVICES. [Online]. Available: hhttp://www.analog.com/static/imported-files/data_sheets/AD8354.pdf,January2012

[128] ALM-1322-BLKG Datasheet. Avago Technologies. [Online]. Available: http://www.avagotech.com/docs/AV02-1855EN,January2012

[129] E. E. M. Woestenburg, R. H. Witvers, and L. Bakker, "Low noise room temperature lnas for the ska," in *Microwave Integrated Circuits Conference (EuMIC), 2011 European*, oct. 2011, pp. 366 –369.

[130] (Jan 2012) PMA-545G1 Datasheet. Mini Circuits. [Online]. Available: http://www.minicircuits.com/pdfs/PMA-545G1+.pdf

[131] (Jan 2012) TAV-551+ Datasheet. Mini Circuits. [Online]. Available: http://www.minicircuits.com/pdfs/TAV-551+.pdf

[132] (Januaury 2012) MGA-13116 Data sheet. Avago Technologies. [Online]. Available: http://www.avagotech.com/docs/AV02-2877EN

[133] (Jan. 2012) WEA107 Datasheet . WanTcom. [Online]. Available: http://www.wantcominc.com/DataSheets/WEA/WEA107.pdf

[134] (Jan 2012) WHM0520-18AE Datasheet. WanTcom. [Online]. Available: http://www.wantcominc.com/DataSheets/WHM/WHM0520-18AE.pdf

[135] (Jan 2012) ZRL-1150LN+ Datasheet. Mini Circuits. [Online]. Available: http://www.minicircuits.com/pdfs/ZRL-1150LN+.pdf

[136] (Jan 2012) ALM-1522 Datasheet. Avago Technologies. [Online]. Available: http://www.avagotech.com/docs/AV02-1723EN

[137] (Jan 2012) TGA2511 Datasheet. TriQuint SemiConductors. [Online]. Available: http://www.triquint.com/products/p/TGA2511

[138] (Jan 2012) WLPA80-4540A Datasheet. WanTcom. [Online]. Available: http://www.wantcominc.com/DataSheets/WLPA/WLPA80-4540A.pdf

[139] S. Bhaumik, M. Roy, and D. George, "Comparative study of hemts for lnas in square kilometre array telescope," in *Microwave Symposium Digest (MTT), 2011 IEEE MTT-S International*, june 2011, pp. 1 –4.